



Catalytic conversion of C1 molecules under mild conditions

Xiaoju Cui,^{a,b,c} Rui Huang,^a and Dehui Deng^{*,a,b,c}

^a State Key Laboratory of Catalysis, Collaborative Innovation Center of Chemistry for Energy Materials, Dalian Institute of Chemical Physics, Chinese Academy of Sciences, Dalian 116023, China

^b Collaborative Innovation Center of Chemistry for Energy Materials, College of Chemistry and Chemical Engineering, Xiamen University, Xiamen 361005, China

^c University of Chinese Academy of Sciences, Beijing 100039, China

*Correspondence: dhdeng@dicp.ac.cn (D. D.)

ABSTRACT: C1 catalysis based on the transformation of methane, carbon monoxide, methanol and carbon dioxide offers great potential for the sustainable production of fuels and chemicals in response to the decrease of the energy consumption and plant maintenance. While the relatively inert nature of C–H and C–O bond (e.g., methane and carbon dioxide) and uncontrollable coupling of C–C bond render the selective activation and controllable transformation of C1 molecules to high-value-added products challenging in C1 chemistry. Catalytic conversion of C1 energy molecules under mild conditions enables a better control of the selectivity of the desired products, however, which requires highly active catalysts to lower the reaction energy barriers. Besides designing efficient catalysts to promote C1 molecules conversion, employing electro-catalysis and photo-catalysis to circumvent the thermodynamic limitations is regarded as promising ways for C1 catalysis at low temperatures. Benefiting from the advanced technology for catalyst synthesis, reactor design, mechanism understanding, catalytic conversion of C1 molecules under mild conditions has made significant progress from 2010 to 2020. In this review, we summarized the typical catalytic processes and representative catalysts for transforming methane, carbon monoxide, methanol and carbon dioxide into high value-added chemicals with a reaction temperatures below 200 °C driven by thermo-catalysis, electro-catalysis, and photo-catalysis. Besides, a short perspective is offered to highlight possible future research directions towards C1 molecules conversion under mild conditions. It is expected to provide a useful reference for the readers to design better catalysts and reaction process for mild conversion of C1 molecules efficiently in future.

KEYWORDS: C1 catalysis, Active sites, Reaction mechanism, Mild reaction conditions

■ INTRODUCTION

As abundant and cheap carbon feedstocks, one-carbon (C1) molecules either exist in nature or can be facilely produced from natural carbon resources (coal, natural gas, biomass, or organic wastes), which mainly addressed methane, carbon monoxide, methanol and carbon dioxide.^{1,2} In response to the crude oil depleting and the serious pollution caused by fossil fuel combustion, transformation of C1 molecules into various high-value-added fuels and chemicals plays a more and more important role in the current supply of energy and chemicals.^{3–5} As such, C1 catalysis has been attracting significant interest from academy and industry and has become one of the most active research fields.^{6–9}

To date, C1 catalysis has occupied an extremely important role in the modern coal chemical industry and the natural gas chemical industry. The conversion of carbon monoxide via Fischer-Tropsch (F-T) synthesis and water gas shift (WGS) reaction have successfully realized the practice from fundamental research to industrial large-scale processes, which serves as an important C1 chemistry platform. Methanol, as a key intermediate, participates in various chemicals production during C1 molecules utilization process, such as the methanol-to-olefins (MTO) process and methanol steam reforming (MSR) process. The fundamental research about methane and carbon dioxide conversion have gained an increasing interest over the past decades, which can not only mitigate the effects of global warming but also turn waste

into resources. While these laboratory findings are far from the requirements of industrial application.

Besides plenty of well-studied high-temperature systems for C1 catalysis, catalytic conversion of C1 molecules under mild conditions attracts much attention in response to the decrease of the energy consumption and plant maintenance. While the relatively inert nature of C–H and C–O bond (e.g., methane and carbon dioxide) and uncontrollable coupling of C–C bond make it harder to achieve the selective activation and oriented conversion of C1 molecules to high-value-added products, particular for these involving C–C bond coupling reactions to form C₂₊ products. As shown in Table 1, these four C1 energy molecules conversion process below 200 °C can be divided into the thermodynamically favored reactions and unfavored ones according to the Gibbs free energy. For these thermodynamically favored reactions, low-temperature reaction conditions enable a better control of the selectivity of the desired products via slowing down the consecutive transformation reactions, however, which requires highly active catalysts to lower the reaction energy barriers. Besides the thermodynamically favored reactions, we find that some reactions could not occur even the reaction tempera-

Received: June 18, 2020

Revised: December 10, 2020

Accepted: December 14, 2020

Published: 16 December 2020

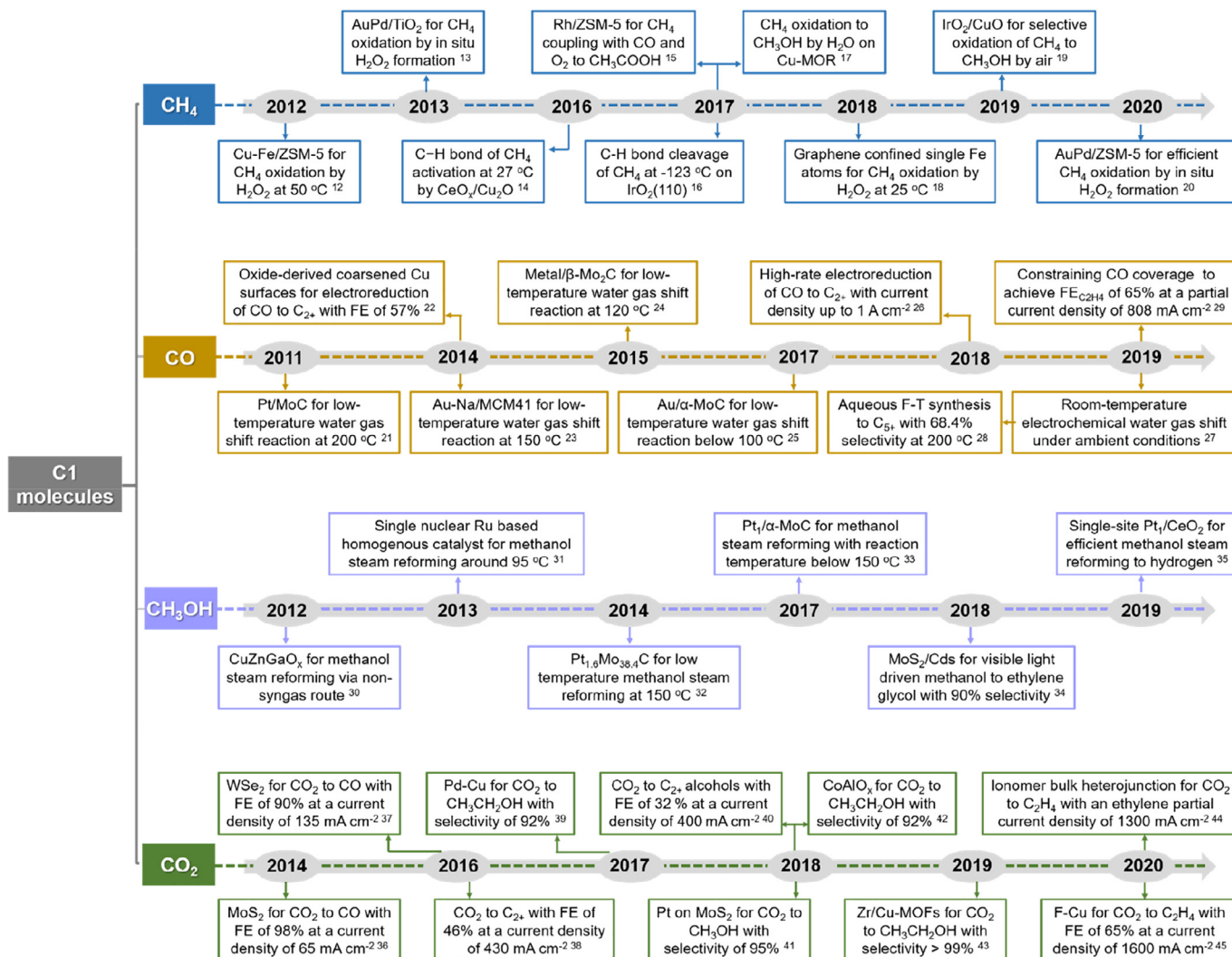


Table 1. Thermodynamical analysis of the representative reactions of the four C1 energy molecules conversion under ambient pressure. The blue and orange columns represent the thermodynamically favored reactions and unfavored ones according to the Gibbs free energy, respectively.

C1 molecules	Reaction Equations	Temperature (°C)	ΔH (kcal/mol)	ΔG (kcal/mol)
CH ₄	2CH ₄ (g) + O ₂ (g) = 2CH ₃ OH(l)	25	-78.440	-55.316
	2CH ₄ (g) + O ₂ (g) = 2CH ₃ OH(g)	200	-60.782	-49.217
	2CH ₄ (g) + O ₂ (g) + 2CO(g) = 2CH ₃ COOH(l)	25	-142.900	-96.329
	2CH ₄ (g) + O ₂ (g) + 2CO(g) = 2CH ₃ COOH(g)	200	-119.889	-73.024
	2CH ₄ (g) + O ₂ (g) = C ₂ H ₄ (g) + 2H ₂ O(l)	25	-88.446	-72.864
	2CH ₄ (g) + O ₂ (g) = C ₂ H ₄ (g) + 2H ₂ O(g)	200	-66.997	-69.675
	2CH ₄ (g) = C ₂ H ₄ (g) + 2H ₂ (g)	25	48.184	40.492
	2CH ₄ (g) = C ₂ H ₄ (g) + 2H ₂ (g)	200	49.403	35.670
	CH ₄ (g) + CO ₂ (g) = 2CO(g) + 2H ₂ (g)	25	59.040	40.759
	CH ₄ (g) + CO ₂ (g) = 2CO(g) + 2H ₂ (g)	200	60.523	29.629
	CH ₄ (g) + CO ₂ (g) = CH ₃ COOH(l)	25	-3.820	13.304
	CH ₄ (g) + CO ₂ (g) = CH ₃ COOH(g)	200	7.836	21.292
	CH ₄ (g) + H ₂ O(l) = CH ₃ OH(l) + H ₂ (g)	25	29.095	29.020
	CH ₄ (g) + H ₂ O(g) = CH ₃ OH(g) + H ₂ (g)	200	27.809	28.064
	CH ₄ (g) + H ₂ O(l) = CO(g) + 3H ₂ (g)	25	59.725	35.968
	CH ₄ (g) + H ₂ O(g) = CO(g) + 3H ₂ (g)	200	50.943	24.498
CO	CO(g) + H ₂ O(l) = CO ₂ (g) + H ₂ (g)	25	0.685	-4.790
	CO(g) + H ₂ O(g) = CO ₂ (g) + H ₂ (g)	200	-9.580	-5.131
	CO(g) + 2H ₂ (g) = CH ₃ OH(l)	25	-30.630	-6.949
	CO(g) + 2H ₂ (g) = CH ₃ OH(g)	200	-23.134	3.567
	2CO(g) + 4H ₂ (g) = C ₂ H ₆ O(l) + H ₂ O(l)	25	-81.675	-32.690
	2CO(g) + 4H ₂ (g) = C ₂ H ₆ O(g) + H ₂ O(g)	200	-63.613	-9.775
	2CO(g) + 4H ₂ (g) = C ₂ H ₄ (g) + 2H ₂ O(l)	25	-71.266	-31.445
	2CO(g) + 4H ₂ (g) = C ₂ H ₄ (g) + 2H ₂ O(g)	200	-52.483	-13.325
CH ₃ OH	CH ₃ OH(l) + H ₂ O(l) = CO ₂ (g) + 3H ₂ (g)	25	31.315	2.158
	CH ₃ OH(g) + H ₂ O(g) = CO ₂ (g) + 3H ₂ (g)	200	13.553	-8.698
	CH ₃ OH(l) = CO(g) + 2H ₂ (g)	25	30.630	6.949
	CH ₃ OH(g) = CO(g) + 2H ₂ (g)	200	23.134	-3.567
	2CH ₃ OH(l) = C ₂ H ₄ (g) + 2H ₂ O(l)	25	-10.006	-17.548
	2CH ₃ OH(g) = C ₂ H ₄ (g) + 2H ₂ O(g)	200	-6.215	-20.458
CO ₂	2CH ₃ OH(l) = C ₂ H ₆ O ₂ (l) + H ₂ (g)	25	5.370	2.218
	2CH ₃ OH(g) = C ₂ H ₆ O ₂ (g) + H ₂ (g)	200	4.625	5.502
	CO ₂ (g) + H ₂ (g) = CO(g) + H ₂ O(l)	25	-0.685	4.790
	CO ₂ (g) + H ₂ (g) = CO(g) + H ₂ O(g)	200	9.580	5.131
	CO ₂ (g) + 3H ₂ (g) = CH ₃ OH(l) + H ₂ O(l)	25	-31.315	-2.158
	CO ₂ (g) + 3H ₂ (g) = CH ₃ OH(g) + H ₂ O(g)	200	-13.553	8.698
	CO ₂ (g) + H ₂ (g) = HCOOH(l)	25	-7.000	8.353
	CO ₂ (g) + H ₂ (g) = HCOOH(g)	200	2.895	14.554
	CO ₂ (g) + 4H ₂ (g) = CH ₄ (g) + 2H ₂ O(l)	25	-60.410	-31.178
	CO ₂ (g) + 4H ₂ (g) = CH ₄ (g) + 2H ₂ O(g)	200	-41.362	-19.366
	2CO ₂ (g) + 6H ₂ (g) = C ₂ H ₆ O(l) + 3H ₂ O(l)	25	-83.045	-23.109
	2CO ₂ (g) + 6H ₂ (g) = C ₂ H ₆ O(g) + 3H ₂ O(g)	200	-44.453	0.487
	2CO ₂ (g) + 6H ₂ (g) = C ₂ H ₄ (g) + 4H ₂ O(l)	25	-72.636	-21.864
	2CO ₂ (g) + 6H ₂ (g) = C ₂ H ₄ (g) + 4H ₂ O(g)	200	-33.322	-3.063

ture increasing from 25 to 200 °C at normal pressures by thermal-catalysis. Electro-catalysis and photo-catalysis can circumvent the thermodynamic limitations to achieve the C1 energy molecules conversion, providing promising ways for C1 catalysis at low temperatures. For example, methane oxidation by water would not take place even the reaction temperature increasing from 25 to 1000 °C, but the electro-catalytic methane oxidation by water to methanol ($\text{CH}_4 + \text{H}_2\text{O} \rightarrow \text{CH}_3\text{OH} + 2\text{H}^+ + 2\text{e}^-$) can be driven at 0.58 V vs standard hydrogen electrode (SHE).¹⁰ In addition, electrochemical reduction of carbon dioxide or carbon monoxide to C₂₊ products has achieved a high current density approaching 1A cm⁻² at room temperature with high Faradic efficiency (FE), in which the energy efficiency can reach almost 40%.¹¹ Compared to the thermal-catalytic C1 energy molecules

conversion with higher reaction rate and conversion, electro-catalysis and photo-catalysis process can achieve a high selectivity for the desired products under lower reaction temperatures. The potential applied to the electrode can be adjusted accurately to control the electrons and protons from electrocatalysis process to boost C1 energy molecules conversion. The excitation of photons with energy of several eV from photocatalysis process can efficiently activate many inert C1 molecules at room temperature. Besides the different types of energy input, the catalysts for electro-catalysis and photo-catalysis should take the conductivity and semiconducting properties into consideration, respectively. Benefiting from the advanced technology for catalyst synthesis, reactor design, characterization techniques and mechanism understanding, catalytic conversion of C1 molecules



Scheme 1. The representative reaction processes and catalyst systems for C1 catalysis operated no higher than 200 °C in the last decade. (I) Methane conversion, (II) Carbon monoxide conversion, (III) Methanol conversion, (IV) Carbon dioxide conversion.

under mild conditions has made significant progress in the last decade.

Herein, we provide a comprehensive overview of C1 catalysis as a whole in this review from 2010 to 2020, which covers the catalytic conversion of four C1 molecules (methane, carbon monoxide, methanol and carbon dioxide). And we mainly focus on the mild conversion of C1 molecules with a reaction temperatures below 200 °C driven by thermal, electric or photonic energy in the last decade, which involves the latest developments on highly efficient catalyst systems and novel reaction processes (**Scheme 1**). Besides, the challenges faced and future prospects have also been discussed.

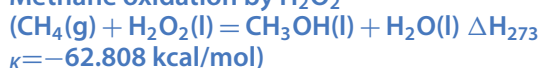
METHANE CONVERSION

Methane, as an abundant and relatively inexpensive feedstock, is expressed to play an important role in chemical industry and energy industry.^{46–48} But the high C-H bond strength ($\Delta H_{C-H} = 104$ kcal/mol) and perfect tetrahedral symmetry make the activation of methane challenging.^{49,50} In addition, the reactivity of target products (e.g., C1 oxygenates) is much higher than that of methane molecule, easily leading to con-

secutive conversions such as deep oxidation to carbon dioxide under the reaction conditions. Hence, orientable conversion of methane to high-value-added products is regarded as one of the most challenging tasks in C1 chemistry.^{51–55} Currently utilized commercial route for methane conversion is to go through an methane reforming step to produce syngas (a mixture of carbon monoxide and hydrogen), and the resulted syngas can be further transformed to olefins, aromatics as well as oxygenates by the well-established technology of FT synthesis.⁵³ Notably, methane reforming is strongly endothermic and requires high temperature above 600 °C.^{6,56} Compared to the indirect route involving the intermediate syngas production step, direct conversion of methane is potentially more economical and environmentally friendly.^{57,58} Methane pyrolysis, nonoxidative methane dehydroaromatization, and oxidative coupling methane are considered as potential avenues for the direct methane conversion.^{49,59,60} However, the required high temperature leads to a rapid deactivation of catalyst and low selectivity for desired products.^{46,61} Hence, it is highly desirable to develop direct methane conversion at low temperature. In the aid of hydrogen peroxide, oxygen, water, ozone, nitrous oxide, partial oxidation of methane into oxygenates become thermodynamically favorable

at low temperatures and thus draw much attention.^{13,17,19,62–65} In addition, the methane coupling with carbon monoxide and carbon dioxide was proposed to produce acetic acid with high atomic economy.^{15,66–70} Benefiting from the advanced technology for precise and controllable material synthesis and highly sensitive detection methods, methane conversion under mild conditions has achieved remarkable progress in many aspects. The representative systems for low-temperature methane conversion are summarized in **Table 2**.

Methane oxidation by H₂O₂



Hydrogen peroxide, as a clean and environmental-friendly oxidant, was usually employed to oxidize methane to produce C1 oxygenates for fundamental research. In these systems, the reaction temperature for methane direct oxidation can efficiently be decreased to 25–95 °C, and the main products are CH₃OH and HCOOH.

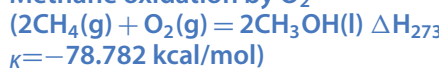
One representative kind of catalysts for methane conversion using hydrogen peroxide is the single metal sites or metal nanoparticles supported on ZSM-5 system. Hutchings et al.^{12,77} reported that an iron- and copper-containing zeolite (Cu promoted Fe-ZSM-5) is capable of selectively transforming methane to methanol with turnover frequencies (TOF) of over 14,000 h⁻¹ in an aqueous medium at 50 °C, and the binuclear iron species were identified as the active sites. Tao et al.⁷¹ reported that Pd₁O₄ single sites anchored on the internal surface of microporous silicate (Pd₁O₄@ZSM-5) is also active for transforming of methane to methanol with a selectivity of 78%–86% in aqueous solution at the reaction temperature of 50–95 °C.

In addition, the single metal atoms or metal nanoparticles supported on the oxides, such as Rh₁/ZrO₂,⁷² Rh-CeO₂,⁷³ Cr₁/TiO₂,⁷⁴ and AuPd/TiO₂,⁷⁵ catalysts were also demonstrated effective for methane conversion to methanol with hydrogen peroxide as the oxidant at the reaction temperature from 30 to 90 °C. The presence of both hydroxyl and methyl radicals during the reaction process indicated that methane oxidation proceeded via a radical pathway.

Besides, the two dimensional materials confined single metal atoms exhibit high activity for methane oxidation by hydrogen peroxide. Lately, Deng and Bao et al.¹⁸ reported graphene-confined single Fe atoms (FeN₄/GN) can be used as an efficient non-precious catalyst to convert methane to CH₃OH, CH₃OOH, HOCH₂OOH and HCOOH at room temperature (25 °C) (**Fig. 1a**). Combined with nuclear magnetic resonance (NMR) and time-of-flight mass spectrometry (TOF-MS), they for the first time identified HOCH₂OOH as a C1 oxygenate product from methane oxidation system. By optimizing the catalyst component, the selectivity of C1-oxygenated products can reach around 94%. To confirm the detected products indeed from methane oxidation, they conducted the control experiments using N₂, CH₄, and ¹³CH₄ as the reactant gas, and demonstrated that C1-oxygenated products came from the oxidation of ¹³CH₄ rather than from the catalyst itself. Combining with electron paramagnetic resonance experiments and density functional theory (DFT) calculations, they indicated that methane oxidation proceeded via a methyl radical mechanism and the unique O-FeN₄-O structure was proposed as the active site. To reveal the reaction process and mechanism, they developed a set of operando TOF-MS to track the evolution of liquid products in real time. The variation of products with reaction time indicated

that the generated methyl radical can combine with hydroxyl and hydroperoxide groups to form CH₃OH and CH₃OOH firstly, and the CH₃OH from CH₄ oxidation can be further converted to produce HOCH₂OOH and HCOOH (**Fig. 1b**). The DFT calculations demonstrated the moderate formation energy of O-FeN₄-O results in the unique activity for methane conversion at room temperature compared with other graphene-confined transition metals. Subsequently, Wu et al.⁷⁷ employed the surface digging effect to prepare the atomic Ni sites anchored on the N-doped carbon, which could also directly catalyze methane to methanol at a low temperature of 50 °C. Much work about methane oxidation by hydrogen peroxide has sprung up in recent years, but the yield of specific products remain still low, and the economic value of the products is not as high as that of hydrogen peroxide.

Methane oxidation by O₂



Hydrogen peroxide have been demonstrated to oxidize methane to methanol efficiently under mild conditions, but the relatively high cost largely hindered its application for an economically viable methane oxidation process. It is of great significance to achieve methane oxidation by molecular oxygen under mild conditions.

Based on the progress that methane can be converted on supported gold-palladium nanoparticles with hydrogen peroxide as an oxidant at 50 °C,⁷⁵ Hutchings et al.⁷⁹ for the first time showed that colloidal gold-palladium nanoparticles can oxidize methane to methanol with high selectivity (92%) in aqueous solution at 50 °C by oxygen in the presence of hydrogen peroxide (**Fig. 2**). The isotopically labeled oxygen indicated that 70% of the oxygen atoms in methanol came from molecular oxygen, and the reaction took place immediately without induction period when methane coming with hydrogen peroxide and oxygen. An increase of adding hydrogen peroxide resulted in the enhanced productivity of total products. For this system, hydrogen peroxide is indispensable for methane initial activation to produce methyl radicals. And once the methyl radicals are generated, which can react quickly with dissolved oxygen, leading to the incorporation of >70% oxygen into the methanol. This research shed light on the importance of hydroxyl radicals for H abstraction to form methyl radicals, and indicate that once methyl radicals can be generated, then the methane oxidation by molecular oxygen can be proceeded.

Further, employing hydrogen and oxygen to in-situ generated hydrogen peroxide for selective oxidation of methane were successfully achieved by gold-palladium alloy nanoparticles supported on TiO₂. The methanol selectivity can reach 67.8% at 50 °C with the hydrogen/oxygen/methane as the reaction gas in water.¹³ But the productivity is lower than that observed in methane oxidation by hydrogen peroxide directly, which may be due to the low concentration of in-situ generated hydrogen peroxide around the active sites. Given the key intermediate hydrogen peroxide generated relatively slowly from hydrogen and oxygen but readily diffusing away from the active sites, Xiao and Wang et al.²⁰ reported a novel strategy of a molecular fence to prevent hydrogen peroxide dilution and thereby keeping a high local concentration of hydrogen peroxide around the metal nanoparticles to promote methane oxidation (**Fig. 3a**). They indicated that hydrophobic zeolite modification can enhance methane oxidation to methanol by in situ generated hydrogen peroxide at 70 °C. The AuPd alloy nanoparticles were firstly

Table 2. Representative systems for low-temperature methane conversion.

Systems	Oxidants	Catalysts	Reaction Temperature (°C)	Products	Active sites	Mechanisms
One-step conversion	H₂O₂	Cu promoted Fe-ZSM-5	50	CH ₃ OH, HCOOH, CH ₃ OOH, CO ₂	Binuclear Fe species	•CH ₃ radical ¹²
		Pd ₁ O ₄ @ZSM-5	50–95	CH ₃ OH, HCOOH, CH ₃ OOH, CO ₂	Single Pd atoms	•CH ₃ radical ⁷¹
		Rh ₁ /ZrO ₂	70	CH ₃ OH, CH ₃ OOH, CO ₂	Single Rh atoms	M-C σ-bond ⁷²
		Rh-CeO ₂	50	CH ₃ OH, CH ₃ OOH, CO, CO ₂	Single Rh atoms	•CH ₃ radical ⁷³
		Cr ₁ /TiO ₂	50	CH ₃ OH, CH ₃ OOH, HOCH ₂ OOH, HCOOH, CO ₂	Single Cr atoms	•CH ₃ radical ⁷⁴
		AuPd/TiO ₂	30–90	CH ₃ OH, CH ₃ OOH, CO ₂	Supported AuPd nanoparticles	•CH ₃ radical ^{13,75,76}
		Graphene confined FeN ₄	25	CH ₃ OH, CH ₃ OOH, HOCH ₂ OOH, HCOOH, CO ₂	Single Fe atoms	•CH ₃ radical ¹⁸
		Atomic Ni sites anchored on the N-doped carbon MOF MIL-53 stabilized Fe active sites	50	CH ₃ OH, CH ₃ OOH	Single Ni atoms	•CH ₃ radical ⁷⁷
	O₂+H₂O₂	Colloidal gold-palladium nanoparticles	50	CH ₃ OH, CH ₃ OOH, HCOOH, CO ₂	Dimeric Fe sites	•CH ₃ radical ⁷⁸
		RuCu nanosheet	50	CH ₃ OH, CH ₃ OOH, CO ₂	AuPd colloids	•CH ₃ radical ⁷⁹
H₂+O₂		CuPdO ₂ /CuO	50	CH ₃ OH, CH ₃ OOH, CO, CO ₂	RuCu nanosheet	•CH ₃ radical ⁸⁰
		AuPd/TiO ₂	2–70	CH ₃ OH, CH ₃ OOH, CO ₂	Interfaces between CuPdO ₂ and CuO	•CH ₃ radical ⁸¹
		AuPd@ZSM-5	70	CH ₃ OH, CH ₃ OOH, HCOOH	AuPd nanoparticles	•CH ₃ radical ¹³
					AuPd nanoparticles	•CH ₃ radical ²⁰
O₂		IrO ₂ (110)	–123 (under ultrahigh vacuum)	CO, CO ₂ , H ₂ O	IrO ₂ (110)	M-C σ-bond ¹⁶
		IrO ₂ /CuO	150	CH ₃ OH, CH ₃ CHO, CH ₃ CH ₂ OH	IrO ₂	M-C σ-bond ¹⁹
		CeO ₂ -Cu ₂ O	177	CH ₃ OH, CO, CO ₂	CeO ₂ -Cu ₂ O/Cu(111) interface	M-C σ-bond ^{14,82}
		Ni-CeO ₂	177	CH ₃ OH, CO, CO ₂	Ni-CeO ₂ surface	M-C σ-bond ⁸³
Step-wise conversion*	H₂O	Cu-MOR	200	CH ₃ OH	Dicopper Cu (II) sites	M-C σ-bond ¹⁷
	O₂	Cu-oxo clusters stabilized in MOF NU-1000	150	CH ₃ OH, CH ₃ OCH ₃ , CO ₂	Trimeric Cu hydroxide	•CH ₃ radical ⁸⁴

(continued on next page)

Table 2 (continued)

Systems	Oxidants	Catalysts	Reaction Temperature (°C)	Products	Active sites	Mechanisms
Coupling with CO/CO ₂	O ₂ /N ₂ O	Metal (Fe, Cu, Co, Ni et al.)-exchanged zeolites (MOR, ZSM-5, SSZ-13, SAPO-34 et al.)	125–200	CH ₃ OH	Monomeric, dimeric, and multimeric metal species	•CH ₃ radical or M-C σ-bond ^{85,86}
	CO+O ₂	Rh-ZSM-5	150	CH ₃ OH, CH ₃ COOH, CO ₂	Single Rh atoms	M-C σ-bond ^{15,70}
	CO ₂	Zn/H-ZSM-5	250	CH ₃ COOH	Zinc sites confined in ZSM-5	M-C σ-bond ⁶⁷
		Metal supported on Al ₂ O ₃ (Metal=Cu, Pt and Au)	30	CH ₃ OH, HCHO, CH ₃ CH ₂ OH, CH ₃ COOH, Acetone	Metal surface	•CH ₃ radical ⁶⁸

* For step-wise conversion, the catalysts were firstly activated by an oxidant at 250–500 °C.

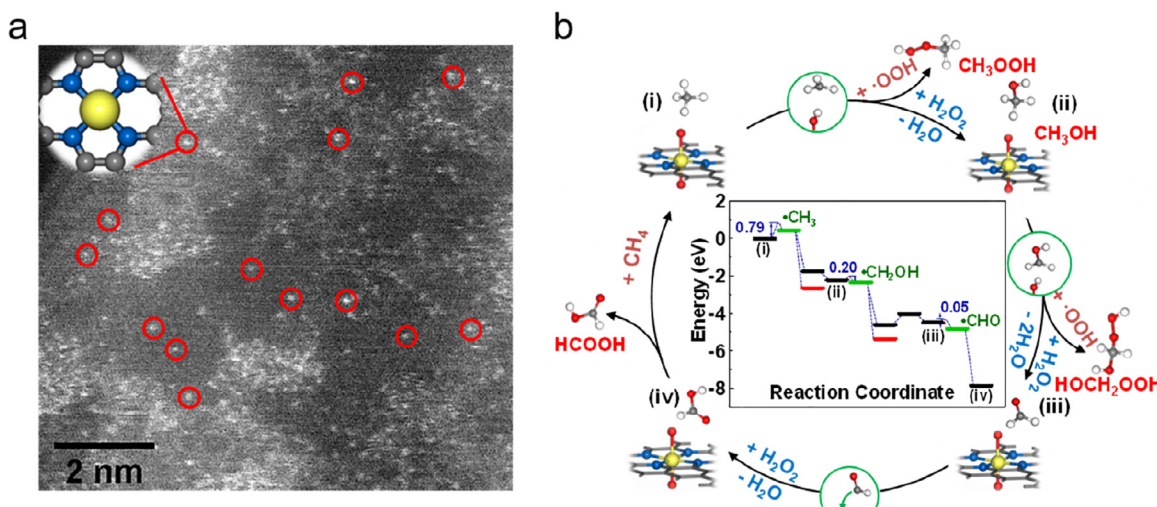


Fig. 1. Graphene-confined single Fe atoms for methane oxidation by hydrogen peroxide. (a) An high-angle annular dark-field scanning transmission electron microscopy (HAADF-STEM) image of graphene-confined single Fe atoms. (e) Reaction pathway of methane conversion to CH₃OH, CH₃OOH, HOCH₂OOH, and HCOOH. Reproduced with permission.¹⁸ Copyright 2018, Elsevier.

fixed within aluminosilicate zeolite crystals, and further treated by organosilanes to enhance the hydrophobic property of the external surface of the zeolite (**Fig. 3b and c**). Via the processing, the diffusion of hydrogen, oxygen, and methane to the catalyst active sites was significantly promoted, while the generated hydrogen peroxide was localized around the catalyst. Thus the high local concentration of hydrogen peroxide in a zeolite nanoreactor can considerably enhance efficient oxidation of methane at 17.3% conversion and a 92% methanol selectivity (**Fig. 3d**). They compared this effect as a hydrophobic sheath to hinder the diffusion of hydrogen peroxide from the encapsulated AuPd nanoparticles, enhancing the local concentration of hydrogen peroxide around the catalyst to promote methane oxidation. The new concept of molecular-fence opens up new horizons for efficient methane conversion under mild conditions.

Besides the strategy of using oxygen and hydrogen to in-situ produce hydrogen peroxide to oxidize methane, the direct methane oxidation only by molecular oxygen was also proposed. Surface science study by Liang et al.¹⁶ demonstrated that methane can be adsorbed at the coordinatively unsaturated Ir center in IrO₂(110) to form the σ complex under ultrahigh-vacuum conditions, leading to a break of the carbon-hydrogen bonds at temperatures as low as –123 °C to form Ir-CH₃ species. With an increase of the reaction temperature, the Ir-CH₃ species can react with surface oxygen to produce carbon dioxide, carbon monoxide, et al. (**Fig. 4a and b**). These results indicated the IrO₂ possessed good activity towards C-H bond cleavage of methane, which was in accordance with the theoretical prediction that IrO₂ exhibited the best activity towards methane activation among a series of catalysts, including MOR zeolites, MOFs and

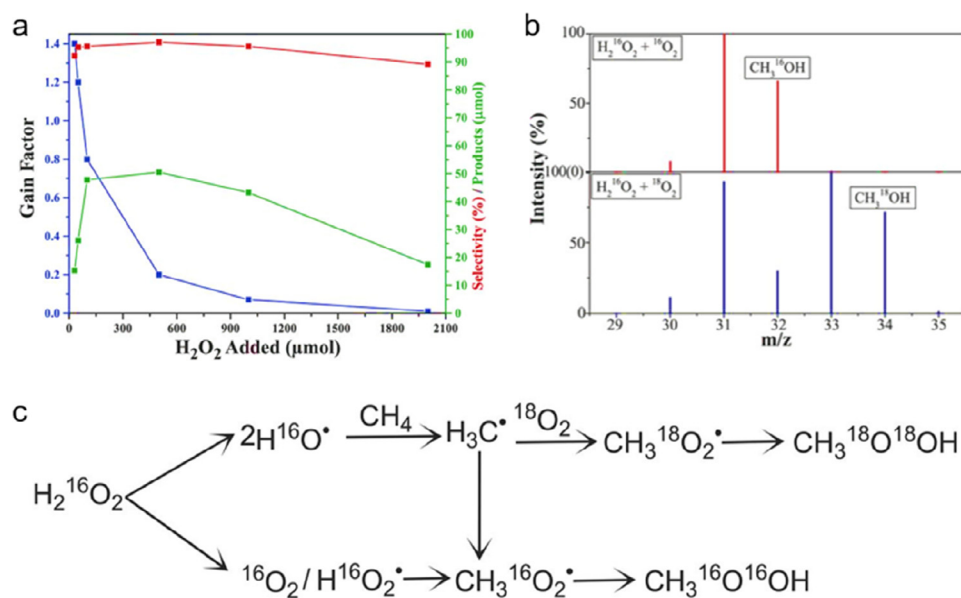


Fig. 2. The activity and reaction mechanism of methane oxidation with oxygen under mild condition by aqueous Au-Pd colloids. (a) The effect of different amounts of hydrogen peroxide on the selectivity and total amount of products. (b) Gas chromatography-mass spectrometry of methanol formed during methane oxidation by isotopically labeled oxygen. (c) Proposed reaction scheme for methane oxidation in the presence of H_2O_2 and molecular O_2 . Reproduced with permission.⁷⁹ Copyright 2017, AAAS.

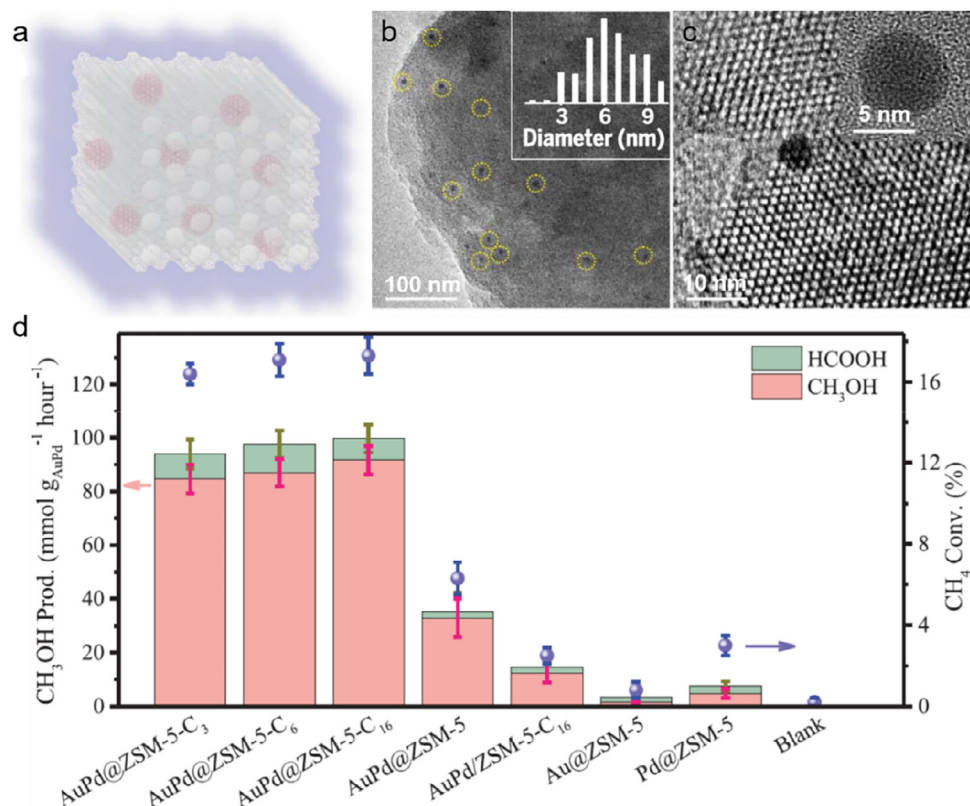


Fig. 3. The structure and activity for methane oxidation of AuPd@ZSM-5-C₁₆ catalysts. (a-c) Models and TEM images of AuPd@ZSM-5-C₁₆. (d) The productivity of methanol and methane conversion by a series of AuPd based catalysts at 70 °C. Reproduced with permission.²⁰ Copyright 2020, AAAS.

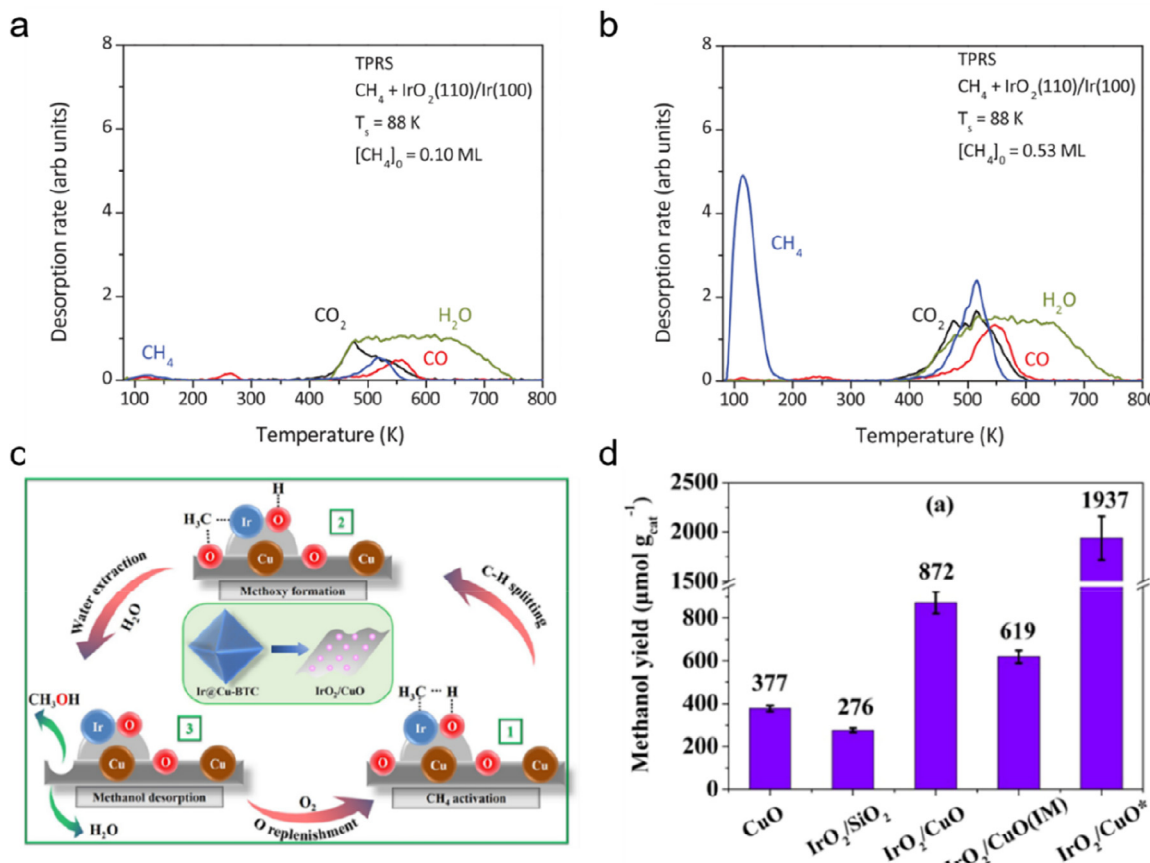


Fig. 4. IrO₂-based catalysts for methane oxidation by oxygen. (a-b) Temperature-programmed reaction spectroscopy of CH₄, H₂O, CO, and CO₂ obtained after adsorbing CH₄ on IrO₂(110) at 88 K with different CH₄ coverages. Reproduced with permission.¹⁶ Copyright 2017, AAAS. (c) The possible reaction pathway of methane conversion on IrO₂/CuO catalyst to methanol. (d) Methanol yield over different catalysts. The reactions were performed with a feedstock of 3 bar CH₄ and 1 bar air, except for IrO₂/CuO*, which was carried out with a feedstock of 20 bar CH₄ and 1 bar air. Reproduced with permission.¹⁹ Copyright 2019, ACS.

other oxides.⁸⁷ Besides, Rui et al.¹⁹ synthesized a highly mixed hybrid IrO₂/CuO catalyst (Fig. 4c), which can catalyze methane oxidation by air to methanol with a yield of 872 $\mu\text{mol g}_{\text{cat}}^{-1}$ in water at 150 °C for 3 h (Fig. 4d). The conversion of methane can reach about 2.5% with a methanol selectivity of 95%. In addition, the catalyst exhibited high stability without obvious activity loss even after 5 cycles test. The reaction mechanism may be that IrO₂ component can promote C–H bond cleavage through Ir–C σ bond to form Ir–CH₃ species, which can further react with oxygen attached at the neighboring Cu atoms to form methoxyl group. The presence of water can facilitate methanol production. The synergy between IrO₂ and CuO enhance the methane oxidation by molecular oxygen, which provides a new route to convert methane via multi-component catalysts. Latest research by Liu, Rodriguez and Senanayake et al.^{14,82} found that water served as a promoter in the process of methane oxidation to methanol by oxygen. Based on the ambient-pressure x-ray photoelectron spectroscopy, they indicated that CeO₂/Cu₂O/Cu(111) surface was able to activate methane at room temperature, producing C, CH_x fragments and CO_x species. The addition of water into the system can change the reaction network on the catalyst surface, yielding only adsorbed CH_x fragments. Once the temperature increasing to 177 °C, the adsorbed CH_x fragments can react with OH from water dissociation to yield methanol. Noting that

water participated during the methane oxidation to methanol as the actual O-provider and hindered oxygen activation by blocking the active Ce sites at the CeO₂–CuO interface. And the oxygen dominantly promoted to re-oxidize CeO_x. Another system also exhibited the similar results that Ni/CeO₂(111) can activate methane at 27 °C and then the introduction of water can inhibit the complete dissociation of methane to produce CO_x and promote a direct catalytic cycle for the generation of methanol at 177 °C.⁸³ These results unveil the significant role of water in the methane oxidation to methanol by oxygen, and provides a new route to tune the products selectivity for methane conversion.

The direct methane oxidation by molecular oxygen can also be achieved by a stepwise process over metal-exchanged zeolites, involving high-temperature activation, low temperature reaction, and extraction by water. The metal-exchanged zeolites (such as Cu-MOR, Fe-ZSM-5, Cu-ZSM-5, Cu-SSZ-13 and Cu-SAPO-34) were first activated in oxygen at 450 °C, and then cooled to 125–200 °C and reacts with methane in the absence of oxygen, which can inhibit the overoxidation of methanol. Subsequently methanol can be extracted by water at 135–200 °C. The methanol selectivity can reach over 70%. The repeated heating and cooling procedure largely hindered the applicability of this technique. More details about the stepped methane conversion can be found in the relevant reviews.^{65,85}

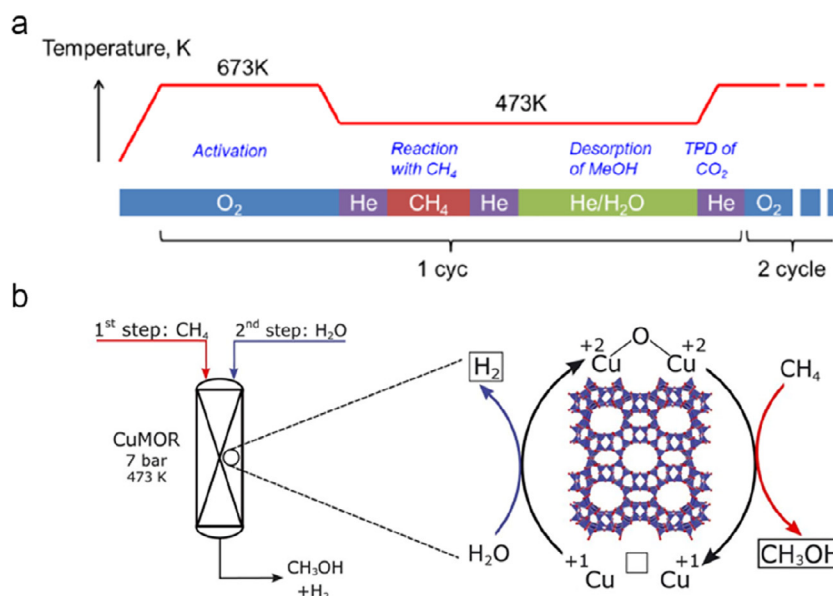
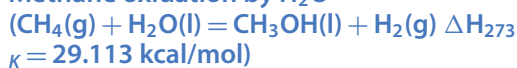


Fig. 5. The stepwise conversion of methane by water. (a) The reaction process for stepwise conversion of methane. (b) The possible reaction pathway of methane oxidation by water. Reproduced with permission.¹⁷ Copyright 2017, AAAS.

Methane oxidation by H₂O



Water was rarely used for methane oxidation in thermal-catalysis due to its weak oxidation property. Recently, a significant breakthrough by Bokhoven et al.¹⁷ demonstrated a watery route for methane oxidation with a methanol productivity of 0.202 mol per mole Cu at an ultrahigh selectivity of 97% over a copper-containing zeolite. They reported that water molecules not only served as a cheap and abundant source of oxygen to partially oxidize methane to methanol, but also promote the desorption of the methanol from the active sites. The stepwise reaction proceeded under the following steps: firstly, the catalyst was activated in helium or oxygen at 400 °C, followed by a consecutive exposure to methane and then water at 200 °C, and finally the methanol was desorbed from the catalyst surface (Fig. 5). The introduction of water in the stepwise process led to an increase of the mass spectral signal of hydrogen, water and methanol, indicating the oxygen atoms from water splitting were inserted into the C–H bond of methane to produce methanol, which was further verified by the isotopic labeling experiments. In addition, the time-resolved *in situ* Fourier transform infrared spectra indicated that the C–H bond cleavage coincided with methoxy and Brønsted acid site formation. Combined with the DFT calculations, they identified the Cu^{II} oxide acting as the active centers and the Cu^I can be reoxidized by water. These results indicated that water can act as an oxidant for methane oxidation in place of molecular oxygen. While some debates on the thermodynamic feasibility, thermal cycling, and the role of water are still pending.^{88,89}

Methane coupling with carbon monoxide



Besides the direct oxidation of methane to C1 oxygenates under mild conditions, the coupling of methane with other C1

molecules to form high-value-added C₂₊ products is another appealing research area. The traditional and indirect way to achieve the methane to acetic acid involves a multi-step process, including the methane steam reforming, methanol synthesis, and subsequent methanol carbonylation on homogeneous catalysts.^{69,90,91} The direct carbonylation of methane to acetic acid is of great significance but remains a great challenge.

Flytzani-Stephanopoulos et al.¹⁸ reported the mononuclear rhodium species, anchored on a zeolite (Rh-ZSM-5) can achieve the direct coupling of methane with oxygen and carbon monoxide to acetic acid at 150 °C with a yield approaching 22,000 μmol g_{cat}⁻¹ and a selectivity of 60% (Fig. 6). In this process, the main products were acetic acid and methanol, but they were produced through independent reaction pathways. The cleavage of C–H bond of methane on the active Rh site led to the formation of Rh-CH₃ species, which can be further inserted by an oxygen atom or carbon monoxide to produce Rh-O-CH₃ or Rh-CO-CH₃ species. After hydrolysis, the methanol and acetic acid can be produced, respectively. The ¹³CO isotope-labeling experiments further evidenced the methyl in methanol and acetic acid is derived solely from methane, not from carbon monoxide.

Meanwhile, Tao et al.⁷⁰ reported the transformation of methane to acetic acid and methanol through coupling of methane, carbon monoxide and oxygen on single-site Rh₁O₅ anchored in microporous aluminosilicates. The yield of acetic acid can reach approximately 80,000 μmol g_{cat}⁻¹ at 150 °C with a selectivity approaching 70%. The isotope experiments indicated that the methyl group of acetic acid came from methane and the carbonyl group from carbon monoxide (Fig. 7), which was in accordance with the results by Flytzani-Stephanopoulos et al. A possible reaction pathway was proposed based on the DFT calculations: firstly, the cleavage of C–H bond of methane occurred on the active site Rh₁O₅ to form a methyl and hydroxyl adsorbed on the Rh site. Then, a carbon monoxide can insert into the Rh–O bond of Rh–O–H, forming a COOH adsorbed on Rh site, which can couple with the adsorbed methyl to form acetic acid. Further desorption yielded the first acetic acid

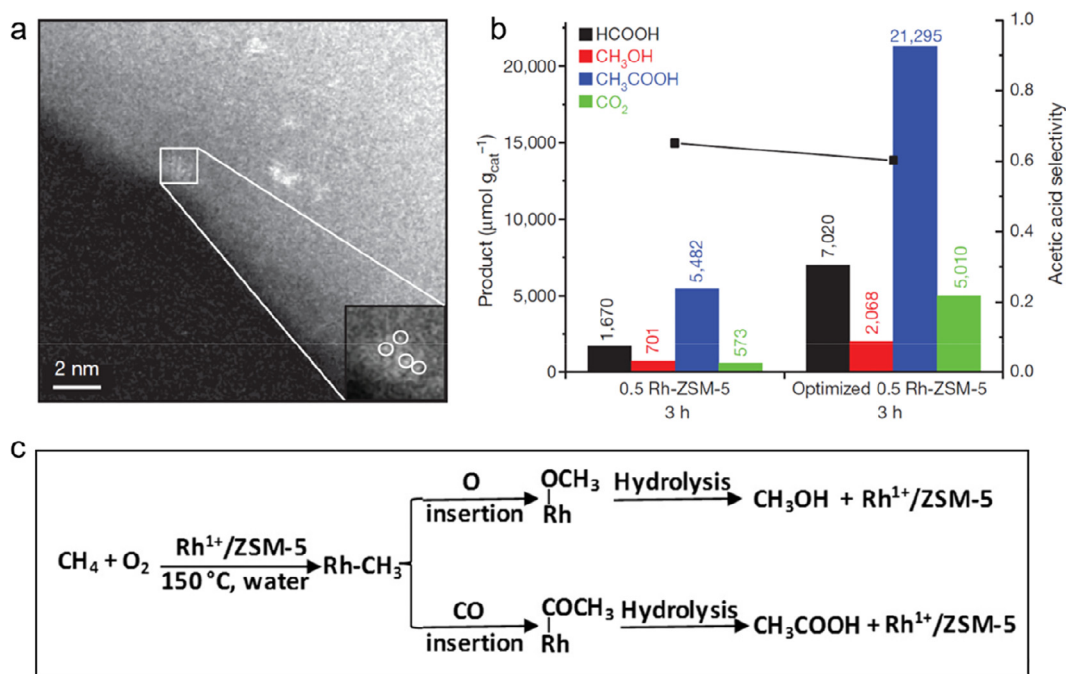


Fig. 6. The structure and activity of methane coupling with carbon monoxide and oxygen on Rh-ZSM-5 catalyst. (a) HAADF-STEM image of Rh-ZSM-5 catalyst. (b) The amount of different products and selectivity of acetic acid. (c) Possible reaction pathways of the catalytic conversion of methane to methanol and acetic acid on Rh-ZSM-5. Reproduced with permission.¹⁵ Copyright 2017, Springer Nature.

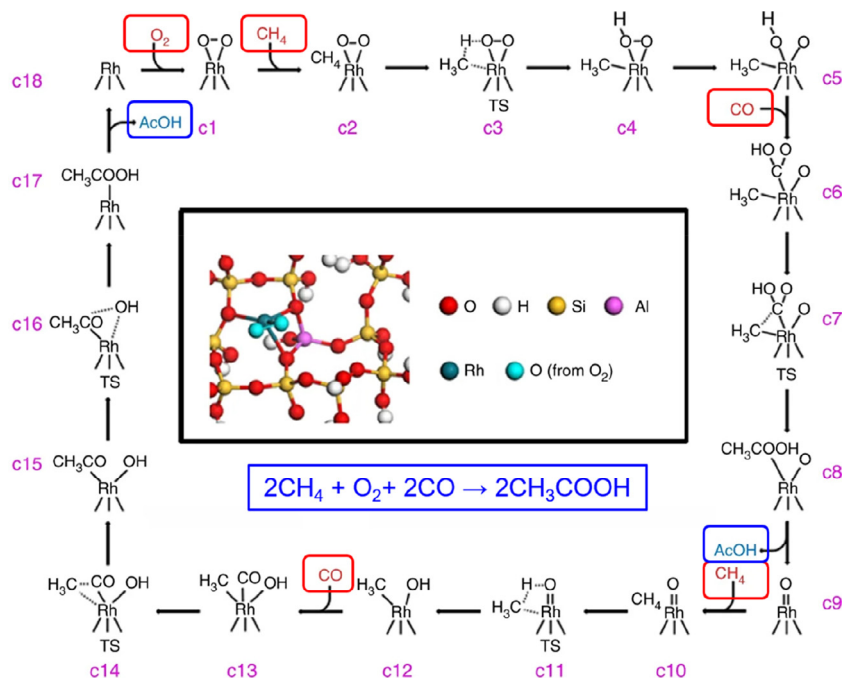


Fig. 7. Reaction mechanism and pathway of methane oxidation by carbon monoxide and oxygen on Rh_1O_5 -ZSM-5 catalyst. Reproduced with permission.⁷⁰ Copyright 2018, Springer Nature..

molecule. The remaining Rh-O oxo group can activate another methane to produce methyl and a hydroxyl group adsorbed on the Rh site. And the second carbon monoxide can insert into the Rh-CH₃ bond to form the acetyl group, which can couple with the hydroxyl group to form the second acetic acid. Although the direct conversion of methane by coupling with

carbon monoxide and oxygen can produce acetic acid under mild conditions, the low conversion of methane and efficiency of carbon monoxide make the process far away from the industrial application. Development of efficient catalysts to enhance the methane conversion and inhibit the carbon dioxide production deserves much attention.

Methane coupling with carbon dioxide

$$\kappa = -4.128 \text{ kcal/mol}$$

Methane and carbon dioxide are not only greenhouse gasses, but also the representative C1 building blocks. The co-conversion of them into high-value-added products plays an important role in the chemical industry. While the inherent stability of both methane and carbon dioxide render their conversion challenging. The methane steam reforming with carbon dioxide usually requires high reaction temperature (above 700 °C) to overcome the high reaction energy barrier. The direct co-conversion of methane and carbon dioxide to C₂₊ products, such as acetic acid, is an attractive process due to the high atom economy, but much efforts should be devoted to exploiting efficient catalysts and process operated under mild reaction conditions.

Previously, Huang et al.⁶⁶ reported the first example of direct conversion of methane and carbon dioxide to oxygenates via a two-step reaction process under heterogeneous conditions. Firstly, the cleavage of C–H bond of methane occurred on the catalyst surface to generate the CH_x species, further introduction of carbon dioxide led to the reaction between CH_x and carbon dioxide to produce acetic acid with a maximum selectivity of 28% at 250 °C. Beside, Wang et al.⁶⁷ employed the solid-state NMR to study the co-conversion of methane and carbon dioxide to acetic acid at 250 °C on a bifunctional zeolite catalyst (Zn/H-ZSM-5). Isotope ¹³C-labeling experiments indicated that the methyl group of acetic acid came from methane and the carbonyl group from carbon dioxide. The proposed mechanism about the co-conversion of methane and carbon dioxide on Zn/H-ZSM-5 zeolite was shown in Fig. 8. Specifically, methane activation was on the zinc site to form the zinc methyl species (-Zn-CH₃) and a Brønsted proton, while carbon dioxide activation resulted in the formation of surface carbonate species. And then the insertion of carbon dioxide into zinc methyl species can produce surface acetate species (-Zn-OOCCH₃), which can further abstract the Brønsted proton to release acetic acid as products. This research provides insights into the significant role of zinc and Brønsted site for methane coupling with carbon dioxide into chemicals over the bifunctional Zn/H-ZSM-5 catalyst by a spectroscopic investigation. Exploitation on the efficient catalytic systems for practical co-conversion of methane and carbon dioxide under mild conditions requires further study.

Besides the traditional thermal method for methane coupling with carbon dioxide, Tu et al.⁶⁸ developed a dielectric barrier discharge reactor to overcome the thermodynamic barrier for the co-conversion of methane and carbon dioxide at 30 °C and atmospheric pressure (Fig. 9). The one-step process can enhance the selectivity of acetic acid approaching 40 %. The production of acetic acid may go through two possible reaction pathways: one is the CO derived from carbon dioxide dissociation can react with a CH₃ radicals derived from the methane dissociation to form an acetyl radical (CH₃CO), followed by recombination with OH to produce acetic acid; the other is the CH₃ radicals derived from methane dissociation can directly combined with carboxyl radicals (COOH) to form acetic acid. The plasma-driven catalysis render the direct co-conversion of methane and carbon dioxide into acetic acid at low temperature (30 °C), which stimulates the non-thermal plasmas for the direct transformation of chemically inert molecules into useful chemicals.

Besides, the photo-oxidation of methane is a fascinating approach in the presence of oxygen or water. The photons with energy of several eV can excite the oxygen or water to

form the reactive and electrophilic oxygen species, which can further initiate the dissociation C–H bond of methane, enabling the methane conversion at room temperature. Kazansky et al.⁹² for the first time realized the photochemically oxidation of methane by TiO₂ based semiconductor photocatalyst under UV irradiation. Due to the oxygen species generated from light excitation possessing high reactivity, the products were mainly carbon dioxide or carbon monoxide. Recent study by Tang and Ma et al.⁹³ reported iron oxide species dispersed on TiO₂ could transform methane to methanol with H₂O₂ as oxidant under ambient conditions and moderate light irradiation (close to one Sun), in which the methane conversion can achieve about 15% with an alcohol selectivity over 97%. Lately, Ye et al.⁹⁴ reported Au/ZnO can realize the methane oxidation to methanol and formaldehyde with a selectivity of 95% by molecular oxygen under solar light at room temperature. The efficient C–H bond activation to methyl radical and controllable activation of oxygen to hydroperoxyl radical were identified as the significant precursors intermediates in the direct photooxidation of methane to liquid oxygenates.

Except for the thermal- or photo-catalytic methods for partial methane oxidation by oxygen under mild conditions, electrocatalytic partial oxidation of methane can be achieved at ambient temperatures on the surface of an electrode, either directly by its reaction with a surface oxygen site (O^{*}) or indirectly via its oxidation by free radicals generated at the electrode/electrolyte interface. The electrocatalytic process can precisely control the rate of generation of these oxidative species by changing the applied potential and is a promising approach to control kinetics and product selectivity for methane oxidation. Although some advances have been achieved, the low current density and energy efficiency still struggle to meet the commercial requirement,^{95,96} which was discussed in the recent reviews.

■ CARBON MONOXIDE CONVERSION

Carbon monoxide, as an important platform molecule in C1 catalysis, which are extensively studied in the commercial catalytic processes of FT synthesis and WGS reaction.^{97–99}

Carbon monoxide reduction

$$\kappa = -71.378 \text{ kcal/mol}$$

FT synthesis, with a history of more than 90 years, is a classic route for the transformation of carbon monoxide and hydrogen into C₂₊ hydrocarbons, e.g., lower olefins, gasoline, jet fuel or diesel, which received renewed interest in recent years because of the shrinking oil resources and the growing environmental concerns. Given the process involving the dissociation of carbon monoxide and hydrogen to form surface CH_x species and C–C bond formation via coupling of CH_x species on catalyst surface without confinement,^{100,101} the selectivity control is one of the greatest challenge for FT synthesis.^{102–104} According to the most widely accepted Anderson-Schulz-Flory (ASF) distribution model, the maximum selectivities of C₂–C₄ (including olefins and paraffins), C₅–C₁₁ (gasoline), C₈–C₁₆ (jet fuel) and C₁₀–C₂₀ (diesel) hydrocarbons are evaluated to be 58%, 48%, 41% and 40%, respectively. Much attention has been paid to the Fe, Co and Ru based catalysts due to their balanced abilities for carbon monoxide dissociation, hydrogenation and chain growth in FT synthesis.^{105–108} Among them, Ru is the most active metal with lower reaction temperature and good selectivity for long-chain hydrocarbons. By contrast, Fe based catalysts are appropriate

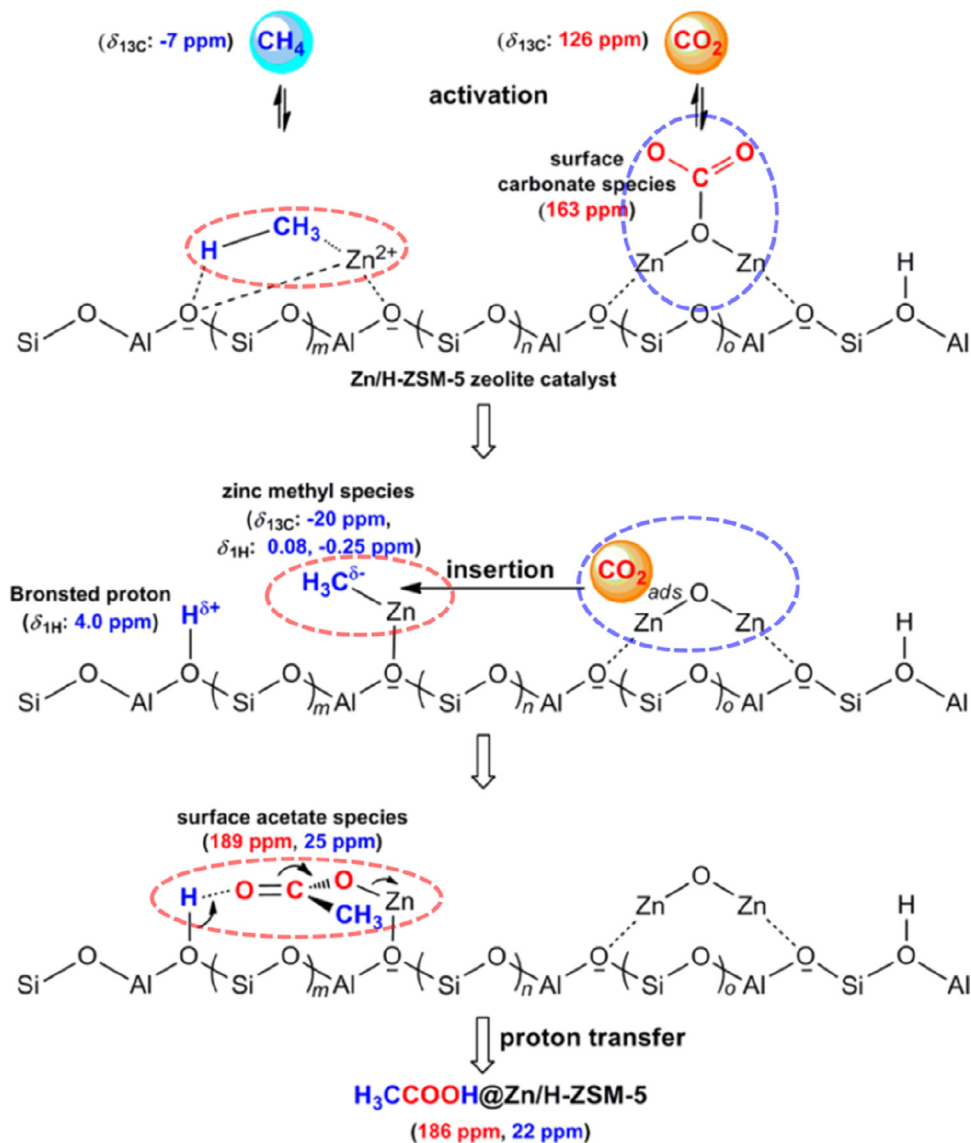


Fig. 8. Possible reaction mechanism for methane coupling with carbon dioxide into acetic acid on the bifunctional Zn/H-ZSM-5 zeolite. Reproduced with permission.⁶⁷ Copyright 2013, American Chemical Society.

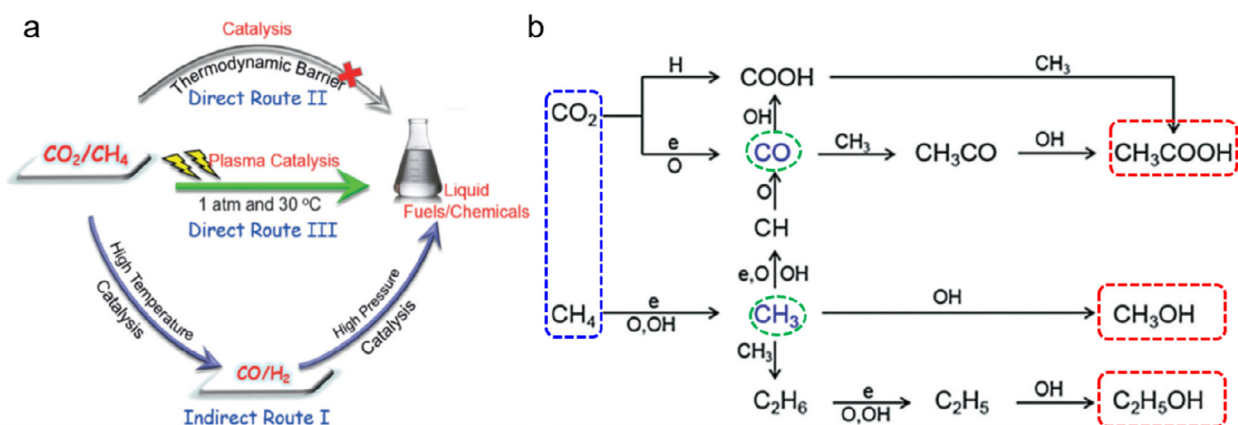


Fig. 9. One-step co-conversion of methane and carbon dioxide by dielectric barrier discharge reactor. (a) Comparison of direct and indirect processes for conversion of methane and carbon dioxide. (b) Scheme of the possible reaction pathways for the formation of acetic acid. Reproduced with permission.⁶⁸ Copyright 2017, Wiley-VCH.

Table 3. Catalytic performance of aqueous-phase CO conversion with different catalysts.²⁸

Catalyst	Reactant	Temperature (°C)	FTS activity (mol _{CH2-} mol _{metal} ⁻¹ h ⁻¹)	Selectivity (%)
				CH ₄ C ₂ –C ₄ C ₅₊
Pt-Mo ₂ C/C	CO	150	–	– – –
Pt-Mo ₂ C/C	CO	200	–	– – –
Pt-Mo ₂ C/C	CO:H ₂ =1:2	150	–	– – –
Ru/C	CO:H ₂ =1:2	200	9.1	24.1 20.9 55.0
RuPt-Mo ₂ C/C (Ru/Pt=2.5,Ru/Mo=0.3)	CO	200	2.2	23.6 29.7 46.7
Pt-Mo ₂ C/C+ Ru/C (Ru/Pt=2.5, Ru/Mo=0.3)	CO	200	8.7	11.4 20.2 68.4

for the production of linear alkanes and oxygenates, which can be used over a wider range of temperature and H₂/CO ratios without generating a large amount of CH₄.¹⁰⁹ Co based catalyst are more sensitive to reaction temperature and H₂/CO ratio, and exhibit higher activity and selectivity for long-chain alkane, as well as low CH₄ and CO₂ selectivity.¹¹⁰ In addition, Fe and Co based catalysts are more suitable for large-scale industrial applications due to their low cost. Modulation of the catalyst compositions and reaction conditions can change the product distribution, but the transformation of syngas to a specific range of useful C₂₊ hydrocarbons still remains a great challenge.

In order to attain a specific range of products with high selectivity, innovative reaction routes beyond FT synthesis are dedicated to breaking the ASF distribution. Recently, Bao and Pan group has made a significant breakthrough by designing a novel oxide-zeolite (OX-ZEO) process involves the activation of CO and C–C coupling proceed separately on partially reduced oxide (ZnCrO_x) surface and in mesoporous SAPO zeolite pores by a composite catalyst.¹¹¹ The C₂–C₄ olefin selectivity reaches as high as 80% at a CO conversion of 17% at 400 °C. This C₂–C₄ olefins selectivity markedly surpasses the optimized FT to olefin catalyst based Fe and Co (~60%), and breaks the limitation predicted by the ASF distribution.¹¹² Soon afterwards, Wang group developed a tandem route that couples methanol-synthesis and methanol-to-olefins reactions by a bifunctional catalyst ZnO-ZrO₂/SAPO-34, which can convert syngas to lower olefins directly with a selectivity of 74% at a 11% CO conversion at 400 °C.¹¹³ The Zr-Zn binary oxide was proposed to facilitate the activation of CO to methanol or methoxide, and the SAPO-34 worked for the selective C–C coupling. Controlling the hydrogenation ability of the bifunctional catalyst can significantly enhance the C₂–C₄ olefins selectivity.

Besides, aqueous-phase FT synthesis process that couples WGS and FT synthesis was proposed to transform syngas to liquid fuels under mild conditions,²⁸ through which the selectivity towards C₅₊ hydrocarbons approached 68.4% at 200 °C by the tandem catalyst Pt-Mo₂C/C+Ru/C (**Table 3**). The in-situ generated hydrogen from water can directly react with carbon monoxide to produce liquid fuels in the aid of the water solvent, which presents a promising energy-efficient catalytic route for carbon monoxide resource utilization under mild conditions.

Typical reaction conditions: 60 mL water, 3.0 MPa gas, reaction times were 12 h (150 °C) and 7 h (200 °C), respectively. The metal ratio in the catalysts was molar ratio.

Except for the traditional thermal catalytic process, much progress has been made in the field of light driven FT synthesis,¹¹⁴ but the catalytic activities are still not sufficient to demand serious consideration in practical applications. A recent review has discussed the research in detail,¹¹⁵ which will be not dealt with here.

Electroreduction of carbon monoxide is an emerging platform with great promise for effective high-value-added C₂₊ production, including ethylene, ethanol, acetic acid and n-propanol.^{11,29,116} Compared to the traditional FT synthesis route, the electroreduction pathway using electric-potential as the driving force is a promising approach of circumventing the harsh conditions (high reaction temperature and high pressure), being of great economic and environmental interest, which can reduce carbon monoxide to hydrocarbons by water under mild conditions without carbon dioxide emission.^{117–119} In addition, the lower reaction temperature can prohibit the catalyst prone to deactivation caused by particle sintering or coke deposition.^{120,121} Cu is the only known elemental electrocatalyst possessing good activity for carbon monoxide electroreduction to C₂₊ products.^{22,122–125} Staged over several years, the current density has increased from less than 1 mA cm⁻² to over 1 A cm⁻², which was mainly caused by the upgradation of the electrolytic cell from H-type reactor to a flow-cell. The gas-diffusion electrode in the flow-cell enables carbon monoxide to flow in a gas phase apart from any liquid catholyte.^{26,126,127} Much work was dedicated to reducing carbon monoxide to C₂₊ products with high faraday efficiency at high rates, which was discussed in detail in the following parts.

H-type (batch-type reactor)

Research on the electrochemical reduction of carbon monoxide is a young field although the hydrogenation of carbon monoxide in the gas phase thermo-catalytically has been widely studied. Before 1987, electroreduction of carbon monoxide did not proceed effectively with the cathodic partial current density for electroreduction of carbon monoxide not exceeding 5 × 10⁻² mA cm⁻².^{117,118,128,129} In 1987, Hori et al.¹²⁷ reported that polycrystalline Cu can electro-reduce carbon monoxide to hydrocarbons with a current density of 1.1 mA cm⁻² and a Faradaic efficiency approaching 23% in 0.1 M KOH at -0.7 V vs. reversible hydrogen electrode (RHE), which opens up a new view of carbon monoxide electroreduction in aqueous medium. But the low current density and Faradaic efficiency make it far away from applicable implementation. The discovery of advanced catalytic sites and approach for overcoming the poor mass transport of carbon monoxide is indeed necessary for enhancement of the activity and selectivity. With the improved overall product detection sensitivity, Wang et al.¹³⁰ reported that polycrystalline Cu could reduce carbon monoxide to oxygenates and hydrocarbons (ethylene and ethanol as the major products) with Faradaic efficiencies up to 65% at a low overpotential of -0.63 V vs. RHE. In 2014, Li et al.²² reported an oxide-derived coarsened Cu surfaces can reduce carbon monoxide to produce multi-carbon oxygenates (ethanol, acetate and n-propanol) with up to 57% Faraday efficiency at modest potentials (-0.25 to

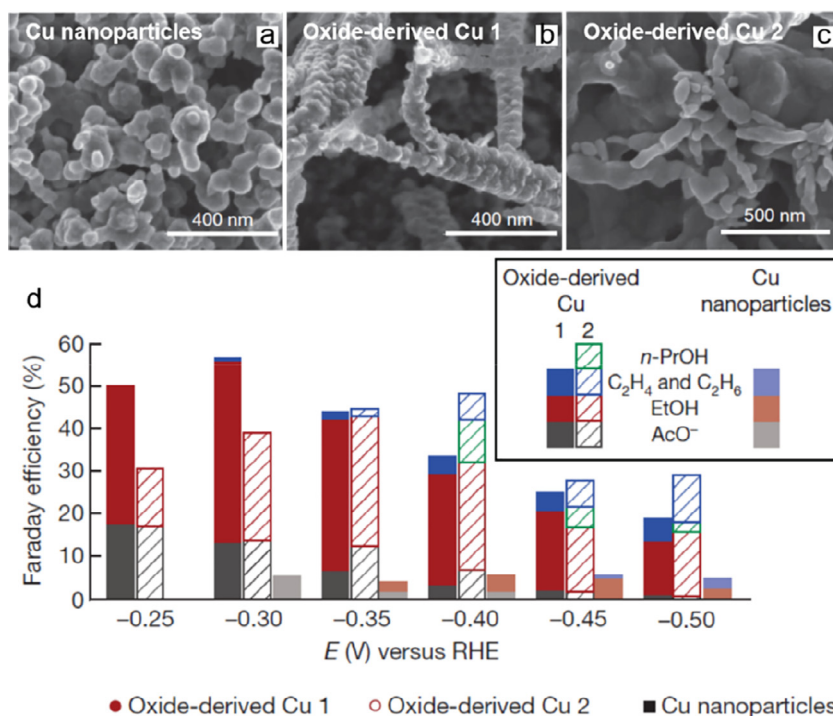


Fig. 10. The morphology structure and performance of Cu-based catalyst for carbon monoxide electroreduction. (a-c) SEM images. (d) Faradaic efficiencies for ethanol (EtOH), acetate (AcO⁻), n-propanol (n-Pr-OH), ethylene (C₂H₄) and ethane (C₂H₆) at different potentials. Reproduced with permission.²² Copyright 2014, Springer Nature.

–0.5 V vs. RHE). They put forward engineering the grain boundaries on the catalysts was favor of the activity and selectivity for carbon monoxide electroreduction to long-chain products (Fig. 10). Afterwards, Feng et al.¹²³ also demonstrated the carbon monoxide electroreduction activity is directly correlated to the density of grain boundaries in Cu nanoparticles. They prepared Cu nanoparticles with different average grain boundary densities to quantitative analysis of surface-area-normalized carbon monoxide reduction current densities with the density of the grain boundaries. In addition, Raciti et al.¹³¹ indicated that the Cu(110) facets with the highest grain boundary density played a key role in carbon monoxide reduction to C₂₊ products. Except for the efforts focusing on the increase of surface active sites for polycrystalline Cu, the electrode structure was designed to possess high-surface-area with better carbon monoxide accessibility. Wang et al.¹³² prepared a three-dimensional (3D) nanostructured oxide-derived Cu catalyst based on commercial Cu foams, which can efficiently enhance the current density and selectivity towards carbon monoxide reduction due to its large surface area facilitating the supply of carbon monoxide to the active sites.

Besides the optimization of the structure of Cu catalyst, researchers also made efforts on the fabrication of cathodic electrode structure. Han et al.¹²⁴ fabricated Cu nanoparticles-based gas diffusion electrodes to render the carbon monoxide gas be directly introduced onto the catalyst surface, which can enhance the partial current density to 50.8 mA cm⁻² for carbon monoxide reduction to ethylene at –15 °C and –0.85 V in 10 M KOH. Recently, Deng et al.¹³³ worked on the optimization of hydrophobic property of cathode structure and Cu catalysts to facilitate carbon monoxide diffusion and C–C bond coupling, achieving a 52.7% Faradaic efficiency of ethylene from carbon monoxide electroreduction. The control experiments that Cu

particles supported on the carbon papers with different hydrophobicity indicated that the electrocatalytic carbon monoxide reduction process was greatly affected by the hydrophobicity and porous structure of the catalyst supports. As shown in Fig. 11a, the hydrophobic carbon fiber with 25% polytetrafluoroethylene (PTFE) treatment can efficiently promote carbon monoxide transport at the interface of gas/liquid/solid (Fig. 11b), and the optimal Faradaic efficiency of C₂₊ products can reach 72.5% at 0.7 V in 1 M KOH (Fig. 11c). Combined with the in situ X-ray absorption near-edge structure spectra of Cu K-edge and DFT calculations, Cu(100) was proposed as the most preferred plane for ethylene formation. (Fig. 11d).

Despite significant progress on the electroreduction of carbon monoxide based on the H-type reactor, the optimal activity achieved remains inadequate at less than 100 mA cm⁻², far from the industrial application. The low solubility of carbon monoxide in the electrolyte largely hinders the transport of carbon monoxide to the catalyst surface. In addition, the competition between carbon monoxide reduction and hydrogen evolution inhibits the Faradaic efficiency of carbon monoxide to C₂₊ products.

Flow-cell reactor

Inspired by the application of flow-cell reactor in carbon dioxide electroreduction, the flow-cell reactor comes into sight for the carbon monoxide electroreduction, which allows the gaseous reactants to be directly fed to the electrode-electrolyte interface achieving a high rates of carbon monoxide reduction. Firstly, Jiao et al.²⁶ fabricated a three-compartment carbon monoxide flow electrolyser shown in Fig. 12a and b, in which the carbon monoxide gas was directly fed on the Cu catalyst surface and the triple-phase boundary benefited for the carbon monoxide transportation. The well-engineered electrode-electrolyte interface promoted the carbon monoxide reduction to C₂₊ products

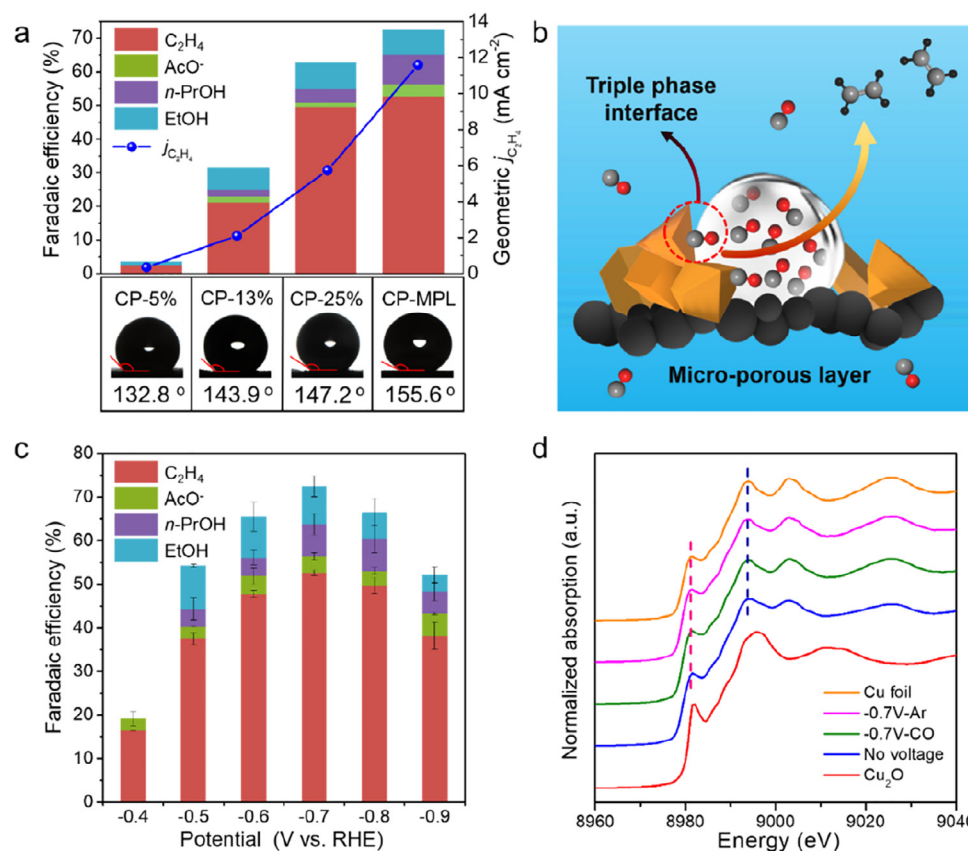


Fig. 11. The carbon monoxide electroreduction performance and characterization of Cu electrode structure. (a) Faradaic efficiency and geometric current density for carbon monoxide electroreduction of Cu nanoparticles supported on carbon papers with different hydrophobicity. (b) Schematic illustration of triple phase interface for carbon monoxide reduction. (c) Faradaic efficiencies of C_2+ products over Cu particles. (d) The in situ X-ray absorption near-edge structure spectra of Cu K-edge. Reproduced with permission.¹³³ Copyright 2020, Wiley-VCH.

with a 91% selectivity at a partial current density of 635 mA cm^{-2} (**Fig. 12c and d**).

Besides the increase of local carbon monoxide concentration to enhance the carbon monoxide electroreduction current density, changing the carbon monoxide concentration can also regulate the selectivity of carbon monoxide electroreduction products. Latest research by Sargent and Sinton group²⁹ indicated that an ethylene Faradaic efficiencies of 65% at a partial current density of 808 mA cm^{-2} were achieved by tuning the local carbon monoxide concentration at the catalyst-electrolyte interface (**Fig. 13a**). They performed carbon monoxide electroreduction in 1 M KOH at various carbon monoxide concentrations and a fixed potential. Combined with the experiments and DFT calculations, they indicated that the carbon monoxide coverage on the catalyst surface influenced the reaction pathways of ethylene versus oxygenate: lower carbon monoxide coverage stabilized the ethylene-relevant intermediates whereas higher carbon monoxide coverage favored oxygenate formation.

In addition, the alkalinity of the electrolyte also has a great effect on the Faradaic efficiencies and current density for carbon monoxide electroreduction. Li et al.²⁹ indicated that alkalinity of the electrolyte above 1 M inhibited the ethylene production but benefited for acetate formation, which was ascribed to a high alkalinity facilitating $*C_2$ intermediates reacting with the abundant hydroxide ions to acetate.

After several years of rapid development, carbon monoxide electroreduction with high rate performance is now beginning to

take shape. The 40% energetic efficiency for C_2+ products can be maintained at 600 mA cm^{-2} (**Fig. 13b-c**). The ethylene Faradaic efficiencies can reach over 65% at a partial current density about 800 mA cm^{-2} , which shows promise for large-scale application of carbon monoxide electroreduction under mild conditions.

Combined with the in-situ characterizations and DFT calculations, much progress has been achieved on the understanding of active sites, key reaction intermediates and reaction pathways of Cu catalysts for carbon monoxide electroreduction to C_2+ products. As shown in **Fig. 14**, the two adsorbed carbon monoxide molecules can firstly form a dimer $CO-CO^*$ species, which can further adsorb the protons from the electrolyte to form $COHCOH^*$ species. Then, the dehydration process occurred to form the $CCOH^*$ species. Further adsorption of the protons and dehydration lead to the formation of CHC^* species. Afterwards, the proton-electron transfer occurred on the CHC^* species to form the C_2H_4 products. Note that the proton-electron transfer of $CHCOH^*$ splits the pathway to C_2H_4 from the pathway to CH_3CH_2OH and CH_3COOH . Via changing the structure of catalysts, we can adjust the reaction pathway to selective electroreduction of carbon monoxide to desired C_2+ products. In addition, the formation of the $C_2O_2^*$ species is regarded as the most endergonic electrochemical step and determines the overpotentials of the cathode reaction. Hence, designing efficient catalysts to lower the formation energy of $C_2O_2^*$ species can significantly enhance the activity of carbon monoxide electroreduction.

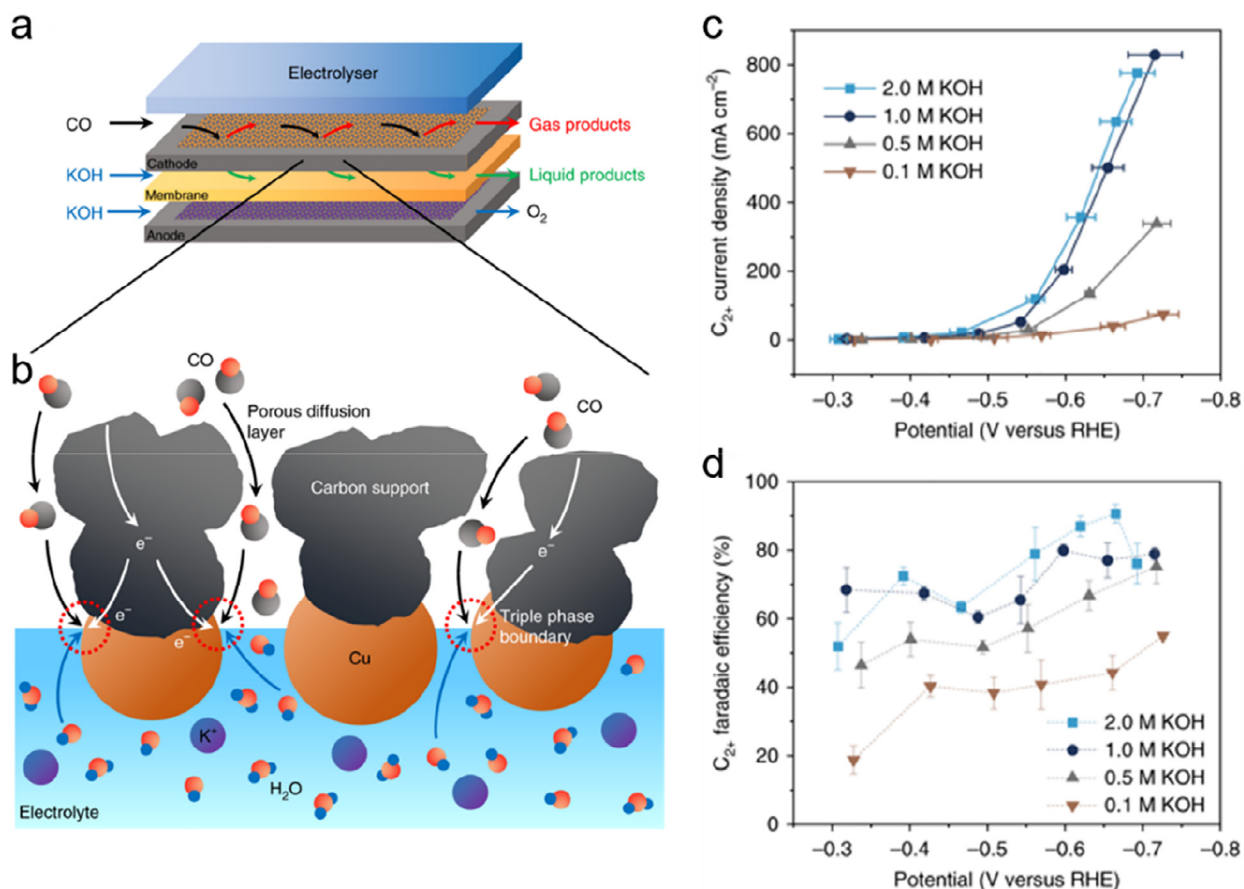
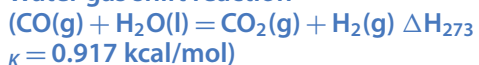


Fig. 12. The scheme of flow-cell reactor and performance of carbon monoxide electroreduction. (a-b) Scheme of the carbon monoxide flow electrolyser and triple-phase boundary for carbon monoxide reduction. (c-d) Partial current density and Faradaic efficiencies of C₂₊ products from carbon monoxide reduction. Reproduced with permission.²⁶ Copyright 2018, Springer Nature.

Water gas shift reaction



WGS reaction ($\text{CO} + \text{H}_2\text{O} \rightarrow \text{CO}_2 + \text{H}_2$) is an essential process for hydrogen production through fossil fuel and carbon monoxide removal in various energy-related chemical industry.^{134–136} The development of efficient low-temperature catalysts for WGS reaction are vital for their applications in fuel cells.^{25,137–139} Compared to the Fe based catalysts operating at high-temperature of 350–450 °C, Au based catalysts, Cu based catalysts and Pt group catalysts are used for the low-temperature WGS reaction operating at 200–300 °C with high activity and good selectivity.^{140–144} Thompson et al.²¹ reported Pt/Mo₂C catalyst possessing much higher WGS rates than oxide-supported Pt catalysts and commercial Cu-Zn-Al catalyst at 200 °C. They ascribed the higher activity to the high density of active sites at the perimeter of the Pt particles. Ribeiro et al.²⁴ screened a series of transition metals (Ag, Cu, Pt, Au, Pd and Ni) supported over Mo₂C for WGS at 120 °C, and found that Pt/Mo₂C showed the highest activity, 4–8 times higher than those of the commercial Cu/ZnO/Al₂O₃ catalyst. Latest research by Ma et al.²⁵ reported Au clusters on a α -MoC substrate exhibiting superior performance for low temperature WGS reaction, which is at least one order of magnitude more active than previous findings for the WGS reaction below 150 °C (Table 4). As shown in Fig. 15, carbon monoxide conversion can reach over 95% at

120 °C and 98% at 150 °C under the product free gas feed. Combined with the DFT calculations, they indicated that the water dissociated on the α -MoC center to produce OH species, which can further reacted with the adsorbed CO at the interface of Au and α -MoC to form CO₂ and H₂ at low temperature. But when changing the reaction gas feed to a full reformate gas containing hydrogen and carbon dioxide, the activity dropped significantly to 62% at 120 °C due to the inhibition by product of hydrogen and carbon dioxide, corresponding to the Au-normalized activity of 0.62 and 2.02 mol_{CO} mol_{Au}⁻¹ s⁻¹, respectively. Besides the metal supported on Mo_xC system for low temperature WGS reaction, Stephanopoulos et al.²³ found that the addition of Na or K to Au on KLTL zeolite and mesoporous MCM-41 silica enabled the single site cationic Au-O(OH)_x-species stabilized by alkali ions in the form of AuO_y(OH)_z(Na or K)_x, leading to a high activity for the low temperature WGS at 150 °C. In addition, Supported Ionic Liquid Phase catalysis (SILP), as one of the most promising approaches, enables a highly efficient WGS reaction at temperatures between 100 °C and 150 °C by homogeneous catalysis.¹⁴⁵ The SILP catalysts consist of a transition metal complex, which is homogeneously dissolved in a thin film of ionic liquid (IL). The best activities were observed for Ruthenium-based catalysts, especially for systems using RuCl₃ as precursor. The novel process provides an efficient way for WGS reaction at low temperature.

Besides designing novel catalysts in thermal catalysis to decrease the reaction temperature, light energy was also employed

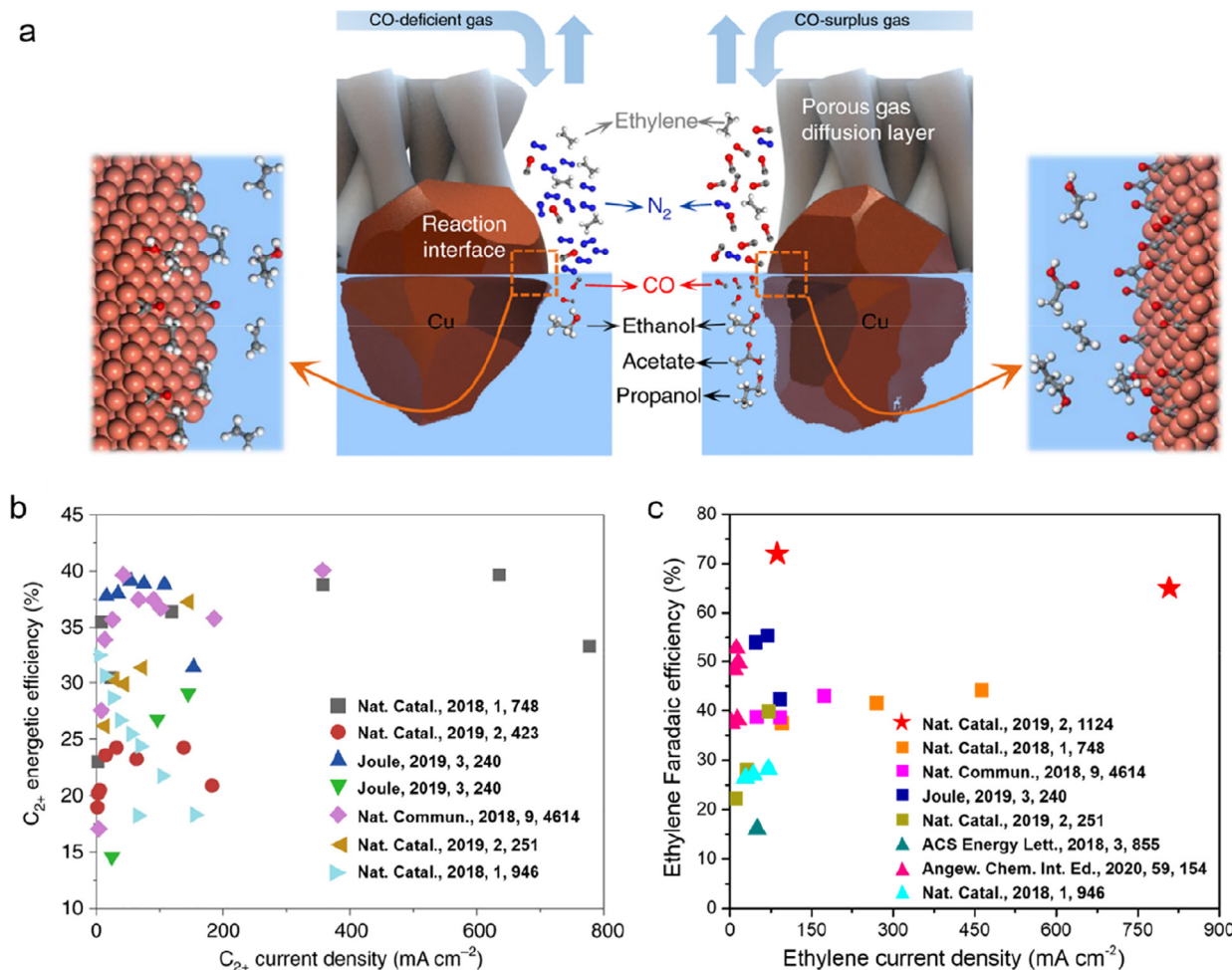


Fig. 13. Representative systems for electroreduction of carbon monoxide. (a) The scheme of the reaction pathway for carbon monoxide reduction at the catalyst-electrolyte interface with carbon monoxide-deficiency and carbon monoxide-surplus conditions. Reproduced with permission.²⁹ Copyright 2019, Springer Nature. (b) C₂₊ energetic efficiencies versus the C₂₊ partial current densities for representative carbon monoxide electroreduction systems and (c) Faradaic efficiencies versus partial current densities for ethylene. Reproduced with permission.^{11,133} Copyright 2019, Springer Nature. Copyright 2020, Wiley-VCH.

to drive the WGS under mild conditions. Ouyang et al.¹³⁹ proposed a solar-driven WGS process instead of traditional thermal catalysis, in which CuO_x/Al₂O₃ catalyst delivered excellent catalytic activity (122 μmol g_{cat}⁻¹ s⁻¹ of H₂ evolution and >95 % of CO conversion) under photothermal condition with UV-light irradiation. The solar-driven WGS reaction with a reaction temperature about 285 °C exhibited more than twice activity of the thermal catalysis operated at 300 °C. The authors ascribed this attractive performance of the solar-driven WGS reaction over CuO_x/Al₂O₃ effect to the combined photo-thermocatalysis and photocatalysis. In addition, Corma et al.¹⁵¹ reported the photocatalytic WGS at ambient temperature with sunlight and visible light by noble-metal (Au, Pd and Pt) nanoparticles loaded on TiO₂ or CeO₂. After 22 h irradiation with concentrated sunlight, Au/TiO₂ showed the highest activity at a carbon monoxide conversion of 71%, with H₂ and CO₂ production rates of 10,506 mmol g_{cat}⁻¹ and 13,447 mmol g_{cat}⁻¹, respectively. These results provide a promising way for the implementation of sunlight-driven, near ambient temperature WGS process.

In addition, a new electrochemical WGS concept was proposed by using electrical energy. Oettel and co-workers^{152,153}

firstly reported an electrochemical membrane reactor, which combined the electrochemical H₂ pumping and the electrochemical CO oxidation in one step. The process was operated about 150 °C with a current density of 28.1 mA cm⁻² at 0.55 V versus RHE employing a H₃PO₄-doped Poly (2,5-benzimidazole) membrane as electrolyte and precious PtRu anode catalyst. Recently, Deng et al.²⁷ put forward a room-temperature electrochemical water-gas shift process (EWGS) for direct production of high purity hydrogen, in which CO was oxidized on the anode and H₂ was produced from H₂O reduction on the cathode. The employment of anion exchange membrane can separate the cathode and anode, and hinder cross-contamination of the anodic (CO₂) and cathodic (H₂) reaction products in the system. Thus a high purity hydrogen can be achieved without the need of additional separation process as required in the traditional WGS. Through improving the hydrophobicity of the catalyst to create solid/liquid/gas interfaces, the diffusion and adsorption of CO can be facilitated, leading to an improvement on the anodic reaction activity. The electrolysis process can be effectively driven at room temperature (25 °C) and atmospheric pressure with a faradaic efficiency of approximately 100% (Fig. 16). Through the rational design of the

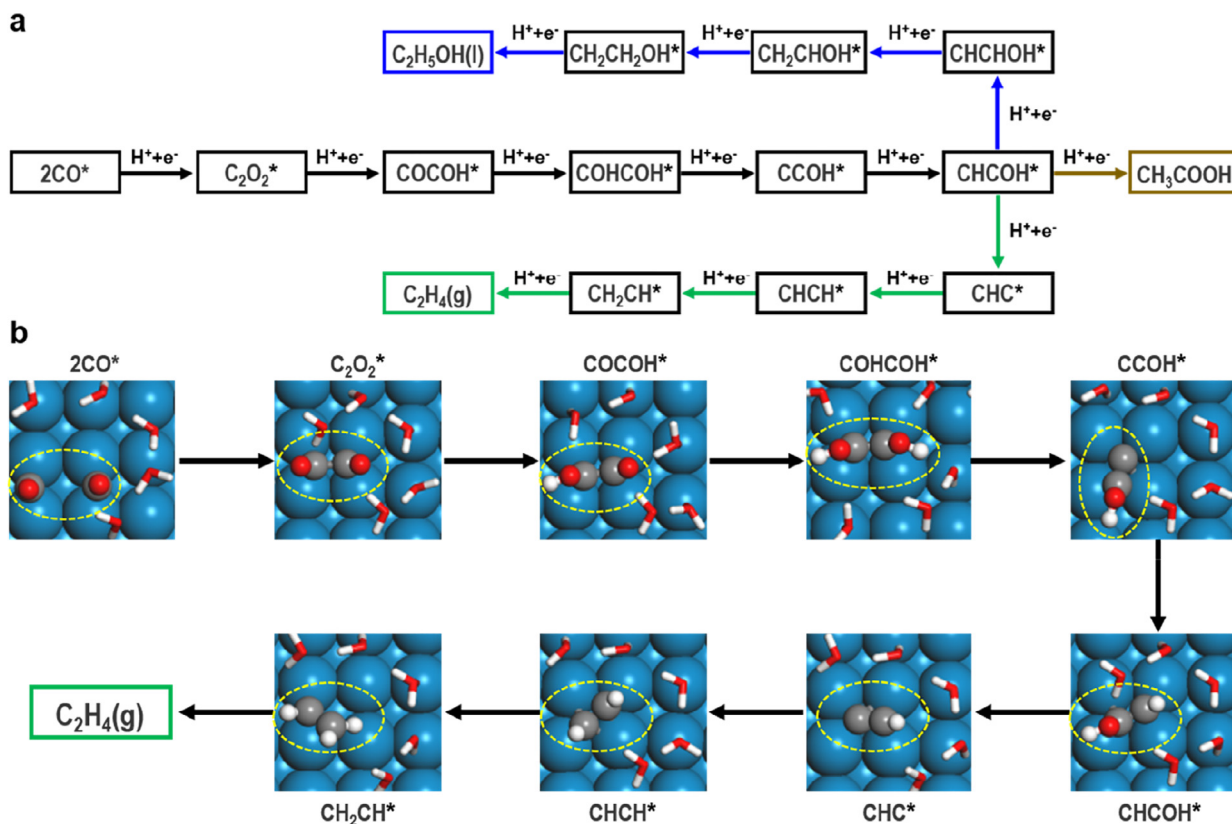


Fig. 14. Schematic representations of CO electroreduction reaction pathways. Reproduced with permission.¹³³ Copyright 2020, Wiley-VCH.

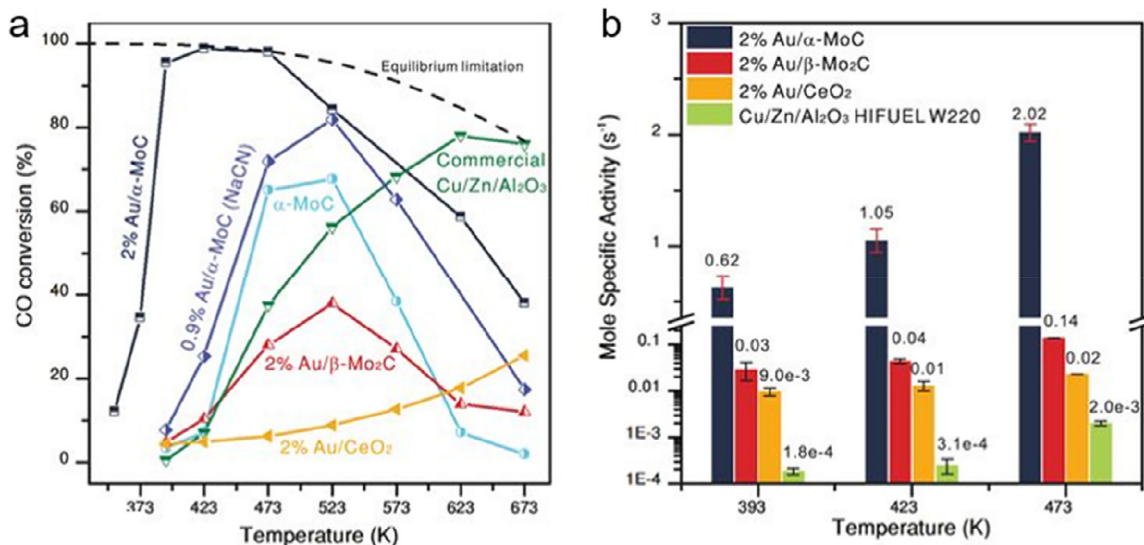


Fig. 15. Catalytic performance and reaction mechanism of Au/α-MoC for low temperature WGS reaction. (a) carbon monoxide conversion on different catalysts at various temperatures. (b) The Au-normalized activity of different catalysts under different temperature. Reproduced with permission.²⁵ Copyright 2017, AAAS.

anode structure and catalyst, the operating voltage for the EWGS process was lowered to almost 0 V vs. RHE. The optimized PtCu catalyst increased the current density up to 70.0 mA cm^{-2} at a moderate potential of 0.6 V, which was more than 12 times that of pristine commercial Pt/C (40 wt.%) catalyst, and remains stable for even more than 475 h. The rate of hydrogen production can

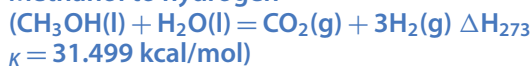
reach $128.2 \text{ mmol h}^{-1} \text{ g}_{\text{cat}}^{-1}$. Electrochemically decoupling the WGS redox reaction to separated cathodic reduction reaction and anodic oxidation reaction in an electrolytic cell and using electric-potential as the driving force of the process provides a new and promising platform for hydrogen production via WGS process under mild conditions.

Table 4. Representative catalytic systems for the low-temperature WGS reaction operating below 300 °C.

Catalysts	Reaction temperature (°C)	Gas feed composition	Mass specific activity ($\mu\text{mol}_{\text{CO}} \text{g}_{\text{cat}}^{-1} \text{s}^{-1}$)	Reference
(2%)Au/ α -MoC	40	3% CO+6% H ₂ O+20% N ₂ in Ar	1.22	25
	80	5% CO+10% H ₂ O+20% N ₂ in Ar	13.06	
	120	10.5% CO+21% H ₂ O+20% N ₂ in Ar	103	
	150		167	
	200		325	
Au/MoC _x	80	3% CO+10% H ₂ O+He in He	5.77	146
	100		18.9	
	140		50.0	
Au/ β -Mo ₂ C	120	7% CO/22% H ₂ O/37% H ₂ /8.5% CO ₂ in Ar	1.6	24
Pt/ β -Mo ₂ C	120	7% CO+22% H ₂ O+37% H ₂ +8.5% CO ₂ in Ar	1.8	24
Pd/ β -Mo ₂ C	120	7% CO+22% H ₂ O+37% H ₂ +8.5% CO ₂ in Ar	1.4	24
Au-Na/MCM41	150	11% CO+26% H ₂ O+26% H ₂ +7% CO ₂ in He	0.83	23
Au/CeFeAl	180	9% CO+30% H ₂ O+50% H ₂ +12% CO ₂	1.79	147
Pt-Na/CNT	200	2% CO/10% H ₂ O in He	1.25	148
Pt-Mo ₂ C	200	11% CO+21% H ₂ O+43% H ₂ +6% CO ₂ in N ₂	100	21
Au/CeO ₂	240		285	149
	250	11% CO/26% H ₂ O/26% H ₂ /7% CO ₂ in He	48	
Pt/CeO ₂	250	11% CO/26% H ₂ O/26% H ₂ /7% CO ₂ in He	22	149
Ir ₁ /FeO _x	300	2% CO/10% H ₂ O in He	1.2	150

METHANOL CONVERSION

Methanol to hydrogen



Methanol, as an important raw material, which participate in many important industrial reactions, such as MSR, methanol to olefins.^{31,32,154,155} MSR has been considered as an important method for the clean hydrogen production, for which the suppression of by-products carbon monoxide and improvement of low temperature activity remain major challenges.¹⁵⁶ It has been discovered that Cu-based catalysts exhibit high activity for low temperature MSR, but they suffer from severe deactivation during the reaction.¹⁵⁷ In contrast, the noble catalysts, such as Pt-based or Pd-based catalysts deliver good stability.^{35,158} The Pd or Pt dispersed on Cu/ZnO are the representative heterogeneous catalysts for the methanol steam reforming.^{154,159} Iwasa et al.¹⁶⁰ carried out the methanol steam reforming over various supported group 8–10 metal catalyst at 220 °C, and reported the highest performance of PdZn alloy catalyst with a 54.2% conversion and

a 99.2% selectivity of carbon dioxide. In order to achieve a high rate of hydrogen production from low-temperature MSR process, bifunctional structures with efficient activation for both the water and the methanol were proposed as promising catalysts. Recent study by Ma et al.³³ found that atomically dispersed platinum over α -MoC can achieve the aqueous-phase reforming of methanol at 150–190 °C, which exhibited a high TOF about 18,046 mol of hydrogen per mole of platinum per hour (Fig. 17). The strong interaction led to an exceptionally high density of electron-deficient surface Pt sites for both the adsorption or activation of methanol. And the α -MoC provided highly active sites for water dissociation, producing abundant surface hydroxyls and thus accelerating the methanol-reforming reaction at the interface between Pt₁ and α -MoC. The synergetic effect make the catalyst possess unprecedented activity and good stability. Notably, the selectivity of carbon monoxide can be even reduced below 0.1%, which shows great potential for commercially hydrogen storage.

Besides the noble-metal catalysts, much attention was attracted by the cheap and more abundant Cu/ZnO systems, but they require higher reaction temperature than the Pt or Pd

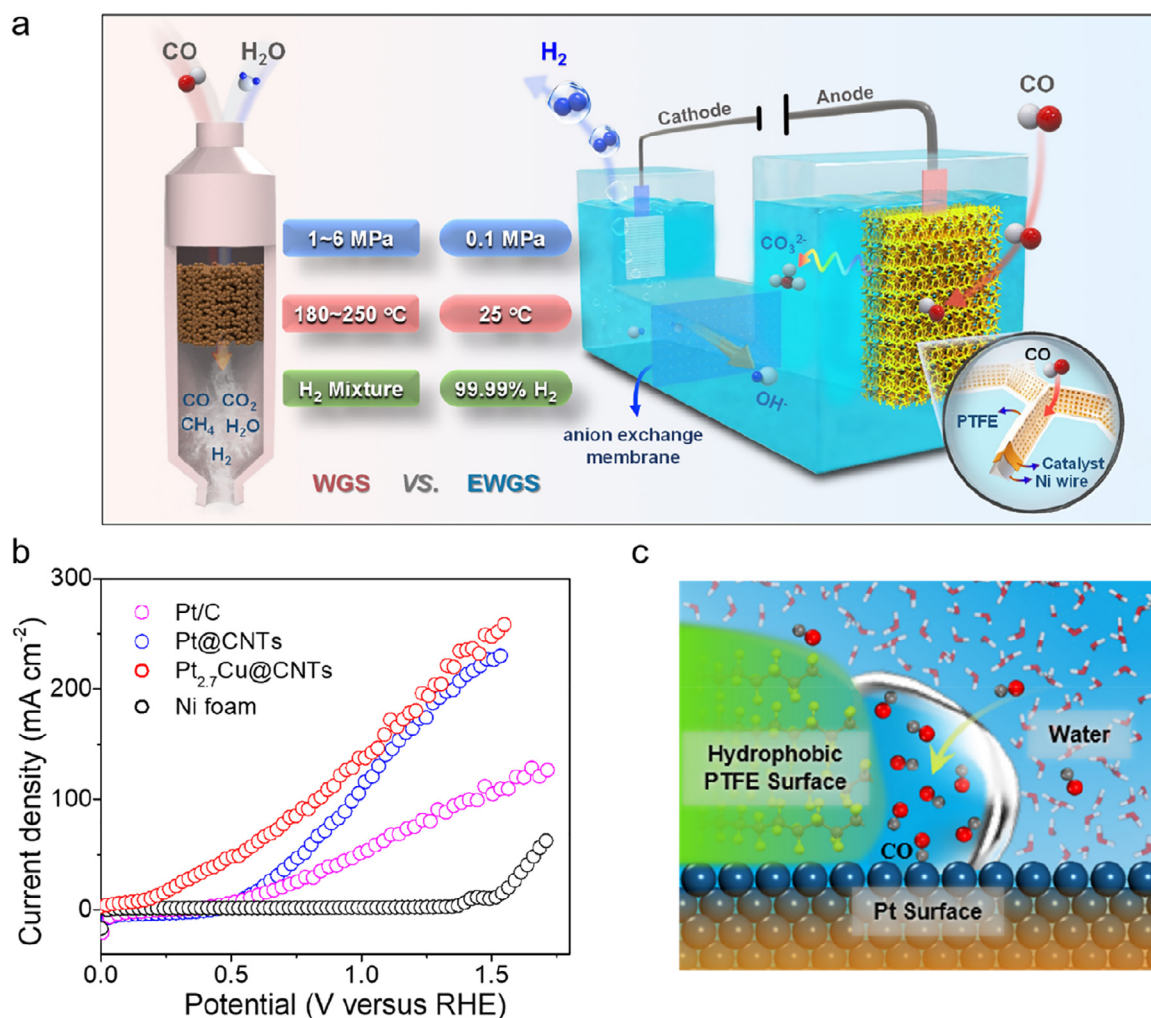
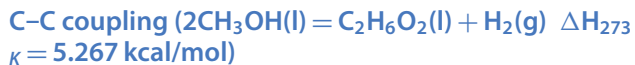


Fig. 16. Room-temperature EWGS for direct production of high purity hydrogen (a) Schematic diagram of the EWGS process compared with the traditional WGS process. (b) Linear sweep voltammetry polarization curves of the CO oxidation catalyzed by different catalysts. (c) Schematic illustration of solid/liquid/gas interfaces on the PTFE-decorated Pt surface. Reproduced with permission.²⁷ Copyright 2019, Springer Nature.

catalysts.¹⁵⁴ Tsang et al.³⁰ reported a CuZnGaO_x catalyst for the direct methanol steam reforming to hydrogen and carbon dioxide via a non-syngas route at 150–200 °C. The balance between metallic Cu⁰ and Cu^I was considered important for the enhancement of activity and selectivity. In contrast to the traditional multi-step process for methanol to hydrogen, the non-syngas route can produce high quality hydrogen with a productivity of 393.6 mL g_{cat}⁻¹ h⁻¹ at 150 °C in a single-step without detectable CO (below detection limit of 1 ppm), which circumvented the steam reforming to syngas at high temperature, water gas shift and carbon monoxide purification. The non-syngas direct steam reforming route provides a promising option for high pure hydrogen production from methanol at mild conditions.



Besides using methanol as a hydrogen carrier, methanol can be converted to other valuable chemicals, such as acetic acid and olefins, which has been extensively studied from fundamental research to industrial applications.^{161–164} MTO process was regarded as a key future technology for transforming coal

or natural gas into the fine chemicals. Since MTO was first proposed by the Mobil Corporation in 1977,¹⁶⁵ great efforts were put into developing the MTO process by systematically exploring catalyst synthesis,^{166–168} reaction mechanism,¹⁶⁹ process engineering^{170,171}, reactor design and commercialization development.¹⁵⁵ The representative MTO catalysts are acid zeolite-based catalysts, with the reaction operated above 400 °C. The world's first MTO unit was constructed and started up by the Dalian Institute of Chemical Physics in 2010 in Baotou, China, which was considered as a crucial milestone for the production of lower olefins from coal. A comprehensive summary about MTO technology from fundamentals to commercialization was reviewed in detail.¹⁵⁵

Except for the C–C coupling of methanol to hydrocarbons and oxygenates under high temperatures, the selectively activate the unreactive C–H bond of methanol but stabilize the hydroxyl group to form the C–C coupling under mild conditions was also reported.^{172,173} In 1982, Yanagida et al. firstly used methanol as the sacrificial electron donors to enhance the photochemical production of hydrogen by ZnS, in which the CH₃OH was converted to ethylene glycol and hydrogen by UV irradiation.¹⁷⁴ After that, they further increased the selectivity of ethylene glycol

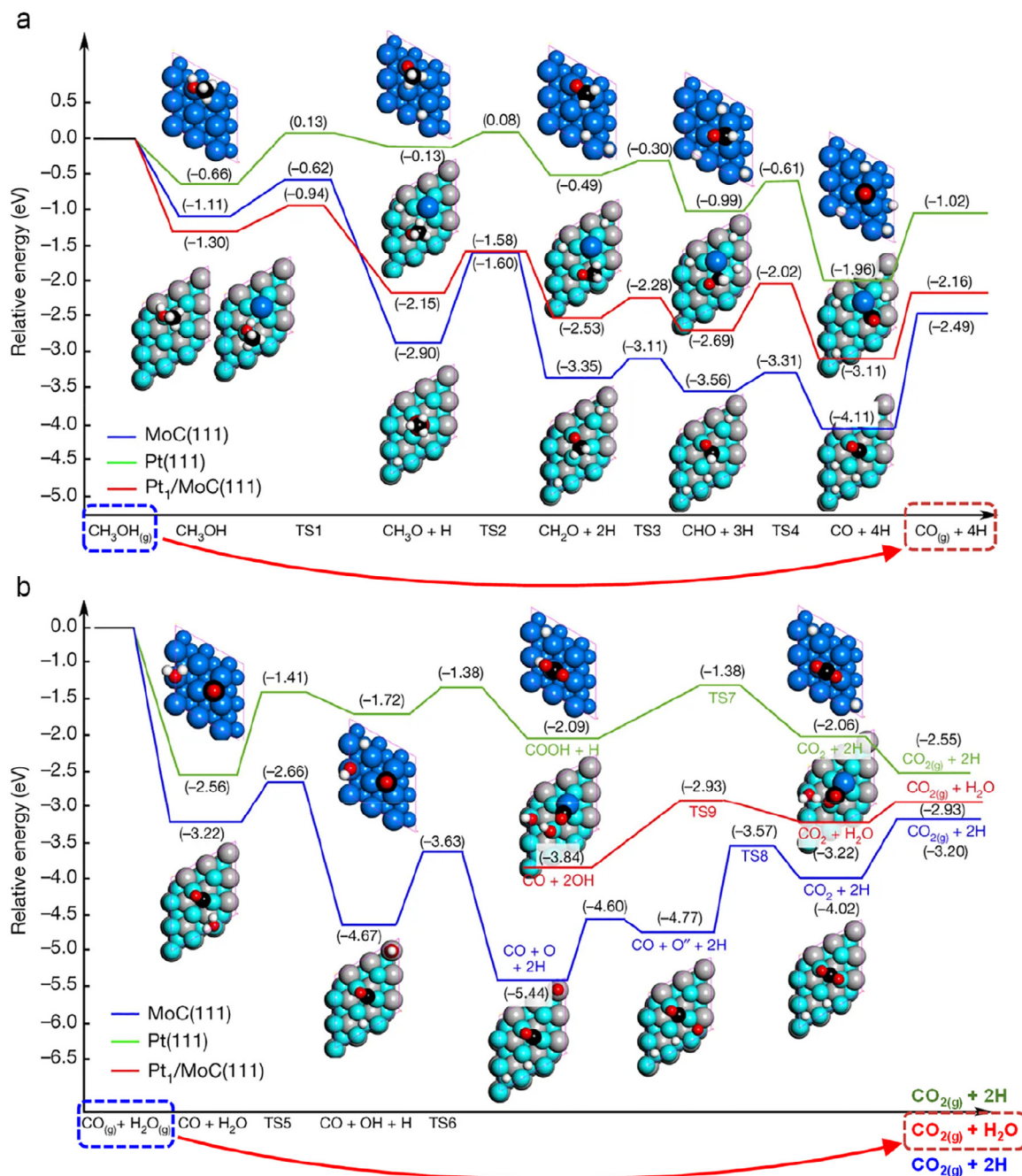


Fig. 17. Reaction mechanism of $\text{Pt}_1/\alpha\text{-MoC}$ for aqueous-phase reforming of methanol. (a) Energy profiles for CH_3OH dissociation into CO and H atoms on different surfaces. (b) Energy profiles for CO_2 formation via the water-gas shift reaction on different surfaces. Reproduced with permission.³³ Copyright 2017, Springer Nature.

to 52% after 60 h irradiation in 1984, and indicated that the first example of photo-assisted process for carbon-carbon formation was achieved via free radical intermediates by ZnS semiconductor particles.¹⁷⁵ Hu et al. then adopted freshly prepared colloidal ZnS to further enhance the selectivity of ethylene glycol to 95% after 6 h irradiation. Moreover, the $\cdot\text{CH}_2\text{OH}$ was confirmed as the main radical intermediate for the formation of ethylene glycol by spin trapping experiments.¹⁷⁶ Recent study by Xie et al.³⁴ present the first visible-light-driven dehydrogenative coupling of methanol to ethylene glycol with 90% selectivity, which was achieved by the catalyst of MoS_2 foam modified CdS nanorod (**Fig. 18**). Specifically, the cleavage of C–H bond in methanol

preferentially occurred on the CdS surface to produce hydroxymethyl radical, which can further coupled with each other to form ethylene glycol. Meanwhile, MoS_2 foam with sufficient edge served as hydrogen evolution active sites, can promote the photocatalytic activity for ethylene glycol formation. In addition, the intimate contact between MoS_2 and CdS benefited for the transfer of photogenerated electrons and holes. Consequently, a 16% yield of ethylene glycol after 100 h reaction by a process-intensified reactor was achieved. The research put forward a promising way for ethylene glycol production under mild conditions and demonstrate a novel strategy for preferential C–H bond activation.

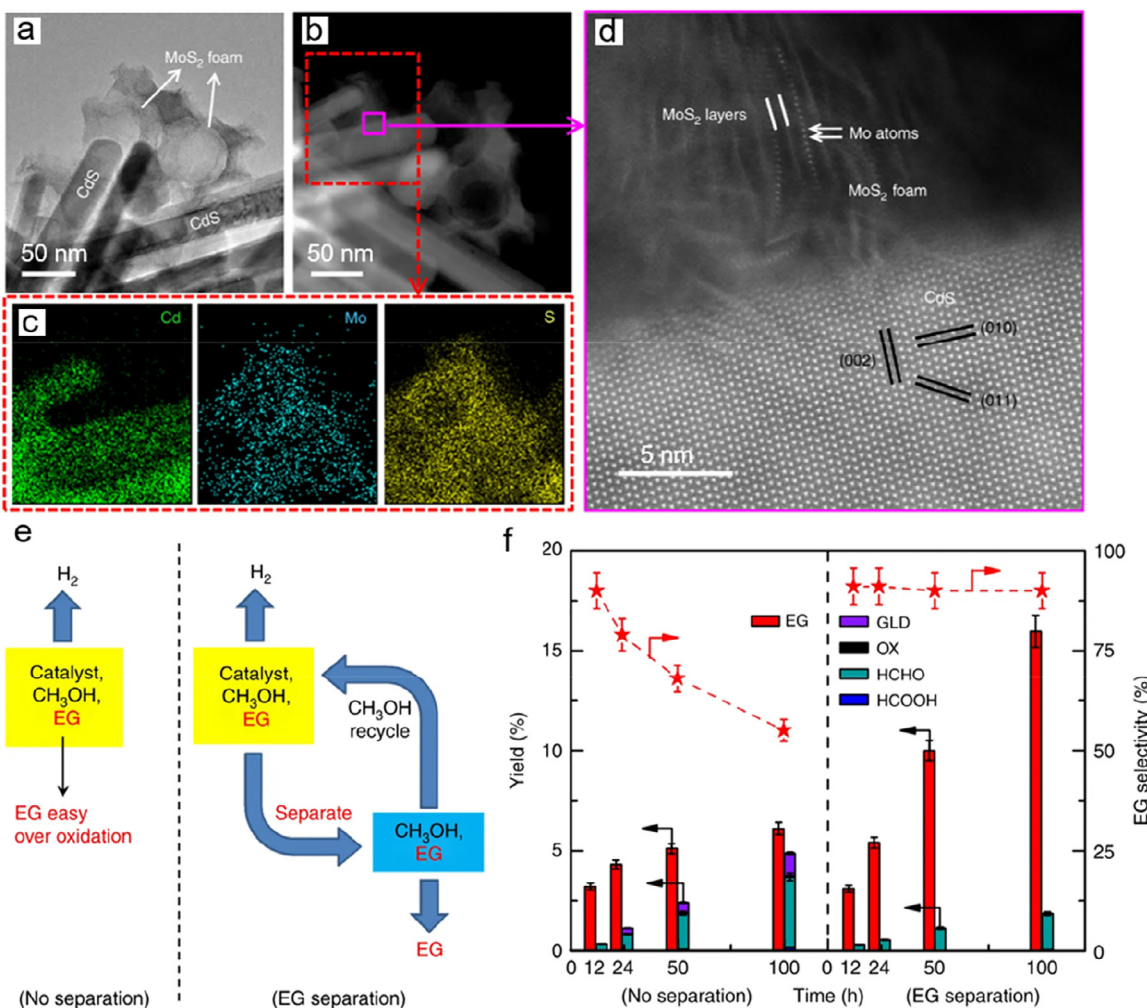
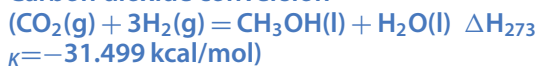


Fig. 18. The structure and activity of MoS₂ foam modified CdS catalyst for visible light-driven methanol to ethylene glycol. (a) TEM image of MoS₂ foam modified CdS catalyst. (b-d) HAADF-STEM images of MoS₂ foam modified CdS catalyst and corresponding elemental mappings. (e) The process-intensified mode with ethylene glycol separation in contrast to the conventional reaction mode. (f) The yield and selectivity of ethylene glycol under different conditions. Reproduced with permission.³⁴ Copyright 2018, Springer Nature.

Carbon dioxide conversion



Carbon dioxide is a cheap, nontoxic and abundant C1 feedstock and its chemical transformation into value-added chemicals and fuels plays a key role for creating a sustainable low-carbon economy in the chemical and energy industry.^{177,178} However, the transformation of carbon dioxide usually needs the co-feeding of a high-energy reactant (e.g., hydrogen) or the supply of external energy (e.g., electric energy or photo energy) due to its thermodynamically stable and kinetically inert property.^{179,180} To date, hydrogenation of carbon dioxide by hydrogen is regarded as the most promising route for the conversion of carbon dioxide to liquid fuels or value-added chemicals. Benefiting from the advanced technology about water electrolysis and solar/wind power, the production of renewable hydrogen become possible and easy to implement.¹⁸¹ Recent progress by Li group from Dalian Institute of Chemical Physics demonstrated a liquid sunshine pilot project that hydrogenation of carbon dioxide by hydrogen to methanol, which involves photovoltaic power technology and water electrolysis for hydrogen (http://www.dicp.ac.cn/xwdt/ttxw/202001/t20200116_5488931.html).

This pilot project provides a promising route for the conversion of carbon dioxide into liquid fuels by solar energy.

Catalytic hydrogenation of carbon dioxide can produce a variety of valuable fuels and chemicals, such as carbon monoxide, methanol, formic acid, ethanol, lower olefins, gasoline and aromatics, etc.^{39,41–43,189,196,203,213–220} The representative catalysts and reaction conditions for the hydrogenation of carbon dioxide are summarized in Table 5. The reported catalysts for carbon dioxide hydrogenation to methanol are mainly focused on Cu-based and Pd-based systems, but most of them were only active when the reaction temperature was higher than 200 °C.^{221–225} The hydrogenation of carbon dioxide to C₂₊ products is usually catalyzed by bifunctional catalysts, which took place through two competing pathways: the modified Fischer-Tropsch synthesis and the methanol-mediated synthesis.²¹⁵

The high reaction temperature and low yield of targeted products remain the major challenges for carbon dioxide hydrogenation. Recently, Zeng group⁴¹ reported a synergistic interaction to enhance the carbon dioxide hydrogenation catalytic activity below 200 °C. They prepared the isolated monomers Pt atoms and neighboring Pt monomers doping MoS₂ nanosheets

Table 5. The representative catalysts for carbon dioxide hydrogenation.

Main Products	Catalysts	Reaction Temperature (°C)	Reference		
C1 products (CH_3OH , HCOOH et al.)	Cu/Zn based	Cu/plate $\text{ZnO}/\text{Al}_2\text{O}_3$ Cu@ ZnO_x Cu/Zn/Al/Y	270 250 250	182 183 184	
	Cu/ ZrO_2 based	Cu/ Zn/ZrO_2 Cu/ $\text{Ga}_2\text{O}_3/\text{NC-ZrO}_2$ La-Cu/ ZrO_2	220 250 220	185 186 187	
		MOF-based	CuZn@UiO-bpy mbpyOH-[Ir]-UiO	250 85	188 189
		Pd-based	Pd/ $\text{ZnO}/\text{Al}_2\text{O}_3$ Pd/Zn/CNTs Pd/ In_2O_3	180 250 300	190 191 192
	Au-based	Au/ ZnO Au/ ZrO_2	220–240 220–240	193 193	
		Bi-metallic	Pd-Cu/SBA-15 Pd-Cu/ CeO_2 PdMn _{0.6} @S-1	250 190–270 80	194 195 196
	Inter-metallic	PdZnAl	250	197	
		NiGa/ SiO_2	200	198	
		CuIn-In ₂ O ₃	280	199	
	Hybrid oxide	In ₂ O ₃ / ZrO_2	300	200	
		Cu-ZnO/ Al_2O_3	260	201	
C_{2+} products ($\text{CH}_3\text{CH}_2\text{OH}$, C_2H_4 et al.)	Fe-based	Fe/ZIF-8 Na-Fe ₃ O ₄ /H-ZSM-5 Fe-Zr-Ce-K	300 320 320	202 203 204	
	Cu-based	Cu-Zn-Cr oxide/zeolite H-Y	400	205	
		FeCu/K/ Al_2O_3	300	206	
	Zn-based	ZnGa ₂ O ₄ /SAPO34	450	207	
		Fe-Zn-Zr@H-beta	340	208	
	Co-based	CoAlO _x	140	42	
		Co-Fe/K/ Al_2O_3	320	209	
	In-based	In ₂ O ₃ /HZSM-5	340	210	
		In ₂ O ₃ -ZrO ₂ /SAPO-34	400	211	
	Cr-based	Cr ₂ O ₃ /H-ZSM-5	350	212	
	MOF-based	Zr ₁₂ -bpdc-CuCs	85–100	43	

(Fig. 19). Compared to the isolated monomers Pt atoms doping MoS_2 , the neighboring Pt monomers doping MoS_2 exhibited better catalytic performance towards carbon dioxide hydrogenation with a TOF of 162.5 h^{-1} for 7.5% Pt/ MoS_2 at 150°C . In addition, the activation energy for 7.5% Pt/ MoS_2 was only about half of that for 0.2% Pt/ MoS_2 . Combined with DFT calculations, they indicated that the synergistic interaction of neighboring Pt monomers can efficiently lower the reaction barrier and optimize the reaction pathway for carbon dioxide hydrogenation.

Metal-organic frameworks (MOFs), as another promising heterogeneous catalysts or supports/precursors, were reported to present good activity for carbon dioxide hydrogenation. Wang et al.¹⁸⁹ indicated that molecular iridium catalysts immobilized in MOFs can efficiently convert carbon dioxide to formic acid/formate with a high TOF of 410 h^{-1} under atmospheric pressure and at 85°C .

Besides, the conversion of carbon dioxide to C_{2+} oxygenates such as ethanol is economically attractive and scientifically challenging because of the requirement of forming C-C bonds while retaining some of the C-O bonds ($2\text{CO}_2(\text{g}) + 6\text{H}_2(\text{g}) = \text{C}_2\text{H}_6\text{O}(\text{l}) + 3\text{H}_2\text{O}(\text{l})$ $\Delta\text{H}=-83.576 \text{ kcal/mol}$). Xiao group⁴² reported a non-noble catalysts (CoAlO_x) for selective hydrogenation of carbon dioxide into ethanol with a selectivity of 92.1% at 140°C , and the ethanol

time yield can reach $0.444 \text{ mmol g}^{-1} \text{ h}^{-1}$. They ascribed the good activity and extraordinary selectivity to the surface oxides with co-existence of Co-CoO phases due to their positive effect on production of $^*\text{CH}_x$ for converting formate into acetate via insertion. The noble Pd-based catalysts, such as Pd-Cu nanoparticles, was also found to be active for carbon dioxide to ethanol, which exhibited high selectivity up to 92% with a TOF of 359 h^{-1} at 200°C .³⁹ Recent study by Wang et al.⁴³ found that carbon dioxide can be hydrogenated to ethanol by cooperative Cu¹ sites on a Zr₁₂ cluster of a MOF (Fig. 20). The Cu- and Cs-functionalized MOF exhibited >99% selectivity towards ethanol for carbon dioxide hydrogenation, with a turnover number (TON) of 4080 in supercritical carbon dioxide at 85°C in 10 h or a TON of 490 at 2 MPa of CO₂/H₂ (1/3) and 100°C . The isotope labeling experiments indicated that the methyl group of methanol can be incorporated into the ethanol product. Further, they proposed a possible catalytic cycle via bimetallic oxidative addition. Firstly, the hydrogen was activated on bimetallic Cu¹₂ sites to form (Cu²⁺-H⁻)₂, and then carbon dioxide was hydrogenated to form methanol and formyl species. Further, a C-C bond coupling occurred on methanol and formyl species to generate C_{2+} oxygenates. The Cu¹₂ sites were regenerated by bimetallic reductive elimination with concomitant formation of methanol, ethanol or water. During the process, the cooperative nature of the bimetallic Cu¹₂

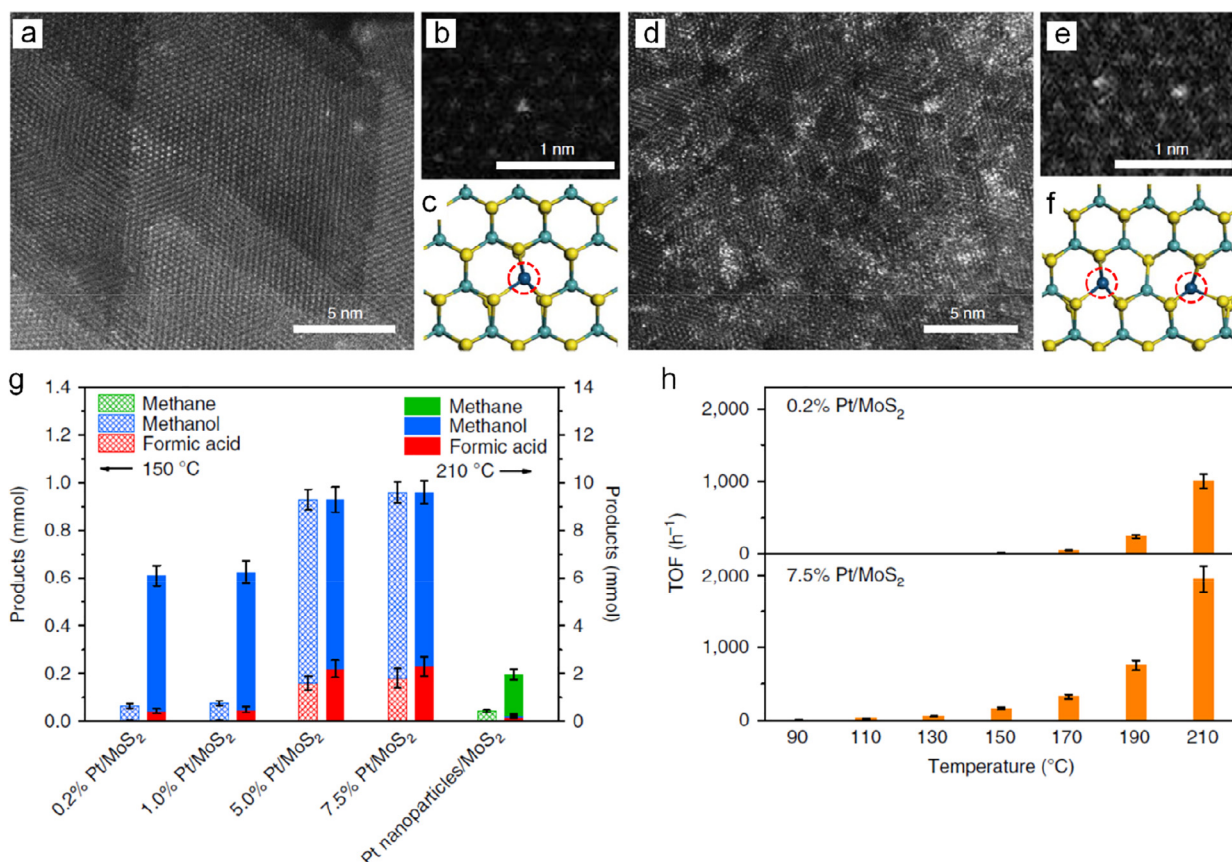


Fig. 19. Structural characterizations of isolated monomers Pt atoms and neighboring Pt monomers doping MoS₂ nanosheets and their catalytic performance for carbon dioxide hydrogenation. (a-c) HAADF-STEM images of isolated Pt monomers in 0.2% Pt/MoS₂ and its corresponding structural model. (d-f) HAADF-STEM image of neighboring Pt monomers doping MoS₂ and its corresponding structural model. (g) The activity of a series of Pt/MoS₂ for carbon dioxide hydrogenation. (h) Comparison of TOF between 0.2% Pt/MoS₂ and 7.5% Pt/MoS₂ catalysts at different reaction temperature. Reproduced with permission.⁴¹ Copyright 2018, Springer Nature.

sites not only facilitated hydrogen activation but also the direct C–C coupling of methanol and formyl species. Latest research²²⁶ by them demonstrated that another Cu-Ru-MOF hybrid by low-intensity light to in situ generating and stabilizing Cu¹ species can selectively hydrogenate carbon dioxide to ethanol with an activity of 9650 μmol g_{Cu}⁻¹ h⁻¹ under 2 MPa of CO₂/H₂ (1/3) at 150 °C. These researches highlight the opportunities in using MOFs as novel catalysts for catalytic hydrogenation of carbon dioxide to C₂₊ products.

Besides, the electrocatalytic and photocatalytic for carbon dioxide reduction emerged as a promising approach for carbon dioxide utilization, which can produce a variety of products, including carbon monoxide, formic acid, methanol, hydrocarbons, and alcohols.^{36–38,40} The recent progress about the carbon dioxide electroreduction and photoreduction has been thoroughly summarized in the relevant reviews.^{227–232} In addition, plasma catalytic reaction for carbon dioxide splitting and dry reforming of methane attracts much attention, which has the potential to enable thermodynamically unfavorable chemical reaction to occur at ambient conditions, which has been discussed in detail in the relevant reviews.^{233–236}

CONCLUSIONS AND PERSPECTIVES

As a promising strategy of reducing the pressure of the depleting fossil resources as well as alleviating the greenhouse effect, C1

catalysis has recently aroused great concern from academics and industry and become one of the most attractive research fields in heterogeneous catalysis. This Review highlighted the latest developments of highly efficient catalysts and reaction processes towards C1 molecules conversion to value-added products under mild conditions, including methane, carbon monoxide, methanol and carbon dioxide. Although significant progress has been made in the activation of C1 molecules under mild conditions, these processes are still far from the scale of industrialization due to their low efficiency. Much efforts are still needed to improve the reaction activity and selectivity simultaneously by developing novel catalysts and reaction processes. Further studies should be conducted to reveal the reaction mechanism by operando characterization and theoretical calculations. Thus, to narrow the gap between laboratory findings and industry performance requirements, the following issues need to be addressed:

Methane conversion is currently one of the most active research area in C1 catalysis. The surge-like eruption of confined single-atom catalysts stimulated the rapid development of selective oxidation of methane, but inefficient activation of C–H bond in methane under mild conditions, and low selectivity of target products have become the greatest bottleneck for their application. Selective oxidation of methane using hydrogen peroxide synthesized in situ from hydrogen and oxygen have been demonstrated to effectively increase product yields. In addition, coupling methane with carbon monoxide and carbon

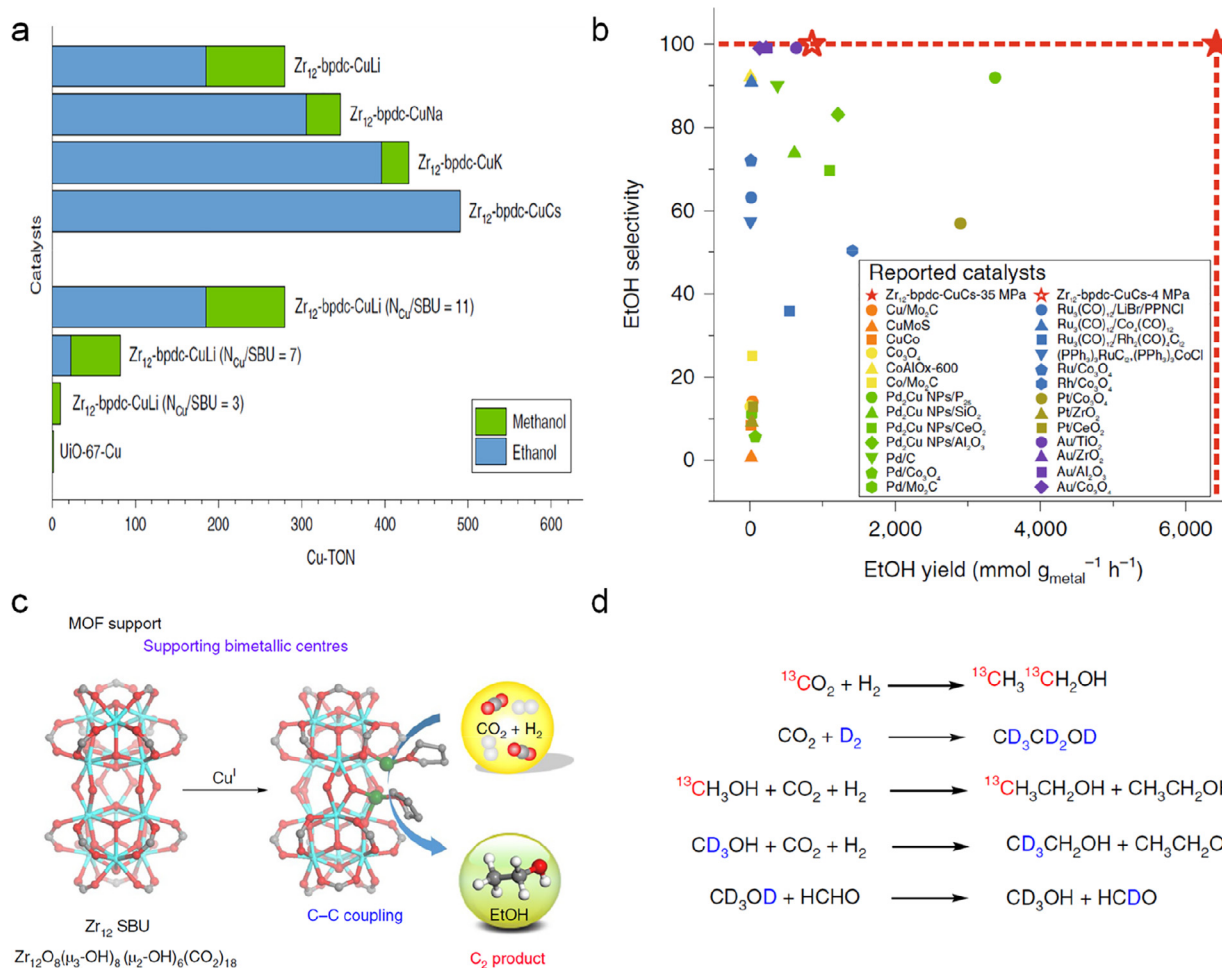


Fig. 20. Cooperative copper centers in a metal-organic framework for selective conversion of carbon dioxide to ethanol. (b) Comparison of TON for different catalysts. (b) Comparisons of ethanol yield and selectivity. (c) Scheme of cooperative copper centers in a metal-organic framework for carbon dioxide hydrogenation. (d) Isotope labeling experiments to unveil the source of carbon and hydrogen in ethanol. Reproduced with permission.⁴³ Copyright 2019, Springer Nature.

dioxide to produce acetic acid are promising system for methane conversion. However, it is still a long way to improve the activity and selectivity. Further studies should pay much attention to the selective oxidation of methane by molecular oxygen even air as the oxidant. Besides, development of novel catalysts and reaction process driven by thermal, electric, and photo energy and integrate the advantages of each approach in one reaction system to jointly enhance the performance will bring new opportunity for low temperature methane conversion.

The conversion of carbon monoxide to hydrocarbons and multi-carbon oxygenates by electrochemical reduction has achieved a significant breakthrough. The flow-cell reactor with well-engineered electrode-electrolyte interface shows promising potential for scale-up industrial application due to its high C₂₊ selectivity and current density. To date, an ethylene Faradaic efficiencies of 65% at a partial current density of 808 mA cm⁻² can be achieved by tuning the local carbon monoxide concentration at the catalyst-electrolyte interface.²⁹ Future work may focus on further improving the Cu-based catalyst stability due to its variability during the reaction. In addition, enhancing the Faradaic efficiency of single products under lower concentration electrolyte should be performed to reduce the cost on products separation and device maintenance. WGS reaction

has been widely applied in industry for hydrogen production and carbon monoxide removal. Despite remarkable improvements in decreasing the reaction temperature by Au/α-MoC²⁵ below 100 °C have been achieved, the products of hydrogen and carbon dioxide inhibited the carbon monoxide conversion significantly. New efforts towards an improved stability are required to obtain superior low temperature WGS catalysts. In addition, the novel concept of EWGS process provide a new avenue for low temperature WGS, further studies can focus on improving the current density and developing non-noble catalysts to satisfy the requirements of industry.

Methanol can not only serve as a carrier for hydrogen production, but also as a key C1 building block to produce C₂₊ products via C–C coupling. The methanol steam reforming for hydrogen production involves the methanol and water activation simultaneously on the catalysts during the process, in which suppressing the CO formation and improving low-temperature activity are the main research targets. Compared with the cheap and abundant Cu based catalyst, the noble metal catalysts exhibit good low-temperature performance and thermal stability. The emerging Pt₁/α-MoC³³ catalyst demonstrated an preceded activity with low selectivity of carbon monoxide. And CuZnGaO_x³⁰ system provides a new non-syngas route for high quality hydrogen pro-

duction without carbon monoxide. The long-term stability and reaction mechanism require further investigation. Light-driven dehydrogenative coupling of methanol offers atom economic way to produce ethylene glycol under mild conditions, which can selectively activate the unreactive C–H bond of methanol but stabilize the hydroxyl group. The fascinating system shed light on the preferential C–H bond activation to achieve C–C coupling under mild conditions.

The direct conversion of carbon dioxide to methanol, olefins or hydrocarbons has been widely studied with considerable progress. Carbon dioxide hydrogenation to methanol has already been industrialized in Iceland by the Carbon Recycling International company, and the needed hydrogen was produced by water electrolysis using cheap geothermally produced electricity.^{213,217} Compared to the C1 products from carbon dioxide hydrogenation, C₂₊ product synthesis is more fascinating but challenging due to the chemical inertness of C–O bond and high C–C coupling energy barrier. Several newly reported catalysts, such as cobalt catalysts (CoAlO_x)⁴², ordered Pd–Cu nanoparticles,³⁹ and MOFs stabilized Cu centers⁴³ are promising catalysts for thermal-catalytical carbon dioxide hydrogenation to ethanol below 200 °C in liquid phase. Further investigation should be paid on the enhancement of carbon dioxide conversion and reaction rate. Except for the thermal catalysis on carbon dioxide hydrogenation, great progress has been made in the electrochemical reduction of carbon dioxide, which delivers an current density greater than 1 A cm⁻² with C₂₊ Faradaic efficiency around 65%, showing great potential for large-scale application.^{44,45} Future work focused on the operando characterizations to identify the nature of the active sites and to understand the reaction mechanism is necessary to guide the rational design of efficient catalysts for carbon dioxide conversion.

For the conversion of inert methane and carbon dioxide under mild conditions, we usually employ another co-reactant with relatively higher Gibbs energy to make their conversion more favorable thermodynamically. In these reaction processes, strong oxidants and reductants were always the good candidates for the conversion of methane and carbon dioxide, respectively. Hence, design of the efficient catalysts to activate the relatively inert C–H and C–O bond is the key to promote the conversion of methane and carbon dioxide, in which the high loading of single metal atoms confined in the two dimensional materials (graphene, transition metal sulfide, MXene et al.) are the promising catalysts. Noting that such single atoms catalysts also deliver good activity for WGS and MSR processes. Developing the new synthesis methods to achieve the high-loading metal atoms and macroscopic preparation can significantly accelerate the development of C1 catalysis field. In addition, the bifunctional metal oxide/zeolite catalysts show great potential for the hydrogenation of carbon dioxide and carbon monoxide to light olefins or aromatics, which can significantly break the ASF distribution. Precise identification of the real active sites will benefit the preparation of the catalysts with well-defined composition and molecular structure so that undesired carbon dioxide and carbon monoxide formation can be suppressed during catalytic syngas conversion and carbon dioxide hydrogenation.

In conclusion, the highly efficient conversion of C1 molecules into high-value-added fuels or chemicals under mild conditions remains a long-pursued target for C1 catalysis. With the aid of advanced operando techniques, researchers will get deep understanding of the nature of active sites and reaction mechanisms. In addition, with the development of machine learning approach in the age of big data, computational approaches in the search for

new catalysts are less human-intensive and easily parallelizable, which will provide important guidance for the design of next-generation catalysts with compositions and morphologies not previously even considered or realized. Hence, researchers now have a better chance to design efficient catalysts with high activity and selectivity. The prospects of C1 molecules conversion under mild conditions have never been brighter, and offers great hope for the safe and renewable use of fossil fuels.

■ ACKNOWLEDGMENTS

The authors gratefully acknowledge financial support from the National Key R&D Program of China (No. 2016YFA0204100 and 2016YFA0200200), the National Natural Science Foundation of China (No. 21890753 and 21988101), the Key Research Program of Frontier Sciences of the Chinese Academy of Sciences (No. QYZDB-SSW-JSC020), and the DNL Cooperation Fund, Chinese Academy of Sciences (No. DNL180201).

■ AUTHOR CONTRIBUTIONS

Xiaoju Cui and Dehui Deng draft the outline. Xiaoju Cui, Rui Huang and Dehui Deng co-wrote and revised the manuscript.

■ CONFLICT OF INTEREST

The authors declare no conflict of interest.

■ REFERENCES

- Mesters, C. A selection of recent advances in C1 chemistry. *Annu. Rev. Chem. Biomol. Eng.* **7**, 223–238 (2016).
- Zhou, W., Cheng, K., Kang, J., Zhou, C., Subramanian, V., Zhang, Q., Wang, Y. New horizon in C1 chemistry: breaking the selectivity limitation in transformation of syngas and hydrogenation of CO₂ into hydrocarbon chemicals and fuels. *Chem. Soc. Rev.* **48**, 3193–3228 (2019).
- Santos, V. P., Pollefeyt, G., Yancey, D. F., Sandikci, A. C., Vanchura, B., Nieskens, D. L. S., de Kok-Kleiberg, M., Kirilin, A., Chojecki, A., Malek, A. Direct conversion of syngas to light olefins (C₂–C₃) over a tandem catalyst CrZn-SAPO-34: tailoring activity and stability by varying the Cr/Zn ratio and calcination temperature. *J. Catal.* **381**, 108–120 (2020).
- Zhang, Y., Zhao, W. J. Direct conversion of syngas and methane to value-added chemicals. *Natl. Sci. Rev.* **6** (2019) 847–847.
- Xu, Y. F., Liu, J. G., Wang, J., Ma, G. Y., Lin, J. H., Yang, Y., Li, Y. W., Zhang, C. H., Ding, M. Y. Selective conversion of syngas to aromatics over Fe₃O₄@MnO₂ and hollow HZSM-5 bifunctional catalysts. *ACS Catal.* **9**, 5147–5156 (2019).
- Bao, J., Yang, G., Yoneyama, Y., Tsubak, N. Significant advances in C1 catalysis: highly efficient catalysts and catalytic reactions. *ACS Catal.* **9**, 3026–3053 (2019).
- Asundi, A. S., Hoffman, A. S., Bothra, P., Boubnov, A., Vila, F. D., Yang, N. Y., Singh, J. A., Zeng, L., Raiford, J. A., Abild-Pedersen, F., et al. Understanding structure-property relationships of MoO₃-promoted Rh catalysts for syngas conversion to alcohols. *J. Am. Chem. Soc.* **141**, 19655–19668 (2019).
- Kang, Y., Tian, M., Huang, C. D., Lin, J., Hou, B. L., Pan, X. L., Li, L., Rykov, A. I., Wang, J. H., Wang, X. D. Improving syngas selectivity of Fe₂O₃/Al₂O₃ with yttrium modification in chemical looping methane conversion. *ACS Catal.* **9**, 8373–8382 (2019).
- Kousi, K., Neagu, D., Bekris, L., Papaioannou, E. I., Metcalfe, I. S. Endogenous nanoparticles strain perovskite host lattice providing oxygen capacity and driving oxygen exchange and CH₄ conversion to syngas. *Angew. Chem. Int. Ed.* **59**, 2510–2519 (2020).

10. Fornaciari, J. C., Primc, D., Kawashima, K., Wygant, B. R., Verma, S., Spanu, L., Mullins, C. B., Bell, A. T., Weber, A. Z. A Perspective on the electrochemical oxidation of methane to methanol in membrane electrode assemblies. *ACS Energy Lett.* **5**, 2954–2963 (2020).
11. Jouny, M., Hutchings, G. S., Jiao, F. Carbon monoxide electroreduction as an emerging platform for carbon utilization. *Nat. Catal.* **2**, 1062–1070 (2019).
12. Hammond, C., Forde, M. M., Ab Rahim, M. H., Thetford, A., He, Q., Jenkins, R. L., Dimitratos, N., Lopez-Sanchez, J. A., Dummer, N. F., Murphy, D. M., et al. Direct catalytic conversion of methane to methanol in an aqueous medium by using copper-promoted Fe-ZSM-5. *Angew. Chem. Int. Ed.* **51**, 5129–5133 (2012).
13. Rahim, Ab, H., M., Forde, M. M., Jenkins, R. L., Hammond, C., He, Q., Dimitratos, N., Lopez-Sanchez, J. A., Carley, A. F., Taylor, S. H., Wilcock, D. J., et al. Oxidation of methane to methanol with hydrogen peroxide using supported gold-palladium alloy nanoparticles. *Angew. Chem. Int. Ed.* **52**, 1280–1284 (2013). **The first heterogeneous catalytic system for methane oxidation by in-situ H₂O₂ formation.**
14. Zuo, Z., Ramírez, P. J., Senanayake, S. D., Liu, P., Rodriguez, J. A. Low-temperature conversion of methane to methanol on Ce_x/Cu₂O catalysts: water controlled activation of the C-H Bond. *J. Am. Chem. Soc.* **138**, 13810–13813 (2016).
15. Shan, J., Li, M., Allard, L. F., Lee, S., Flytzani-Stephanopoulos, M. Mild oxidation of methane to methanol or acetic acid on supported isolated rhodium catalysts. *Nature* **551**, 605–608 (2017). **The first work for heterogeneous methane coupling with carbon monoxide and oxygen to produce acetic acid at 150 °C.**
16. Liang, Z., Li, T., Kim, M., Asthagiri, A., Weaver, J. F. Low-temperature activation of methane on the IrO₂(110) surface. *Science* **356**, 299–303 (2017). **The work demonstrating the C-H cleavage of methane even occurred at -123 °C.**
17. Sushkevich, V. L., Palatin, D., Ranocchiari, M., van Bokhoven, J. A. Selective anaerobic oxidation of methane enables direct synthesis of methanol. *Science* **356**, 523–527 (2017).
18. Cui, X. J., Li, H. B., Wang, Y., Hu, Y. L., Hua, L., Li, H. Y., Han, X. W., Liu, Q. F., Yang, F., He, L. M., et al. Room-temperature methane conversion by graphene-confined single iron atoms. *Chem* **4**, 1902–1910 (2018).
19. Yang, L., Huang, J., Ma, R., You, R., Zeng, H., Rui, Z. Metal-organic framework-derived IrO₂/CuO catalyst for selective oxidation of methane to methanol. *ACS Energy Lett.* **4**, 2945–2951 (2019).
20. Jin, Z., Wang, L., Zuidema, E., Mondal, K., Zhang, M., Zhang, J., Wang, C., Meng, X., Yang, H., Mesters, C., et al. Hydrophobic zeolite modification for in situ peroxide formation in methane oxidation to methanol. *Science* **367**, 193–197 (2020).
21. Schweitzer, N. M., Schaidle, J. A., Ezekeye, O. K., Pan, X., Linic, S., Thompson, L. T. High activity carbide supported catalysts for water gas shift. *J. Am. Chem. Soc.* **133**, 2378–2381 (2011).
22. Li, C. W., Ciston, J., Kanan, M. W. Electroreduction of carbon monoxide to liquid fuel on oxide-derived nanocrystalline copper. *Nature* **508**, 504–507 (2014).
23. Yang, M., Li, S., Wang, Y., Herron, J. A., Xu, Y., Allard, L. F., Lee, S., Huang, J., Mavrikakis, M., Flytzani-Stephanopoulos, M. Catalytically active Au-O(OH)_x species stabilized by alkali ions on zeolites and mesoporous oxides. *Science* **346**, 1498–1501 (2014). **The work showing the promotion of alkali ions to gold on water gas shift reaction.**
24. Sabnis, K. D., Cui, Y., Akatay, M. C., Shekhar, M., Lee, W.- S., Miller, J. T., Delgass, W. N., Ribeiro, F. H. Water-gas shift catalysis over transition metals supported on molybdenum carbide. *J. Catal.* **331**, 162–171 (2015).
25. Yao, S., Zhang, X., Zhou, W., Gao, R., Xu, W., Ye, Y., Lin, L., Wen, X., Liu, P., Chen, B., et al. Atomic-layered Au clusters on α -MoC as catalysts for the low-temperature water-gas shift reaction. *Science* **357**, 389–393 (2017).
- The work showing water-gas shift reaction happened below 100 °C.**
26. Jouny, M., Luc, W., Jiao, F. High-rate electroreduction of carbon monoxide to multi-carbon products. *Nat. Catal.* **1**, 748–755 (2018). **The work reporting electroreduction of CO to C₂₊ with current density up to 1 A cm⁻².**
27. Cui, X. J., Su, H. Y., Chen, R. X., Yu, L., Dong, J. C., Ma, C., Wang, S. H., Li, J. F., Yang, F., Xiao, J. P., et al. Room-temperature electrochemical water-gas shift reaction for high purity hydrogen production. *Nat. Commun.* **10**, 86 (2019). **The work reporting room-temperature electrochemical water-gas shift reaction for high purity hydrogen production.**
28. Xu, Y., Li, J., Li, W. J., Li, W. Z., Zhang, X. C., Zhao, Y., Xie, J. L., Wang, X. P., Liu, X., Li, Y. W., et al. Direct conversion of CO and H₂O into liquid fuels under mild conditions. *Nat. Commun.* **10**, 1389 (2019).
29. Li, J., Wang, Z., McCallum, C., Xu, Y., Li, F., Wang, Y., Gabardo, C. M., Dinh, C.- T., Zhuang, T.- T., Wang, L., et al. Constraining CO coverage on copper promotes high-efficiency ethylene electroproduction. *Nat. Catal.* **2**, 1124–1131 (2019).
30. Yu, K. M. K., Tong, W., West, A., Cheung, K., Li, T., Smith, G., Guo, Y., Tsang, S. C. E Non-syngas direct steam reforming of methanol to hydrogen and carbon dioxide at low temperature. *Nat. Commun.* **3**, 1230 (2012).
31. Nielsen, M., Alberico, E., Baumann, W., Drexler, H.- J., Junge, H., Gladiali, S., Beller, M. Low-temperature aqueous-phase methanol dehydrogenation to hydrogen and carbon dioxide. *Nature* **495**, 85–89 (2013).
32. Ma, Y., Guan, G., Shi, C., Zhu, A., Hao, X., Wang, Z., Kusakabe, K., Abudula, A. Low-temperature steam reforming of methanol to produce hydrogen over various metal-doped molybdenum carbide catalysts. *Int. J. Hydrogen Energy* **39**, 258–266 (2014).
33. Lin, L., Zhou, W., Gao, R., Yao, S., Zhang, X., Xu, W., Zheng, S., Jiang, Z., Yu, Q., Li, Y.- W., et al. Low-temperature hydrogen production from water and methanol using Pt/ α -MoC catalysts. *Nature* **544**, 80–83 (2017).
34. Xie, S. J., Shen, Z. B., Deng, J., Guo, P., Zhang, Q. H., Zhang, H. K., Ma, C., Jiang, Z., Cheng, J., Deng, D. H., et al. Visible light-driven C-H activation and C-C coupling of methanol into ethylene glycol. *Nat. Commun.* **9**, 1181 (2018). **First work about visible light driven methanol to ethylene glyco.**
35. Chen, L. N., Hou, K. P., Liu, Y. S., Qi, Z. Y., Zheng, Q., Lu, Y. H., Chen, J. Y., Chen, J. L., Pao, C. W., Wang, S. B., et al. Efficient hydrogen production from methanol using a single-site Pt₁/CeO₂ catalyst. *J. Am. Chem. Soc.* **141**, 17995–17999 (2019).
36. Asadi, M., Kumar, B., Behranginia, A., Rosen, B. A., Baskin, A., Repnin, N., Pisasale, D., Phillips, P., Zhu, W., Haasch, R., et al. Robust carbon dioxide reduction on molybdenum disulfide edges. *Nat. Commun.* **5**, 4470 (2014).
37. Asadi, M., Kim, K., Liu, C., Addepalli, A. V., Abbasi, P., Yasaei, P., Phillips, P., Behranginia, A., Cerrato, J. M., Haasch, R., et al. Nanosstructured transition metal dichalcogenide electrocatalysts for CO₂ reduction in ionic liquid. *Science* **353**, 467–470 (2016).
38. Ma, S., Sadakiyo, M., Luo, R., Heima, M., Yamauchi, M., Keen, P. J. A One-step electrosynthesis of ethylene and ethanol from CO₂ in an alkaline electrolyzer. *J. Power Sources* **301**, 219–228 (2016).
39. Bai, S., Shao, Q., Wang, P., Dai, Q., Wang, X., Huang, X. Highly active and selective hydrogenation of CO₂ to ethanol by ordered Pd-Cu nanoparticles. *J. Am. Chem. Soc.* **139**, 6827–6830 (2017).
40. Zhuang, T.- T., Liang, Z.- Q., Seifitokaldani, A., Li, Y., De Luna, P., Burdyny, T., Che, F., Meng, F., Min, Y., Quintero-Bermudez, R., et al. Steering post-C-C coupling selectivity enables high efficiency

- electroreduction of carbon dioxide to multi-carbon alcohols. *Nat. Catal.* **1**, 421–428 (2018).
41. Li, H., Wang, L., Dai, Y., Pu, Z., Lao, Z., Chen, Y., Wang, M., Zheng, X., Zhu, J., Zhang, W., et al. Synergetic interaction between neighbouring platinum monomers in CO₂ hydrogenation. *Nat. Nanotechnol.* **13**, 411–417 (2018).
 42. Wang, L., Wang, L., Zhang, J., Liu, X., Wang, H., Zhang, W., Yang, Q., Ma, J., Dong, X., Yoo, S. J., et al. Selective hydrogenation of CO₂ to ethanol over cobalt catalysts. *Angew. Chem. Int. Ed.* **57**, 6104–6108 (2018).
 43. An, B., Li, Z., Song, Y., Zhang, J., Zeng, L., Wang, C., Lin, W. Cooperative copper centres in a metal-organic framework for selective conversion of CO₂ to ethanol. *Nat. Catal.* **2**, 709–717 (2019).
The work demonstrating Zr/Cu-MOFs for CO₂ to CH₃CH₂OH with selectivity above 99%.
 44. García de Arquer, F. P., Dinh, C.- T., Ozden, A., Wicks, J., McCallum, C., Kirmani, A. R., Nam, D.- H., Gabardo, C., Seifitokaldani, A., Wang, X., et al. CO₂ electrolysis to multcarbon products at activities greater than 1 A cm⁻². *Science* **367**, 661–666 (2020).
The work showing a ionomer bulk heterojunction for CO₂ electroreduction with C₂H₄ partial current density of 1300mA cm⁻².
 45. Ma, W., Xie, S., Liu, T., Fan, Q., Ye, J., Sun, F., Jiang, Z., Zhang, Q., Cheng, J., Wang, Y. Electrocatalytic reduction of CO₂ to ethylene and ethanol through hydrogen-assisted C-C coupling over fluorine-modified copper. *Nat. Catal.* **3**, 478–487 (2020).
 46. Dyballa, M., Pappas, D. K., Kvande, K., Borfecchia, E., Arstad, B., Beato, P., Olsbye, U., Svelle, S. On how copper mordenite properties govern the framework stability and activity in the methane-to-methanol conversion. *ACS Catal.* **9**, 365–375 (2019).
 47. Okolie, C., Belhseine, Y. F., Lyu, Y., Yung, M. M., Engelhard, M. H., Kovarik, L., Stavitski, E., Sievers, C. Conversion of methane into methanol and ethanol over nickel oxide on ceria-zirconia catalysts in a single reactor. *Angew. Chem. Int. Ed.* **56**, 13876–13881 (2017).
 48. Kim, H. J., Huh, J., Kwon, Y. W., Park, D., Yu, Y., Jang, Y. E., Lee, B. R., Jo, E., Lee, E. J., Heo, Y., et al. Biological conversion of methane to methanol through genetic reassembly of native catalytic domains. *Nat. Catal.* **2**, 342–353 (2019).
 49. Oh, S. C., Schulman, E., Zhang, J. Y., Fan, J. F., Pan, Y., Meng, J. Q., Liu, D. X. Direct non-oxidative methane conversion in a millisecond catalytic wall reactor. *Angew. Chem. Int. Ed.* **58**, 7083–7086 (2019).
 50. Hao, J. Q., Schwach, P., Fang, G. Z., Guo, X. G., Zhang, H. L., Shen, H., Huang, X., Eggart, D., Pan, X. L., Bao, X. H. Enhanced methane conversion to olefins and aromatics by H-donor molecules under nonoxidative condition. *ACS Catal.* **9**, 9045–9050 (2019).
 51. Dipu, A. L., Ohbuchi, S., Nishikawa, Y., Iguchi, S., Ogihara, H., Yamanaka, I. Direct nonoxidative conversion of methane to higher hydrocarbons over silica-supported nickel phosphide catalyst. *ACS Catal.* **10**, 375–379 (2020).
 52. Guo, X., Fang, G., Li, G., Ma, H., Fan, H., Yu, L., Ma, C., Wu, X., Deng, D., Wei, M., et al. Direct, nonoxidative conversion of methane to ethylene, aromatics, and hydrogen. *Science* **344**, 616–619 (2014).
 53. Schwach, P., Pan, X., Bao, X. Direct conversion of methane to value-added chemicals over heterogeneous catalysts: challenges and prospects. *Chem. Rev.* **117**, 8497–8520 (2017).
 54. Wang, P., Zhao, G., Wang, Y., Lu, Y. MnTiO₃-driven low-temperature oxidative coupling of methane over TiO₂-doped Mn₂O₃·Na₂WO₄/SiO₂ catalyst. *Sci. Adv.* **3**, e1603180 (2017).
 55. Gallagher, J. Liquid metal methane conversion. *Nat. Energy* **3**, 3 (2018).
 56. Latimer, A. A., Kakekhani, A., Kulkarni, A. R., Norskov, J. K. Direct methane to methanol: the selectivity-conversion limit and design strategies. *ACS Catal.* **8**, 6894–6907 (2018).
 57. Zhu, C. L., Hou, S. S., Hu, X. L., Lu, J. H., Chen, F. L., Xie, K. Electrochemical conversion of methane to ethylene in a solid oxide electrolyzer. *Nat. Commun.* **10**, 1173 (2019).
 58. Yu, X., De Waele, V., Lofberg, A., Ordovsky, V., Khodakov, A. Y. Selective photocatalytic conversion of methane into carbon monoxide over zinc-heteropolyacid-titania nanocomposites. *Nat. Commun.* **10**, 700 (2019).
 59. Song, H., Meng, X. G., Wang, Z. J., Liu, H. M., Ye, J. H. Solar-energy-mediated methane conversion. *Joule* **3**, 1606–1636 (2019).
 60. Huang, K. F., Miller, J. B., Huber, G. W., Dumesic, J. A., Maravelias, C. T. A general framework for the evaluation of direct nonoxidative methane conversion strategies. *Joule* **2**, 349–365 (2018).
 61. Han, Q., Tanaka, A., Matsumoto, M., Endo, A., Kubota, Y., Inagaki, S. Conversion of methane to C₂ and C₃ hydrocarbons over TiO₂/ZSM-5 core-shell particles in an electric field. *RSC Adv* **9**, 34793–34803 (2019).
 62. Xie, P. F., Pu, T. C., Nie, A. M., Hwang, S., Purdy, S. C., Yu, W. J., Su, D., Miller, J. T., Wang, C. Nanoceria-supported single-atom platinum catalysts for direct methane conversion. *ACS Catal.* **8**, 4044–4048 (2018).
 63. Wang, Y. Room-temperature conversion of methane becomes true. *Joule* **2**, 1399–1401 (2018).
 64. Sushkevich, V. L., Palagin, D., van Bokhoven, J. A. The effect of the active-site structure on the activity of copper mordenite in the aerobic and anaerobic conversion of methane into methanol. *Angew. Chem. Int. Ed.* **57**, 8906–8910 (2018).
 65. Tomkins, P., Ranocchiari, M., van Bokhoven, J. A. Direct conversion of methane to methanol under mild conditions over Cu-zeolites and beyond. *Acc. Chem. Res.* **50**, 418–425 (2017).
 66. Huang, W., Xie, K. C., Wang, J. P., Gao, Z. H., Yin, L. H., Zhu, Q. M. Possibility of direct conversion of CH₄ and CO₂ to high-value products. *J. Catal.* **201**, 100–104 (2001).
 67. Wu, J. F., Yu, S. M., Wang, W. D., Fan, Y. X., Bai, S., Zhang, C. W., Gao, Q., Huang, J., Wang, W. Mechanistic insight into the formation of acetic acid from the direct conversion of methane and carbon dioxide on zinc-modified H-ZSM-5 zeolite. *J. Am. Chem. Soc.* **135**, 13567–13573 (2013).
 68. Wang, L., Yi, Y., Wu, C., Guo, H., Tu, X. One-step reforming of CO₂ and CH₄ into high-value liquid chemicals and fuels at room temperature by plasma-driven catalysis. *Angew. Chem. Int. Ed.* **56**, 13679–13683 (2017).
 69. Lin, M., Sen, A. Direct catalytic conversion of methane to acetic acid in an aqueous medium. *Nature* **368**, 613–615 (1994).
 70. Tang, Y., Li, Y., Fung, V., Jiang, D. E., Huang, W., Zhang, S., Iwasawa, Y., Sakata, T., Nguyen, L., Zhang, X., et al. Single rhodium atoms anchored in micropores for efficient transformation of methane under mild conditions. *Nat. Commun.* **9**, 1231 (2018).
 71. Huang, W., Zhang, S., Tang, Y., Li, Y., Nguyen, L., Li, Y., Shan, J., Xiao, D., Gagne, R., Frenkel, A. I., et al. Low-temperature transformation of methane to methanol on Pd₁O₄ single sites anchored on the internal surface of microporous silicate. *Angew. Chem. Int. Ed.* **55**, 13441 (2016).
 72. Kwon, Y., Kim, T. Y., Kwon, G., Yi, J., Lee, H. Selective activation of methane on single-atom catalyst of rhodium dispersed on zirconia for direct conversion. *J. Am. Chem. Soc.* **139**, 17694–17699 (2017).
 73. Bai, S., Liu, F., Huang, B., Li, F., Lin, H., Wu, T., Sun, M., Wu, J., Shao, Q., Xu, Y., et al. High-efficiency direct methane conversion to oxygenates on a cerium dioxide nanowires supported rhodium single-atom catalyst. *Nat. Commun.* **11**, 954 (2020).
 74. Song, W. G., Shen, Q., Cao, C., Huang, R., Zhu, L., Zhou, X., Zhang, Q., Gu, L. Single chromium atoms supported on titanium dioxide nanoparticles for synergic catalytic methane conversion under mild conditions. *Angew. Chem. Int. Ed.* **59**, 1216–1219 (2019).
 75. Williams, C., Carter, J. H., Dummer, N. F., Chow, Y. K., Morgan, D. J., Yacob, S., Serna, P., Wilcock, D. J., Meyer, R. J., Taylor, S. H., et al. Selective oxidation of methane to methanol using supported AuPd catalysts prepared by stabilizer-free sol-immobilization. *ACS Catal.* **8**, 2567–2576 (2018).

76. Rahim, Ab, M., Forde, M., Hammond, C., Jenkins, R. L., Dimitratos, N., Lopez-Sanchez, J. A., Carley, A. F., Taylor, S. H., Willock, D. J., Hutchings, G. J. Systematic study of the oxidation of methane using supported gold palladium nanoparticles under mild aqueous conditions. *Top. Catal.* **56**, 1843–1857 (2013).
77. Zhou, H., Liu, T., Zhao, X., Zhao, Y., Lv, H., Fang, S., Wang, X., Zhou, F., Xu, Q., Xu, J., et al. A supported nickel catalyst stabilized by a surface digging effect for efficient methane oxidation. *Angew. Chem. Int. Ed.* **131**, 18559–18564 (2019).
78. Osadchii, D. Y., Olivos-Suarez, A. I., Szécsényi, Á., Li, G., Nasalevich, M. A., Dugulan, I. A., Crespo, P. S., Hensen, E. J. M., Veber, S. L., Fedin, M. V., et al. Isolated Fe sites in metal organic frameworks catalyze the direct conversion of methane to methanol. *ACS Catal.* **8**, 5542–5548 (2018).
79. Agarwal, N., Freakley, S. J., McVicker, R. U., Althahban, S. M., Dimitratos, N., He, Q., Morgan, D. J., Jenkins, R. L., Willock, D. J., Taylor, S. H., et al. Aqueous Au-Pd colloids catalyze selective CH₄ oxidation to CH₃OH with O₂ under mild conditions. *Science* **358**, 223–227 (2017).
80. Bai, S., Yao, Q., Xu, Y., Cao, K., Huang, X. Strong synergy in a lichen-like RuCu nanosheet boosts the direct methane oxidation to methanol. *Nano Energy* **71**, 104566 (2020).
81. Bai, S., Xu, Y., Wang, P., Shao, Q., Huang, X. Activating and converting CH₄ to CH₃OH via the CuPdO₂/CuO nanointerface. *ACS Catal.* **9**, 6938–6944 (2019).
82. Liu, Z., Huang, E., Orozco, I., Liao, W., Palomino1, R. M., Rui, N., Duchoň, T., Nemšák, S., Grinter, D. C., Mahapatra, M., et al. Water-promoted interfacial pathways in methane oxidation to methanol on a CeO₂-Cu₂O catalyst. *Science* **368**, 513–517 (2020).
83. Lustemberg, P. G., Palomino, R. M., Gutiérrez, R. A., Grinter, D. C., Vorokhta, M., Liu, Z., Ramírez, P. J., Matolín, V., Ganduglia-Pirovano, M. V., Senanayake, S. D., et al. Direct conversion of methane to methanol on Ni-Ceria surfaces: metal-support interactions and water-enabled catalytic conversion by site blocking. *J. Am. Chem. Soc.* **140**, 7681–7687 (2018).
84. Ikuno, T., Zheng, J., Vjunov, A., Sanchez-Sanchez, M., Ortuño, M. A., Pahls, D. R., Fulton, J. L., Camaiomi, D. M., Li, Z., Ray, D. Methane oxidation to methanol catalyzed by Cu-Oxo clusters stabilized in NU-1000 metal-organic framework. *J. Am. Chem. Soc.* **139**, 10294–10301 (2017).
85. Mahyuddin, M. H., Shiota, Y., Yoshizawa, K. Methane selective oxidation to methanol by metal-exchanged zeolites: a review of active sites and their reactivity. *Catal. Sci. Technol.* **9**, 1744–1768 (2019).
86. Sushkevich, V. L., Verel, R., van Bokhoven, J. A. Pathways of methane transformation over copper-exchanged mordenite as revealed by in situ NMR and IR spectroscopy. *Angew. Chem. Int. Ed.* **59**, 910–918 (2019).
87. Latimer, A. A., Kulkarni, A. R., Aljama, H., Montoya, J. H., Yoo, J. S., Tsai, C., Abild-Pedersen, F., Studt, F., Nørskov, J. K. Understanding trends in C–H bond activation in heterogeneous catalysis. *Nat. Mater.* **16**, 225–229 (2017).
88. Labinger, J. A. Comment on “Selective anaerobic oxidation of methane enables direct synthesis of methanol”. *Science* **359**, eaar4968 (2018).
89. Periana, R. A. Comment on “Selective anaerobic oxidation of methane enables direct synthesis of methanol”. *Science* **358**, eaan5970 (2017).
90. Paulik, F. E., Roth, J. F. Novel catalysts for the low-pressure carbonylation of methanol to acetic acid. *Chem. Commun.* **24**, 1578 (1968).
91. Lin, M., Hogan, T. E., Sen, A. Catalytic carbon-carbon and carbon-hydrogen bond cleavage in lower alkanes. Low-temperature hydroxylations and hydroxycarbonylations with dioxygen as the oxidant. *J. Am. Chem. Soc.* **118**, 4574–4580 (1996).
92. Kalaguine, S. L., Shelimov, B. N., Kazansky, V. B. Reactions of methane and ethane with hole centers O[−]. *J. Catal.* **55**, 384–393 (1978).
93. Xie, J., Jin, R., Li, A., Bi, Y., Ruan, Q., Deng, Y., Zhang, Y., Yao, S., Sankar, G., Ma, D., et al. Highly selective oxidation of methane to methanol at ambient conditions by titanium dioxide-supported iron species. *Nat. Catal.* **1**, 889–896 (2018).
94. Song, H., Meng, X., Wang, S., Zhou, W., Wang, X., Kako, T., Ye, J. Direct and selective photocatalytic oxidation of CH₄ to oxygenates with O₂ on cocatalysts/ZnO at room temperature in water. *J. Am. Chem. Soc.* **141**, 20507–20515 (2019).
95. Jang, J., Shen, K., Morales-Guio, C. G. Electrochemical direct partial oxidation of methane to methanol. *Joule* **3**, 2589–2593 (2019).
96. Xie, S., Lin, S., Zhang, Q., Tian, Z., Wang, Y. Selective electrocatalytic conversion of methane to fuels and chemicals. *J. Energy Chem.* **27**, 1629–1636 (2018).
97. Su, J. J., Zhou, H. B., Liu, S., Wang, C. M., Jiao, W. Q., Wang, Y. D., Liu, C., Ye, Y. C., Zhang, L., Zhao, Y., et al. Syngas to light olefins conversion with high olefin/paraffin ratio using ZnCrOx/AIPO-18 bifunctional catalysts. *Nat. Commun.* **10**, 1297 (2019).
98. Zhou, W., Kang, J. C., Cheng, K., He, S., Shi, J. Q., Zhou, C., Zhang, Q. H., Chen, J. C., Peng, L. M., Chen, M. S., et al. Direct conversion of syngas into methyl acetate, ethanol, and ethylene by relay catalysis via the intermediate dimethyl ether. *Angew. Chem. Int. Ed.* **57**, 12012–12016 (2018).
99. Gupta, M., Smith, M. L., Spivey, J. J. Heterogeneous catalytic conversion of dry syngas to ethanol and higher alcohols on Cu-based catalysts. *ACS Catal.* **1**, 641–656 (2011).
100. Ma, S. C., Huang, S. D., Liu, Z. P. Dynamic coordination of cations and catalytic selectivity on zinc-chromium oxide alloys during syngas conversion. *Nat. Catal.* **2**, 671–677 (2019).
101. Li, G., Jiao, F., Miao, D. Y., Wang, Y., Pan, X. L., Yokoi, T., Meng, X. J., Xiao, F. S., Parvulescu, A. N., Muller, U., et al. Selective conversion of syngas to propane over ZnCrOx-SSZ-39 OX-ZEO catalysts. *J. Energy Chem.* **36**, 141–147 (2019).
102. Lin, T. J., Qi, X. Z., Wang, X. X., Xia, L., Wang, C. Q., Yu, F., Wang, H., Li, S. G., Zhong, L. S., Sun, Y. H. Direct production of higher oxygenates by syngas conversion over a multifunctional catalyst. *Angew. Chem. Int. Ed.* **58**, 4627–4631 (2019).
103. Li, N., Jiao, F., Pan, X. L., Ding, Y., Feng, J. Y., Bao, X. H. Size effects of ZnO nanoparticles in bifunctional catalysts for selective syngas conversion. *ACS Catal.* **9**, 960–966 (2019).
104. Cheng, K., Zhou, W., Kang, J. C., He, S., Shi, S. L., Zhang, Q. H., Pan, Y., Wen, W., Wang, Y. Bifunctional catalysts for one-step conversion of syngas into aromatics with excellent selectivity and stability. *Chem* **3**, 334–347 (2017).
105. Peña, D., Jensen, L., Cognigni, A., Myrstad, R., Neumayer, T., van Beek, W., Rønning, M. The effect of copper loading on iron carbide formation and surface species in iron-based Fischer-Tropsch synthesis catalysts. *ChemCatChem* **10**, 1300–1312 (2018).
106. Li, S., Krishnamoorthy, S., Li, A., Meitzner, G. D., Iglesia, E. Promoted iron-based catalysts for the fischer-tropsch synthesis: design, synthesis, site densities, and catalytic properties. *J. Catal.* **206**, 202–217 (2002).
107. Iglesia, E. Design, synthesis, and use of cobalt-based Fischer-Tropsch synthesis catalysts. *Appl. Catal. A: Gen.* **161**, 59–78 (1997).
108. Lyu, S., Wang, L., Zhang, J., Liu, C., Sun, J., Peng, B., Wang, Y., Rappé, K. G., Zhang, Y., Li, J., et al. Role of active phase in Fischer-Tropsch synthesis: experimental evidence of CO activation over single-phase cobalt catalysts. *ACS Catal.* **8**, 7787–7798 (2018).
109. Dry, M. E. Fischer-Tropsch synthesis over iron catalysts. *Catal. Lett.* **7**, 241–251 (1990).
110. Khodakov, A. Y., Chu, W., Fongarland, P. Advances in the development of novel cobalt Fischer-Tropsch catalysts for synthesis of long-chain hydrocarbons and clean fuels. *Chem. Rev.* **107**, 1692–1744 (2007).
111. Jiao, F., Li, J. J., Pan, X. L., Xiao, J. P., Li, H. B., Ma, H., Wei, M. M., Pan, Y., Zhou, Z. Y., Li, M. R., et al. Selective conversion of syngas to light olefins. *Science* **351**, 1065–1068 (2016).
112. Wang, Y. A new horizon in C1 chemistry: highly selective

- conversion of syngas to light olefins by a novel OX-ZEO process. *J. Energy Chem.* **25**, 169–170 (2016).
113. Cheng, K., Gu, B., Liu, X. L., Kang, J. C., Zhang, Q. H., Wang, Y. Direct and highly selective conversion of synthesis gas into lower olefins: design of a bifunctional catalyst combining methanol synthesis and carbon-carbon coupling. *Angew. Chem. Int. Ed.* **55**, 4725–4728 (2016).
 114. Guo, X.- N., Jiao, Z.- F., Jin, G.- Q., Guo, X.- Y. Photocatalytic fischer-tropsch synthesis on graphene-supported worm-like ruthenium nanostructures. *ACS Catal.* **5**, 3836–3840 (2015).
 115. Chen, G. B., Waterhouse, G. I. N., Shi, R., Zhao, J. Q., Li, Z. H., Wu, L. Z., Tung, C. H., Zhang, T. R. From solar energy to fuels: recent advances in light-driven C₁ chemistry. *Angew. Chem. Int. Ed.* **58**, 17528–17551 (2019).
 116. Pang, Y., Li, J., Wang, Z., Tan, C.- S., Hsieh, P.- L., Zhuang, T.- T., Liang, Z.- Q., Zou, C., Wang, X., De Luna, P., et al. Efficient electrocatalytic conversion of carbon monoxide to propanol using fragmented copper. *Nat. Catal.* **2**, 251–258 (2019).
 117. Uribe, F. A. S., P. , R., Bard, A. J. Electrochemistry in liquid ammonia—Part VI. Reduction of carbon monoxide. *J. Electroanal. Chem.* **152**, 173–182 (1983).
 118. Petrova, G. N. E., O. , N., Strelets, V. V. Electroreduction of carbon monoxide in aqueous solutions of molybdenum (III)-pyrocatechol complex. *Izv. Akad. Nauk SSSR. Ser. Khim.*, 2608–2610 (1982).
 119. Lum, Y., Cheng, T., Goddard, W. A. 3rd, Ager, J. W. Electrochemical CO reduction builds solvent water into oxygenate products. *J. Am. Chem. Soc.* **140**, 9337–9340 (2018).
 120. Gao, W., Gao, R., Zhao, Y. F., Peng, M., Song, C. Q., Li, M. Z., Li, S. W., Liu, J. J., Li, W. Z., Deng, Y. C., et al. Photo-driven syngas conversion to lower olefins over oxygen-decorated Fe₅C₂ catalyst. *Chem* **4**, 2917–2928 (2018).
 121. Xiong, H. F., Jewell, L. L., Coville, N. J. Shaped carbons as supports for the catalytic conversion of syngas to clean fuels. *ACS Catal.* **5**, 2640–2658 (2015).
 122. Cheng, T., Xiao, H., Goddard, W. A. Full atomistic reaction mechanism with kinetics for CO reduction on Cu(100) from ab initio molecular dynamics free-energy calculations at 298K. *Proc. Natl. Acad. Sci. U. S. A.* **114**, 1795–1800 (2017).
 123. Feng, X. F., Jiang, K. L., Fan, S. S., Kanan, M. W. A direct grain-boundary-activity correlation for CO electroreduction on Cu nanoparticles. *ACS Central Sci.* **2**, 169–174 (2016).
 124. Han, L., Zhou, W., Xiang, C. High-rate electrochemical reduction of carbon monoxide to ethylene using Cu-nanoparticle-based gas diffusion electrodes. *ACS Energy Lett.* **3**, 855–860 (2018).
 125. Bertheussen, E., Hogg, T. V., Abghouli, Y., Engstfeld, A. K., Chorkendorff, I., Stephens, I. E. L. Electroreduction of CO on polycrystalline copper at low overpotentials. *ACS Energy Lett.* **3**, 634–640 (2018).
 126. Ripatti, D. S., Veltman, T. R., Kanan, M. W. Carbon monoxide gas diffusion electrolysis that produces concentrated C₂ products with high single-pass conversion. *Joule* **3**, 240–256 (2019).
 127. Hori, Y. M. A., Takahashi, R., Suzuki, S. Electroreduction of carbon monoxide to methane and ethylene at a copper electrode in aqueous solutions at ambient temperature and pressure. *J. Am. Chem. Soc.* **109**, 5022–5023 (1987).
 128. Yamamura, S. K. H., Kawai, W. Photoelectrochemical reduction of carbon monoxide using p-Si. *J. Electroanal. Chem.* **186**, 309–312 (1985).
 129. Yoneyama, H. W. K., Hatanaka, N., Tamura, H. Photoelectrochemical reduction of carbon monoxide on iron (II) tetraphenylporphyrin-coated p-type GaP electrodes. *Chem. Lett.*, 539–542 (1985).
 130. Wang, L., Nitopi, S. A., Bertheussen, E., Orazov, M., Morales-Guio, C. G., Liu, X., Higgins, D. C., Chan, K., Nørskov, J. K., Hahn, C., et al. Electrochemical carbon monoxide reduction on polycrystalline copper: effects of potential, pressure, and pH on selectivity toward multicarbon and oxygenated products. *ACS Catal.* **8**, 7445–7454 (2018).
 131. Raciti, D., Cao, L., Liv, K. J. T., Rottmann, P. F., Tang, X., Li, C. Y., Hicks, Z., Bowen, K. H., Hemker, K. J., Mueller, T., et al. Low-overpotential electroreduction of carbon monoxide using copper nanowires. *ACS Catal.* **7**, 4467–4472 (2017).
 132. Wang, Y., Raciti, D., Wang, C. High-flux CO reduction enabled by three-dimensional nanostructured copper electrodes. *ACS Catal.* **8**, 5657–5663 (2018).
 133. Chen, R., Su, H.- Y., Liu, D., Huang, R., Meng, X., Cui, X., Tian, Z., Zhang, D.- H., Deng, D. Highly selective production of ethylene by electroreduction of carbon monoxide. *Angew. Chem. Int. Ed.* **59**, 154–160 (2020).
 134. Rodriguez, J. A., Remesal, E. R., Ramirez, P. J., Orozco, I., Liu, Z. Y., Graciani, J., Senanayake, S. D., Sanz, J. F. Water gas shift reaction on K/Cu(111) and Cu/K/TiO₂(110) surfaces: alkali promotion of water dissociation and production of H₂. *ACS Catal.* **9**, 10751–10760 (2019).
 135. Zhu, T., Liu, C., Tan, X. Y., Huan, B., Bian, G. Q., Shao, Q., Bai, S. X., Qian, Y., Li, Y. Y., Huang, X. Q. Se-incorporation stabilizes and activates metastable MoS₂ for efficient and cost-effective water gas shift reaction. *ACS Nano* **13**, 11303–11309 (2019).
 136. Stepić, R., Wick, C. R., Strobel, V., Berger, D., Vučemilović-Alagić, N., Haumann, M., Wasserscheid, P., Smith, A. S., Smith, D. M. Mechanism of the water-gas shift reaction catalyzed by efficient ruthenium-based catalysts: a computational and experimental study. *Angew. Chem. Int. Ed.* **58**, 741–745 (2019).
 137. Zhu, M. H., Tian, P. F., Kurtz, R., Lunkenbein, T., Xu, J., Schlogl, R., Wachs, I. E., Han, Y. F. Strong metal-support interactions between copper and iron oxide during the high-temperature water-gas shift reaction. *Angew. Chem. Int. Ed.* **58**, 9083–9087 (2019).
 138. Liu, N., Xu, M., Yang, Y. S., Zhang, S. M., Zhang, J., Wang, W. L., Zheng, L. R., Hong, S., Wei, M. Au^{δ+}–O_v–Ti⁴⁺ interfacial site: catalytic active center toward low-temperature water gas shift reaction. *ACS Catal.* **9**, 2707–2717 (2019).
 139. Zhao, L., Qi, Y., Song, L., Ning, S., Ouyang, S., Xu, H., Ye, J. Solar-driven water-gas shift reaction over CuO_x/Al₂O₃ with 1.1 % of light-to-energy storage. *Angew. Chem. Int. Ed.* **58**, 7708–7712 (2019).
 140. Andreeva, D., Idakiev, V., Tabakova, T., Andreev, A. Low-temperature water-gas shift reaction over Au/α-Fe₂O₃. *J. Catal.* **158**, 354–355 (1996).
 141. Ratnasamy, C., Wagner, J. P. Water gas shift catalysis. *Catal. Rev.* **51**, 325–440 (2009).
 142. Li, Y., Fu, Q., Flytzani-Stephanopoulos, M. Low-temperature water-gas shift reaction over Cu- and Ni-loaded cerium oxide catalysts. *Appl. Catal. B: Environ.* **27**, 179–191 (2000).
 143. Ammal, S. C., Heyden, A. Understanding the nature and activity of supported platinum catalysts for the water-gas shift reaction: from metallic nanoclusters to alkali-stabilized single-atom cations. *ACS Catal.* **9**, 7721–7740 (2019).
 144. Bahmanpour, A. M., Heroguel, F., Kilic, M., Baranowski, C. J., Artiglia, L., Rothlisberger, U., Luterbacher, J. S., Krocher, O. Cu-Al spinel as a highly active and stable catalyst for the reverse water gas shift reaction. *ACS Catal.* **9**, 6243–6251 (2019).
 145. Stepić, R., Wick, C. R., Strobel, V., Berger, D., Vučemilović-Alagić, N., Haumann, M., Wasserscheid, P., Smith, A.- S., Smith, D. M. Mechanism of the water-gas shift reaction catalyzed by efficient ruthenium-based catalysts: a computational and experimental study. *Angew. Chem. Int. Ed.* **58**, 741–745 (2019).
 146. Dong, J., Fu, Q., Jiang, Z., Mei, B., Bao, X. Carbide-supported Au catalysts for water-gas shift reactions: a new territory for the strong metal-support interaction effect. *J. Am. Chem. Soc.* **140**, 13808–13816 (2018).
 147. Gonzalez Castaño, M., Reina, T. R., Ivanova, S., Centeno, M. A., Odriozola, J. A. Pt vs. Au in water-gas shift reaction. *J. Catal.* **314**, 1–9 (2014).
 148. Zugic, B., Zhang, S., Bell, D. C., Tao, F., Flytzani-Stephanopoulos, M. Probing the low-temperature water-gas shift activity of

- alkali-promoted platinum catalysts stabilized on carbon supports. *J. Am. Chem. Soc.* **136**, 3238–3245 (2014).
149. Fu, Q., Saltsburg, H., Flytzani-Stephanopoulos, M. Active non-metallic Au and Pt species on ceria-based water-gas shift catalysts. *Science* **301**, 935–938 (2003).
 150. Lin, J., Wang, A., Qiao, B., Liu, X., Yang, X., Wang, X., Liang, J., Li, J., Liu, J., Zhang, T. Remarkable performance of Ir₁/FeO_x single-atom catalyst in water gas shift reaction. *J. Am. Chem. Soc.* **135**, 15314–15317 (2013).
 151. Sastre, F., Oteri, M., Corma, A., García, H. Photocatalytic water gas shift using visible or simulated solar light for the efficient, room-temperature hydrogen generation. *Energy Environ. Sci.* **6**, 2211–2215 (2013).
 152. Oettel, C., Rihko-Struckmann, L., Sundmacher, K. Characterisation of the electrochemical water gas shift reactor (EWGSR) operated with hydrogen and carbon monoxide rich feed gas. *Int. J. Hydrogen Energy.* **37**, 11759–11771 (2012).
 153. Oettel, C., Rihko-Struckmann, L., Sundmacher, K. Combined generation and separation of hydrogen in an electrochemical water gas shift reactor (EWGSR). *Int. J. Hydrg. Energy.* **37**, 6635–6645 (2012).
 154. Palo, D. R., Dagle, R. A., Holladay, J. D. Methanol steam reforming for hydrogen production. *Chem. Rev.* **107**, 3992–4021 (2007).
 155. Tian, P., Wei, Y., Ye, M., Liu, Z. Methanol to olefins (MTO): from fundamentals to commercialization. *ACS Catal.* **5**, 1922–1938 (2015).
 156. Sá, S., Silva, H., Brandão, L., Sousa, J. M., Mendes, A. Catalysts for methanol steam reforming-a review. *Appl. Catal. B: Environ.* **99**, 43–57 (2010).
 157. Mateos-Pedrero, C., Silva, H., Tanaka, D. A. P., Liguori, S., Iulianelli, A., Basile, A., Mendes, A. CuO/ZnO catalysts for methanol steam reforming: the role of the support polarity ratio and surface area. *Appl. Catal. B: Environ.* **174**, 67–76 (2015).
 158. Zhang, H., Sun, J., Dagle, V. L., Halevi, B., Datye, A. K., Wang, Y. Influence of ZnO facets on Pd/ZnO catalysts for methanol steam reforming. *ACS Catal.* **4**, 2379–2386 (2014).
 159. Qing, S., Hou, X., Liu, Y., Li, L., Wang, X., Gao, Z., Fan, W. Strategic use of CuAlO₂ as a sustained release catalyst for production of hydrogen from methanol steam reforming. *Chem. Commun.* **54**, 12242–12245 (2018).
 160. Iwasa, N., Mayanagi, T., Ogawa, N., Sakata, K., Takezawa, N. New catalytic functions of Pd-Zn, Pd-Ga, Pd-In, Pt-Zn, Pt-Ga and Pt-In alloys in the conversions of methanol. *Catal. Lett.* **54**, 119–123 (1998).
 161. Zhu, X., Hofmann, J. P., Mezari, B., Kosinov, N., Wu, L., Qian, Q., Weckhuysen, B. M., Asahina, S., Ruiz-Martínez, J., Hensen, E. J. M. Trimodal porous hierarchical SSZ-13 zeolite with improved catalytic performance in the methanol-to-olefins reaction. *ACS Catal.* **6**, 2163–2177 (2016).
 162. Zhang, J., Qian, W., Kong, C., Wei, F. Increasing para-xylene selectivity in making aromatics from methanol with a surface-modified Zn/P/ZSM-5 catalyst. *ACS Catal.* **5**, 2982–2988 (2015).
 163. Xu, S., Zhi, Y., Han, J., Zhang, W., Wu, X., Sun, T., Wei, Y., Liu, Z. Chapter Two-Advances in catalysis for methanol-to-olefins conversion. *Adv. Catal.*, 37–122 (2017).
 164. Sun, Q., Xie, Z., Yu, J. The state-of-the-art synthetic strategies for SAPO-34 zeolite catalysts in methanol-to-olefin conversion. *Natl. Sci. Rev.* **5**, 542–558 (2017).
 165. Chang, C. D., Silvestri, A. J. The conversion of methanol and other O-compounds to hydrocarbons over zeolite catalysts. *J. Catal.* **47**, 249–259 (1977).
 166. Olsbye, U., Svelle, S., Bjørgen, M., Beato, P., Janssens, T. V. W., Joensen, F., Bordiga, S., Lillerud, K. P Conversion of methanol to hydrocarbons: how zeolite cavity and pore size controls product selectivity. *Angew. Chem. Int. Ed.* **51**, 5810–5831 (2012).
 167. Li, C., Paris, C., Martínez-Triguero, J., Boronat, M., Moliner, M., Corma, A. Synthesis of reaction-adapted zeolites as methanol-to-olefins catalysts with mimics of reaction intermediates as organic structure-directing agents. *Nat. Catal.* **1**, 547–554 (2018).
 168. Hereijgers, B. P. C., Bleken, F., Nilsen, M. H., Svelle, S., Lillerud, K.- P., Bjørgen, M., Weckhuysen, B. M., Olsbye, U Product shape selectivity dominates the methanol-to-olefins (MTO) reaction over H-SAPO-34 catalysts. *J. Catal.* **264**, 77–87 (2009).
 169. Ilias, S., Bhan, A. Mechanism of the catalytic conversion of methanol to hydrocarbons. *ACS Catal.* **3**, 18–31 (2013).
 170. Keil, F. J. Methanol-to-hydrocarbons: process technology. *Micropor. Mesopor. Mat.* **29**, 49–66 (1999).
 171. Chen, J. Q., Bozzano, A., Glover, B., Fuglerud, T., Kvistle, S. Recent advancements in ethylene and propylene production using the UOP/Hydro MTO process. *Catal. Today.* **106**, 103–107 (2005).
 172. Haynes, A. Acetic acid synthesis by catalytic carbonylation of methanol. *Catalytic carbonylation reactions*, 179–205 (2006).
 173. Moran, J., Preetz, A., Mesch, R. A., Krische, M. J. Iridium-catalysed direct C-C coupling of methanol and allenes. *Nat. Chem.* **3**, 287–290 (2011).
 174. Shozo, Y., Takayuki, A., Hiroshi, S. Photocatalytic hydrogen evolution from water using zinc-sulfide and sacrificial electron-donors. *Chem. Lett.* **11**, 1069–1070 (1982).
 175. Yanagida, S., Azuma, T., Kawakami, H., Kizumoto, H., Sakurai, H. Photocatalytic carbon-carbon bond formation with concurrent hydrogen evolution on colloidal zinc sulphide. *J. Chem. Soc. Chem. Commun.* **1**, 21–22 (1984).
 176. Chen, L., Gu, W., Zhu, X., Wang, F., Song, Y., Hu, J. Highly efficient hydrogen and ethylene glycol photoproduction from aqueous methanol solution by ZnS and an in situ spin trapping investigation. *J. Photoch. Photobio. A.* **74**, 85–89 (1993).
 177. Centi, G., Quadrelli, E. A., Perathoner, S. Catalysis for CO₂ conversion: a key technology for rapid introduction of renewable energy in the value chain of chemical industries. *Energy Environ. Sci.* **6**, 1711–1731 (2013).
 178. Olah, G. A., Prakash, G. K. S., Goeppert, A Anthropogenic chemical carbon cycle for a sustainable future. *J. Am. Chem. Soc.* **133**, 12881–12898 (2011).
 179. Shih, C. F., Zhang, T., Li, J., Bai, C. Powering the future with liquid sunshine. *Joule* **2**, 1–25 (2018).
 180. Shaner, M. R., Atwater, H. A., Lewis, N. S., McFarland, E. W. A comparative technoeconomic analysis of renewable hydrogen production using solar energy. *Energy Environ. Sci.* **9**, 2354–2371 (2016).
 181. Guan, J., Duan, Z., Zhang, F., Kelly, S. D., Si, R., Dupuis, M., Huang, Q., Chen, J. Q., Tang, C., Li, C. Water oxidation on a mononuclear manganese heterogeneous catalyst. *Nat. Catal.* **1**, 870–877 (2018).
 182. Liao, F. L., Huang, Y. Q., Ge, J. W., Zheng, W. R., Tedsree, K., Collier, P., Hong, X. L., Tsang, S. C. Morphology-dependent interactions of ZnO with Cu nanoparticles at the materials' interface in selective hydrogenation of CO₂ to CH₃OH. *Angew. Chem. Int. Ed.* **50**, 2162–2165 (2011).
 183. Le Valant, A., Comminges, C., Tisseraud, C., Canaff, C., Pinard, L., Pouilloux, Y The Cu-ZnO synergy in methanol synthesis from CO₂, Part 1: origin of active site explained by experimental studies and a sphere contact quantification model on Cu plus ZnO mechanical mixtures. *J. Catal.* **324**, 41–49 (2015).
 184. Gao, P., Li, F., Zhao, N., Xiao, F. K., Wei, W., Zhong, L. S., Sun, Y. H. Influence of modifier (Mn, La, Ce, Zr and Y) on the performance of Cu/Zn/Al catalysts via hydrotalcite-like precursors for CO₂ hydrogenation to methanol. *Appl. Catal. A: Gen.* **468**, 442–452 (2013).
 185. Guo, X. M., Mao, D. S., Lu, G. Z., Wang, S., Wu, G. S. Glycine-nitrate combustion synthesis of CuO-ZnO-ZrO₂ catalysts for methanol synthesis from CO₂ hydrogenation. *J. Catal.* **271**, 178–185 (2010).
 186. Liu, X. M., Lu, G. Q., Yan, Z. F. Nanocrystalline zirconia as catalyst support in methanol synthesis. *Appl. Catal. A: Gen.* **279**, 241–245 (2005).
 187. Guo, X. M., Mao, D. S., Lu, G. Z., Wang, S., Wu, G. S. The influence of La doping on the catalytic behavior of Cu/ZrO₂ for methanol

- synthesis from CO₂ hydrogenation. *J. Mol. Catal. A-Chem.* **345**, 60–68 (2011).
188. An, B., Zhang, J. Z., Cheng, K., Ji, P. F., Wang, C., Lin, W. B. Confinement of ultrasmall Cu/ZnOx nanoparticles in metal-organic frameworks for selective methanol synthesis from catalytic hydrogenation of CO₂. *J. Am. Chem. Soc.* **139**, 3834–3840 (2017).
189. An, B., Zeng, L., Jia, M., Li, Z., Lin, Z., Song, Y., Zhou, Y., Cheng, J., Wang, C., Lin, W. Molecular iridium complexes in metal-organic frameworks catalyze CO₂ hydrogenation via concerted proton and hydride transfer. *J. Am. Chem. Soc.* **139**, 17747–17750 (2017).
190. Xu, J. H., Su, X., Liu, X. Y., Pan, X. L., Pei, G. X., Huang, Y. Q., Wang, X. D., Zhang, T., Geng, H. R. Methanol synthesis from CO₂ and H₂ over Pd/ZnO/Al₂O₃: catalyst structure dependence of methanol selectivity. *Appl. Catal. A: Gen.* **514**, 51–59 (2016).
191. Liang, X. L., Dong, X., Lin, G. D., Zhang, H. B. Carbon nanotube-supported Pd-ZnO catalyst for hydrogenation of CO₂ to methanol. *Appl. Catal. B: Environ.* **88**, 315–322 (2009).
192. Rui, N., Wang, Z. Y., Sun, K. H., Ye, J. Y., Ge, Q. F., Liu, C. J. CO₂ hydrogenation to methanol over Pd/In₂O₃: effects of Pd and oxygen vacancy. *Appl. Catal. B: Environ.* **218**, 488–497 (2017).
193. Hartadi, Y., Widmann, D., Behm, R. J. CO₂ hydrogenation to methanol on supported Au catalysts under moderate reaction conditions: support and particle size effects. *ChemSusChem* **8**, 456–465 (2015).
194. Jiang, X., Jiao, Y., Moran, C., Nie, X. W., Gong, Y. T., Guo, X. W., Walton, K. S., Song, C. S. CO₂ hydrogenation to methanol on Pd-Cu bimetallic catalysts with lower metal loadings. *Catal. Commun.* **118**, 10–14 (2019).
195. Choi, E. J., Lee, Y. H., Lee, D. W., Moon, D. J., Lee, K. Y. Hydrogenation of CO₂ to methanol over Pd-Cu/CeO₂ catalysts. *Mol. Catal.* **434**, 146–153 (2017).
196. Sun, Q., Chen, B. W. J., Wang, N., He, Q., Chang, A., Yang, C.-. M., Asakura, H., Tanaka, T., Hulse, M. J., Wang, C.-. H., et al. Zeolite-encaged Pd-Mn nanocatalysts for CO₂ hydrogenation and formic acid dehydrogenation. *Angew. Chem. Int. Ed.* **59**, 2–11 (2020).
197. Ota, A., Kunkes, E. L., Kasatkin, I., Groppo, E., Ferri, D., Poceiro, B., Yerga, R. M. N., Behrens, M. Comparative study of hydrotalcite-derived supported Pd₂Ga and PdZn intermetallic nanoparticles as methanol synthesis and methanol steam reforming catalysts. *J. Catal.* **293**, 27–38 (2012).
198. Studt, F., Sharafutdinov, I., Abild-Pedersen, F., Elkjaer, C. F., Hummelshøj, J. S., Dahl, S., Chorkendorff, I., Norskov, J. K. Discovery of a Ni-Ga catalyst for carbon dioxide reduction to methanol. *Nat. Chem.* **6**, 320–324 (2014).
199. Shi, Z. S., Tan, Q. Q., Tian, C., Pan, Y., Sun, X. W., Zhang, J. X., Wu, D. F. CO₂ hydrogenation to methanol over Cu-In intermetallic catalysts: effect of reduction temperature. *J. Catal.* **379**, 78–89 (2019).
200. Martin, O., Martin, A. J., Mondelli, C., Mitchell, S., Segawa, T. F., Hauert, R., Drouilly, C., Curulla-Ferre, D., Perez-Ramirez, J. Indium oxide as a superior catalyst for methanol synthesis by CO₂ hydrogenation. *Angew. Chem. Int. Ed.* **55**, 6261–6265 (2016).
201. Bansode, A., Urakawa, A. Towards full one-pass conversion of carbon dioxide to methanol and methanol-derived products. *J. Catal.* **309**, 66–70 (2014).
202. Hu, S., Liu, M., Ding, F. S., Song, C. S., Zhang, G. L., Guo, X. W. Hydrothermally stable MOFs for CO₂ hydrogenation over iron-based catalyst to light olefins. *J. CO₂ Util.* **15**, 89–95 (2016).
203. Wei, J., Ge, Q., Yao, R., Wen, Z., Fang, C., Guo, L., Xu, H., Sun, J. Directly converting CO₂ into a gasoline fuel. *Nat. Commun.* **8**, 15174 (2017).
204. Zhang, J. L., Su, X. J., Wang, X., Ma, Q. X., Fan, S. B., Zhao, T. S. Promotion effects of Ce added Fe-Zr-K on CO₂ hydrogenation to light olefins. *React. Kinet. Mech. Cat.* **124**, 575–585 (2018).
205. Fujiwara, M., Kieffer, R., Ando, H., Souma, Y. Development of composite catalysts made of Cu-Zn-Cr oxide zeolite for the hydrogenation of carbon-dioxide. *Appl. Catal. A: Gen.* **121**, 113–124 (1995).
206. Wang, . W. . J., Jiang, . X., Wang, X. X., Song, C. S. Fe-Cu bimetallic catalysts for selective CO₂ hydrogenation to olefin-rich C₂₊ hydrocarbons. *Ind. Eng. Chem. Res.* **57**, 4535–4542 (2018).
207. Liu, X. L., Wang, M. H., Zhou, C., Zhou, W., Cheng, K., Kang, J. C., Zhang, Q. H., Deng, W. P., Wang, Y. Selective transformation of carbon dioxide into lower olefins with a bifunctional catalyst composed of ZnGa₂O₄ and SAPO-34. *Chem. Commun.* **54**, 140–143 (2018).
208. Wang, X., Yang, G., Zhang, J., Chen, S., Wu, Y., Zhang, Q., Wang, J., Han, Y., Tan, Y. Synthesis of isoalkanes over a core (Fe-Zn-Zr)-shell (zeolite) catalyst by CO₂ hydrogenation. *Chem. Commun.* **52**, 7352–7355 (2016).
209. Numpilai, T., Witoon, T., Chanlek, N., Limphirat, W., Bonura, G., Chareonpanich, M., Limtrakul, J. Structure activity relationships of Fe-Co/K-Al₂O₃ catalysts calcined at different temperatures for CO₂ hydrogenation to light olefins. *Appl. Catal. A: Gen.* **547**, 219–229 (2017).
210. Gao, P., Li, S. G., Bu, X. N., Dang, S. S., Liu, Z. Y., Wang, H., Zhong, L. S., Qiu, M. H., Yang, C. G., Cai, J., et al. Direct conversion of CO₂ into liquid fuels with high selectivity over a bifunctional catalyst. *Nat. Chem.* **9**, 1019–1024 (2017).
211. Gao, P., Dang, S. S., Li, S. G., Bu, X. N., Liu, Z. Y., Qiu, M. H., Yang, C. G., Wang, H., Zhong, L. S., Han, Y., et al. Direct production of lower olefins from CO₂ conversion via bifunctional catalysis. *ACS Catal.* **8**, 571–578 (2018).
212. Wang, Y., Tan, L., Tan, M. H., Zhang, P. P., Fang, Y., Yoneyama, Y., Yang, G. H., Tsubaki, N. Rationally designing bifunctional catalysts as an efficient strategy to boost CO₂ hydrogenation producing value-added aromatics. *ACS Catal.* **9**, 895–901 (2019).
213. Ye, R.-. P., Ding, J., Gong, W., Argyle, M. D., Zhong, Q., Wang, Y., Russell, C. K., Xu, Z., Russell, A. G., Li, Q., et al. CO₂ hydrogenation to high-value products via heterogeneous catalysis. *Nat. Commun.* **10**, 5698 (2019).
214. Wang, Y., Gao, W., Li, K., Zheng, Y., Xie, Z., Na, W., Chen, J. G., Wang, H. Strong evidence of the role of H₂O in affecting methanol selectivity from CO₂ hydrogenation over Cu-ZnO-ZrO₂. *Chem* **6**, 419–430 (2019).
215. Ronda-Lloret, M., Rothenberg, G., Shiju, N. R. A critical look at direct catalytic hydrogenation of carbon dioxide to olefins. *ChemSusChem* **12**, 3896–3914 (2019).
216. Ma, J., Sun, N., Zhang, X., Zhao, N., Xiao, F., Wei, W., Sun, Y. A short review of catalysis for CO₂ conversion. *Catal. Today* **148**, 221–231 (2009).
217. Goeppert, A., Czaun, M., Jones, J.-. P., Surya Prakash, G. K., Olah, G. A. Recycling of carbon dioxide to methanol and derived products—closing the loop. *Chem. Soc. Rev.* **43**, 7995–8048 (2014).
218. An, B., Zhang, J., Cheng, K., Ji, P., Wang, C., Lin, W. Confinement of ultrasmall Cu/ZnOx nanoparticles in metal-organic frameworks for selective methanol synthesis from catalytic hydrogenation of CO₂. *J. Am. Chem. Soc.* **139**, 3834–3840 (2017).
219. Zhong, J., Yang, X., Wu, Z., Liang, B., Huang, Y., Zhang, T. State of the art and perspectives in heterogeneous catalysis of CO₂ hydrogenation to methanol. *Chem. Soc. Rev.* **49**, 1385–1413 (2020).
220. Jiang, X., Nie, X., Guo, X., Song, C., Chen, J. G. Recent advances in carbon dioxide hydrogenation to methanol via heterogeneous catalysis. *Chem. Rev.* **120**, 7984–8034 (2020).
221. Natesakhawat, S., Lekse, J. W., Baltrus, J. P., Ohodnicki, P. R., Howard, B. H., Deng, X., Matranga, C. Active sites and structure-activity relationships of copper-based catalysts for carbon dioxide hydrogenation to methanol. *ACS Catal.* **2**, 1667–1676 (2012).
222. Guo, X., Mao, D., Lu, G., Wang, S., Wu, G. CO₂ hydrogenation to methanol over Cu/ZnO/ZrO₂ catalysts prepared via a route of solid-state reaction. *Catal. Commun.* **12**, 1095–1098 (2011).
223. Kattel, S., Ramirez, P. J., Chen, J. G., Rodriguez, J. A., Liu, P. Active sites for CO₂ hydrogenation to methanol on Cu/ZnO catalysts. *Science* **355**, 1296–1299 (2017).
224. Jiang, X., Koizumi, N., Guo, X., Song, C. Bimetallic Pd-Cu

- catalysts for selective CO₂ hydrogenation to methanol. *Appl. Catal. B: Environ.* **170-171**, 173–185 (2015).
225. Bahruji, H., Bowker, M., Hutchings, G., Dimitratos, N., Wells, P., Gibson, E., Jones, W., Brookes, C., Morgan, D., Lalev, G. Pd/ZnO catalysts for direct CO₂ hydrogenation to methanol. *J. Catal.* **343**, 133–146 (2016).
226. Zeng, L., Wang, Z., Wang, Y., Wang, J., Guo, Y., Hu, H., He, X., Wang, C., Lin, W. Photoactivation of Cu centers in metal-organic frameworks for selective CO₂ conversion to ethanol. *J. Am. Chem. Soc.* **142**, 75–79 (2020).
227. Qiao, J., Liu, Y., Hong, F., Zhang, J. A review of catalysts for the electroreduction of carbon dioxide to produce low-carbon fuels. *Chem. Soc. Rev.* **43**, 631–675 (2014).
228. Ross, M. B., De Luna, P., Li, Y., Dinh, C.- T., Kim, D., Yang, P., Sargent, E. H. Designing materials for electrochemical carbon dioxide recycling. *Nat. Catal.* **2**, 648–658 (2019).
229. Li, L., Huang, Y., Li, Y. Carbonaceous materials for electrochemical CO₂ reduction. *EnergyChem.* **2**, 100024 (2020).
230. Nitopi, S., Bertheussen, E., Scott, S. B., Liu, X., Engstfeld, A. K., Horch, S., Seger, B., Stephens, I. E. L., Chan, K., Hahn, C., et al. Progress and perspectives of electrochemical CO₂ reduction on copper in aqueous electrolyte. *Chem. Rev.* **119**, 7610–7672 (2019).
231. Gao, D., Arán-Ais, R. M., Jeon, H. S., Roldan Cuenya, B. Rational catalyst and electrolyte design for CO₂ electroreduction towards multicarbon products. *Nat. Catal.* **2**, 198–210 (2019).
232. Tackett, B. M., Gomez, E., Chen, J. G. Net reduction of CO₂ via its thermocatalytic and electrocatalytic transformation reactions in standard and hybrid processes. *Nat. Catal.* **2**, 381–386 (2019).
233. Ashford, B., Tu, X. Non-thermal plasma technology for the conversion of CO₂. *Curr. Opin. Green Sust.* **3**, 45–49 (2017).
234. Ma, X., Li, S., Ronda-Lloret, M., Chaudhary, R., Lin, L., van Rooij, G., Gallucci, F., Rothenberg, G., Raveendran Shiju, N., Hessel, V. Plasma assisted catalytic conversion of CO₂ and H₂O over Ni/Al₂O₃ in a DBD reactor. *Plasma Chem. Plasma Process.* **39**, 109–124 (2019).
235. Zhang, D., Huang, Q., Devid, E. J., Schuler, E., Shiju, N. R., Rothenberg, G., van Rooij, G., Yang, R., Liu, K., Kleyn, A. W. Tuning of conversion and optical emission by electron temperature in inductively coupled CO₂ plasma. *J. Phys. Chem. C.* **122**, 19338–19347 (2018).
236. Ronda-Lloret, M., Wang, Y. L., Oulego, P., Rothenberg, G., Tu, X., Shiju, N. R. CO₂ hydrogenation at atmospheric pressure and low temperature using plasma-enhanced catalysis over supported cobalt oxide catalysts. *ACS Sustainable Chem. Eng.* **8**, 17397–17407 (2020).

■ AUTHOR BIOGRAPHIES

Xiaoju Cui received her B.S. in Light Industry Engineering from Sichuan University in 2012 and her Ph.D. in Physical Chemistry from Dalian Institute of Chemical Physics (DICP), Chinese Academy of Sciences (CAS) in 2017. Following that, she served as an iChEM postdoctoral fellow at Xiamen University from 2017 to 2019. She is currently an associate professor at DICP and focusing on the development of new heterogeneous catalysts and catalytic process for C1 energy molecule conversion.



Rui Huang received his Ph.D. in Materials Physics and Chemistry from Dalian University of Technology (DUT, China) in 2015. In 2015–2016, he was a postdoctoral associate at Institute of Metal Research (CAS). He then received a Marie Curie COFUND fellow position at the Institute of Chemical Research of Catalonia (ICIQ) in 2016–2018. He is currently a professor at DUT and focusing on the development of new heterogeneous catalysts and catalytic process for small molecule activation, and the in-depth understanding of catalytic mechanism in combination with reaction kinetics and *in situ/operando* methodologies.



Dehui Deng received his Ph.D. in physical chemistry from DICP in 2013. He subsequently joined the State Key Laboratory of Catalysis, DICP, as an associate Professor and became a full Professor in 2017. Since January 2015, he has served as an iChEM Professor at Xiamen University. He also served as a visiting scholar at Stanford University between 2015 and 2016. He is dedicated to the research of precious metal-substituted nanocatalysts for fundamental and applied research in heterogeneous catalysis and electrocatalysis, aiming at highly efficient activation and conversion of small molecules such as C1 molecules, O₂, N₂, H₂ and H₂O.

